PNL-7200 Pt. 3
UC-402

17

Pacific Northwest Laboratory Annual Report for 1989 to the DOE Office of Energy Research

Part 3: Atmospheric Sciences
June 1990

Prepared for the U.S. Department of Energy
under Contract DE-AC06-76RLO 1830

Pacific Northwest Laboratory
Operated for the U.S. Department of Energy
by Battelle Memorial Institute

Battelle

DISCLAIMER

PACIFIC NORTHWEST LABORATORY
operated by
BATTELLE MEMORIAL INSTITUTE
for the
UNITED STATES DEPARTMENT OF ENERGY
under Contract DE-AC06-76RLO 1830

Printed in the United States of America

Available to DOE and DOE contractors from the
Office of Scientific and Technical Information, P.O. Box 62, Oak Ridge, TN 37831;
prices available from (615) 576-8401. FTS 626-8401.

Available to the public from the National Technical Information Service,
U.S. Department of Commerce, 5285 Port Royal Rd., Springfield, VA 22161.

NTIS Price Codes, Microfiche A01

Printed Copy

Price Code	Page Range
A02	1- 10
A03	11- 50
A04	51- 75
A05	76-100
A06	101-125
A07	126-150
A08	151-175
A09	176-200
A10	201-225
A11	226-250
A12	251-275
A13	276-300
A14	301-325

Price Code	Page Range
A15	326-350
A16	351-375
A17	376-400
A18	401-425
A19	426-450
A20	451-475
A21	476-500
A22	501-525
A23	526-550
A24	551-575
A25	576-600
A99	601-Up

PNL-7200 Pt. 3
UC-402

Pacific Northwest Laboratory Annual Report for 1989 to the DOE Office of Energy Research

Part 3 Atmospheric Sciences

Staff Members of Pacific Northwest Laboratory

June 1990

Prepared for
the U.S. Department of Energy
under Contract DE-AC06-76RLO 1830

Pacific Northwest Laboratory
Richland, Washington 99352

PREFACE

This 1989 Annual Report from Pacific Northwest Laboratory (PNL) to the U.S. Department of Energy (DOE) describes research in environment, safety, and health conducted during fiscal year 1989. The report again consists of five parts, each in a separate volume.

The five parts of the report are oriented to particular segments of the PNL program. Parts 1 to 4 report on research performed for the DOE Office of Health and Environmental Research in the Office of Energy Research. Part 5 reports progress on all research performed for the Assistant Secretary for Environment, Safety and Health. In some instances, the volumes report on research funded by other DOE components or by other governmental entities under interagency agreements. Each part consists of project reports authored by scientists from several PNL research departments, reflecting the multidisciplinary nature of the research effort.

The parts of the 1989 Annual Report are:

Part 1: Biomedical Sciences		
Program Manager:	J. F. Park	J. F. Park, Report Coordinator S. A. Kreml, Editor
Part 2: Environmental Sciences		
Program Manager:	R. E. Wildung	M. G. Hefty, Report Coordinator and Editor
Part 3: Atmospheric Sciences		
Program Manager:	C. E. Elderkin	C. E. Elderkin, Report Coordinator E. L. Owczarski, Editor
Part 4: Physical Sciences		
Program Manager:	L. H. Toburen	L. H. Toburen, Report Coordinator K. A. Parnell, Editor
Part 5: Environment, Safety, Health, and Quality Assurance		
Program Managers:	L. G. Faust P. G. Doctor J. M. Selby	S. K. Ennor, Report Coordinator and Editor

Activities of the scientists whose work is described in this annual report are broader in scope than the articles indicate. PNL staff have responded to numerous requests from DOE during the year for planning, for service on various task groups, and for special assistance.

Credit for this annual report goes to the many scientists who performed the research and wrote the individual project reports, to the program managers who directed the research and coordinated the technical progress reports, to the editors who edited the individual project reports and assembled the five parts, and to Ray Baalman, editor in chief, who directed the total effort.

W. J. Bair and T. S. Tenforde
Environment, Health and Safety
Research Program

Previous reports in this series:

Annual Report for

1951	HW-25021, HW-25709
1952	HW-27814, HW-28636
1953	HW-30437, HW-30464
1954	HW-30306, HW-33128, HW-35905, HW-35917
1955	HW-39558, HW-41315, HW-41500
1956	HW-47500
1957	HW-53500
1958	HW-59500
1959	HW-63824, HW-65500
1960	HW-69500, HW-70050
1961	HW-72500, HW-73337
1962	HW-76000, HW-77609
1963	HW-80500, HW-81746
1964	BNWL-122
1965	BNWL-280, BNWL-235, Vol. 1-4; BNWL-361
1966	BNWL-480, Vol. 1; BNWL-481, Vol. 2, Pt. 1-4
1967	BNWL-714, Vol. 1; BNWL-715, Vol. 2, Pt. 1-4
1968	BNWL-1050, Vol. 1, Pt. 1-2; BNWL-1051, Vol. 2, Pt. 1-3
1969	BNWL-1306, Vol. 1, Pt. 1-2; BNWL-1307, Vol. 2, Pt. 1-3
1970	BNWL-1550, Vol. 1, Pt. 1-2; BNWL-1551, Vol. 2, Pt. 1-2
1971	BNWL-1650, Vol. 1, Pt. 1-2; BNWL-1651, Vol. 2, Pt. 1-2
1972	BNWL-1750, Vol. 1, Pt. 1-2; BNWL-1751, Vol. 2, Pt. 1-2
1973	BNWL-1850, Pt. 1-4
1974	BNWL-1950, Pt. 1-4
1975	BNWL-2000, Pt. 1-4
1976	BNWL-2100, Pt. 1-5
1977	PNL-2500, Pt. 1-5
1978	PNL-2850, Pt. 1-5
1979	PNL-3300, Pt. 1-5
1980	PNL-3700, Pt. 1-5
1981	PNL-4100, Pt. 1-5
1982	PNL-4600, Pt. 1-5
1983	PNL-5000, Pt. 1-5
1984	PNL-5500, Pt. 1-5
1985	PNL-5750, Pt. 1-5
1986	PNL-6100, Pt. 1-5
1987	PNL-6500, Pt. 1-5
1988	PNL-6800, Pt. 1-5

FOREWORD

The Atmospheric Sciences Program at PNL has been studying atmospheric transport and processing of materials since the days of the Atomic Energy Commission (AEC). Early tracer developments were used in dispersion experiments to produce an extensive data base defining instantaneous and continuous plumes diffusing over a limited, relatively flat portion of the Hanford Site. Plume characteristics for a uniform surface in steady-state conditions were evaluated as a function of meteorological parameters. In fallout studies, very sensitive radiological detection methods permitted detailed characterization of seasonal and year-to-year variations in air concentrations of radionuclides over western North America.

As the program evolved, early research also dealt with wet and dry scavenging of nuclear contaminants. Much of the field experimentation on scavenging processes involved simulation of nuclear particulates with tracers. Releases of tracers at the surface investigated dry removal and below-cloud wet removal processes and, later in our initial research aircraft operations, tracers were released into clouds to study in-cloud scavenging processes. As energy development was undertaken more broadly, our research extended beyond nuclear concerns to include the transport, transformation, and wet removal of fossil energy contaminants on a local to multistate basis, preceding by several years the recognition of acid rain as a national problem.

Currently, the broad goals of atmospheric research at PNL are to describe and predict the nature and fate of atmospheric contaminants and to develop an understanding of the atmospheric processes contributing to their distribution on local, regional, continental, and global scales in the air, in clouds, and on the surface. For several years, studies of transport and diffusion have been extended to mesoscale areas of complex terrain. Atmospheric cleansing research has expanded to a regional-scale, multilaboratory investigation of precipitation scavenging processes involving the transformation and wet deposition of chemicals composing "acid rain." In addition, the redistribution and long-range transport of transformed contaminants passing through clouds is recognized as a necessary extension of our research to even larger scales in the future. Eventually, large-scale experiments on cloud processing and redistribution of contaminants will be integrated into the national program on global change, investigating how energy pollutants affect aerosols and clouds and the transfer of radiant energy through them. As the significance of this effect becomes clear, its global impact on climate will be studied through experimental and modeling research.

The description of ongoing atmospheric research at PNL is organized in terms of the following study areas:

- **Atmospheric Studies in Complex Terrain**
- **Large-Scale Atmospheric Transport and Processing of Emissions**
- **Climate Change.**

This report describes the progress in FY 1989 in each of these areas. A divider page summarizes the goals of each area and lists project titles that support research activities.

CONTENTS

Atmospheric Studies in Complex Terrain

ATMOSPHERIC STUDIES IN COMPLEX TERRAIN

The Atmospheric Studies in Complex Terrain (ASCOT) program investigates the role of energy exchange, terrain configuration, and scale interactions for coupled flows (e.g., slope, valley, and gradient) in developing and destroying boundary-layer circulations and in dispersing contained contaminants. Research consists of both field experiments and modeling studies.

Experiments are conducted at sites with prominent terrain features where strong diurnal variations in energy fluxes can be well documented. Temperature, wind, and turbulence fields in the thermally generated mesoscale circulations are measured in situ and remotely. The general flow features over the region to which the terrain-induced circulations and contaminant plumes are periodically linked are characterized with soundings and tracers.

Numerical computer models are used to help analyze the results of measurement programs and to carry out numerical experiments that extend the range of conditions being studied. These investigations are systematically increasing the reliability of theoretical descriptions and models. Such models hold the promise of translating descriptive and forecasting capabilities to the great number of other locations where boundary-layer flow and contaminant dispersion are significantly influenced by terrain features and surface energy exchange processes.

While maintaining their longer-term commitment to basic research in complex terrain meteorology, ASCOT program participants are also focusing more closely on applications of the understanding of complex meteorology; in particular, problems of emergency preparedness relevant to DOE needs. PNL is participating in an ASCOT field experiment at the Oak Ridge National Laboratory (ORNL) in early 1990. The improved understanding of the wind, temperature, and turbulence fields in the vicinity of ORNL and in the Tennessee Valley will improve transport and dispersion forecast tools for the region. Results from measurements and numerical models will be combined to provide a clearer picture of the interaction among ambient winds aloft, thermal forcing in the valley, channeling by nearby mountains, and the effects of smaller scale ridges within the Tennessee Valley. PNL will work closely with other ASCOT investigators to analyze the data collected during this measurement program as well as to integrate the results of a mesoscale modeling program into a study of the mechanisms responsible for the observed wind characteristics.

Three projects at PNL investigate related aspects of the ASCOT research and are closely coordinated with ASCOT projects at other DOE laboratories:

- **Atmospheric Boundary-Layer Studies**
- **Atmospheric Diffusion in Complex Terrain**
- **Coupling/Decoupling of Synoptic and Valley Circulations.**

Atmospheric Studies in Complex Terrain

Direct Numerical Simulation of Turbulent Boundary Layer Flows

T. W. Horst and R. M. Kerr[a]

Horst and Doran (1988a) investigated the local turbulence structure of nocturnal slope flow, using both observations from the Rattlesnake Mountain slope wind site and numerical simulations with a turbulence covariance model that was developed by Brost and Wyngaard (1978) for stably stratified flow. One of the parameters of the model is a turbulent length scale, and two different formulations were used to modify the length scale to account for the change from horizontal to sloped terrain (Horst and Doran 1988b). The model predictions were in most cases insensitive to the length scale formulation, and the predictions were found to compare reasonably well with the observations from Rattlesnake Mountain. The most significant differences between the predictions of the two model formulations occurred for the eddy thermal diffusivity; the predictions of the two models were essentially identical for small values of atmospheric stability, but the difference increased with stability.

A more definitive investigation of the local turbulence structure of nocturnal slope flow (and determination of the proper formulation of the length scale for turbulence covariance modeling) requires either a more extensive data base than presently available from the Rattlesnake Mountain slope wind site or numerical simulation with a more detailed turbulence model. The latter course has been initiated over the past year, using the geophysical turbulence code written by Robert Kerr at the National Center for Atmospheric Research (NCAR).

The boundary-layer algorithms in Kerr's geophysical turbulence code use mesh refinement and a sophisticated pressure elimination scheme to directly simulate no-slip boundary layers at moderate turbulent Reynolds numbers. The Navier-Stokes equations, including the viscous term, are integrated directly and thus no subgrid scale parameterization (e.g., a turbulent length scale) is required to account for an unresolved turbulent portion of the flow field. It has been shown that most of the important dynamical regimes of boundary layers, such as the viscous subrange, the transition regime, and the interior turbulent regime, can be resolved with this approach, and the results agree with moderate Reynolds-number experiments. Since these regimes can generally be scaled to high- Reynolds-number atmospheric flows, this approach provides a basis for studying effects in geophysical boundary layers that have eluded earlier modeling efforts. It also provides simulation data that can be used for comparison with parameterized turbulence models when atmospheric or laboratory observational data are not available.

Since Kerr's model had not been used previously for shear-driven boundary-layer flows, the work during the past year has primarily focused on becoming familiar with and debugging the code by reproducing existing channel flow simulations with a constant pressure gradient and no thermal stratification. Future work will extend the simulations to stably stratified channel flow and finally to nocturnal slope flow.

Several calculated statistics were used to verify application of Kerr's code to channel (Pousille) flow. Simulations were run with a constant mass flux constraint until the pressure gradient and total turbulent kinetic energy approached a quasi-steady-state. Statistics were then averaged for several large-eddy turnover times. Adequate domain size was verified by requiring that the correlation coefficients approach zero at spatial separations equal to one-half of the domain dimensions. Adequate grid resolution was determined by requiring that the energy density at high wave numbers be several decades lower than that at low wave numbers and that there be no evidence of energy pileup at high wave numbers.

Physical realism of the model requires, then, that statistics of the simulated flow field match reliable available observations. Figure 1 shows the mean velocity versus distance from the wall, plotted in

(a) National Center for Atmospheric Research, Boulder, Colorado.

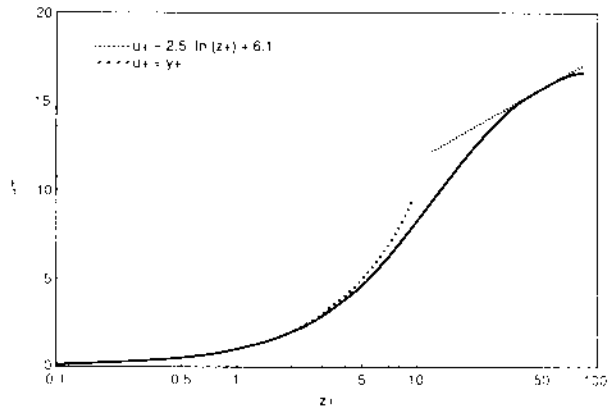

FIGURE 1. Mean Velocity Profiles, Plotted in Wall Coordinates.

wall coordinates, for a simulation on a 64 x 64 x 64 mesh with a streamwise domain equal to 6d and a spanwise domain equal to 3d, where d is one-half the wall separation. Also shown in Figure 1 are the theoretical velocity profiles in the viscous sublayer and in the inertial sublayer. The extent of the inertial sublayer is limited by the low Reynolds number of the simulation (Re=1300, based on the centerline velocity and channel half width). Figure 2 shows the root-mean-square (rms) turbulent intensities, normalized by the wall-shear velocity, as a function of distance from the wall. These profiles agree well with laboratory data and with previous direct numerical simulations of channel flow (Kim et al. 1987).

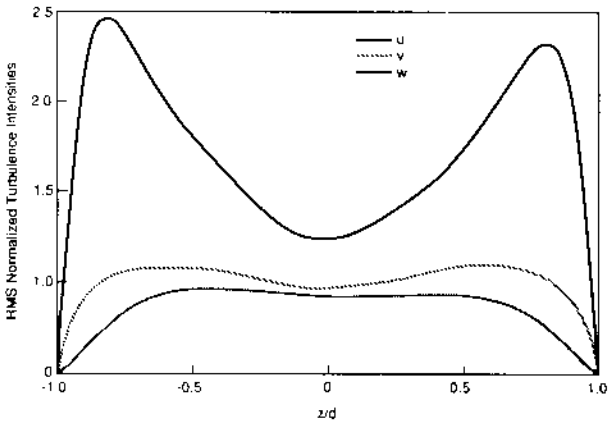

FIGURE 2. Profiles of Root-Mean-Square Velocity Fluctuations, Normalized by the Wall-Shear Velocity.

Acknowledgment

This work was partially supported by the National Science Foundation and the U.S. Army Research Office.

References

Brost, R. A., and J. C. Wyngaard. 1978. "A Model Study of the Stably Stratified Planetary Boundary Layer." *J. Atm. Sci.* 35:1427-1440.

Horst, T. W., and J. C. Doran. 1988a. "The Turbulence Structure of Nocturnal Slope Flow." *J. Atm. Sci.* 45:605-616.

Horst, T. W., and J. C. Doran. 1988b. "The Turbulence Length Scale in Nocturnal Slope Flow." In *Pacific Northwest Laboratory Annual Report for 1987 to the DOE Office of Energy Research, Part 3 Atmospheric Sciences.* PNL-6500 Pt.3. Pacific Northwest Laboratory, Richland, Washington.

Kim, J., P. Moin, and R. Moser. 1987. "Turbulence Statistics in Fully Developed Channel Flow at Low Reynolds Number." *J. Fluid Mech.* 177:133-166.

Modeling of Slope Flows in a Simple Valley

J. C. Doran

A two-dimensional slope flow model (Doran 1989; Doran et al. 1988) has been used in the analysis of data collected over the slope of a simple valley. Observations were used to describe the ambient environment that provided the boundary conditions for the model. The model was then used to perform a series of numerical experiments to examine the mechanisms responsible for the observed features of the slope flows.

Three sets of numerical simulations were carried out. The first set utilized relatively simple temperature profiles to examine the basic response of the modeled slope flows to ambient stratification in the valley. This also allowed a comparison of the model results with results obtained by previous investigators. The second set of simulations used measured temperature profiles from the valley experiments in an effort to reproduce the observed behavior of the slope flows on selected nights.

Finally, a series of sensitivity tests was carried out to isolate those features of the ambient conditions that were most important in determining the slope flow characteristics.

The model was used to compute inversion and momentum depths, denoted h and h', respectively. These depths are defined by the expressions

$$T(n)=T(9m) + \Delta T \cdot \exp(-n/h),$$

where n is the height above the surface, T is the temperature, ΔT is the magnitude of the inversion strength, and

$$Uh' = \int_0^\infty u dn'$$

and

$$U^2h' = \int_0^\infty u^2 dn'$$

where u is the katabatic wind down the valley sidewall and U is a scaling parameter for the wind.

The first set of simulations, which used an ambient temperature profile with constant stratification, was comparable to simulations carried out with another two-dimensional model by Nappo and Rao (1987). Results for the dependence of h and h' were qualitatively similar in the two sets of simulations. The second set of simulations showed that the model was capable of reproducing many of the important features of the slope flows on the valley sidewalls. Comparisons were made between observed and modeled inversion depths, inversion strengths, the product of these two quantities, and their variation with downslope distance. Results were generally good.

The principal finding from the third set of simulations was the importance of the valley temperature structure. The ambient temperature profile in the valley frequently showed extended layers in which the potential temperature was constant. Observations and numerical simulations showed that these layers are associated with decreases in the slope flow inversion depth scale h, but the numerical simulations also showed that this does not necessarily imply a decrease in the momentum depth scale, h'. Over simple slopes, the two depth scales will generally evolve similarly with downslope distance, but in a valley this need not be true.

Model results were also consistent with the observation that as down-valley winds increase, the local inversion strengths on the sidewall drop below the maximum values attained during a transition period shortly after sunset. The effect appears to be related to enhanced vertical mixing on the sidewalls arising from the larger wind shear associated with the stronger winds.

References

Doran, J. C. 1989. "Slope FLow Model for Nesting with a Mesoscale Code." In *Pacific Northwest Laboratory Annual Report for 1988 to the DOE Office of Energy Research, Part 3 Atmospheric Sciences*. PNL-6800 Pt. 3, Pacific Northwest Laboratory, Richland, Washington.

Doran, J. C., T. W. Horst, and C. D. Whiteman. 1988. *The Development and Structure of Nocturnal Slope Winds in a Simple Valley*. Final Report to the Army Research Office, Research Triangle Park, North Carolina.

Nappo, C. J., and K. S. Rao. 1987. "A Model Study of Pure Katabatic Flows." *Tellus* 39A:61-71.

Modeling and Observations of a Valley's Atmospheric Heat Budget

D. C. Bader, T. W. Horst, and C. D. Whiteman

During the 1984 ASCOT field studies in Brush Creek, Colorado, extensive measurements of the nocturnal wind and temperature fields were made that subsequently were used to develop a thermal energy budget of the valley flow system (Horst et al. 1987). The calculated thermal energy budgets did not balance, however. Possible explanations for the discrepancies are that the measurements contained significant errors and that one or more of the several assumptions used in computing the budget terms was not valid. To determine the reasons for the imbalances, valley thermal energy budgets were calculated from numerical simulations of valley drainage flow using a three-dimensional dynamical mesoscale model. The model uses an idealized version of the valley topography to simplify the calculations and more

clearly reveal the small-scale processes that determine the various contributions to the budgets. The model simulation had no externally imposed wind field. The modeled results were compared to an observed case when the winds overlying the valley were light.

Observations and Calculations

The observations used to evaluate the thermal energy budget consisted of lidar measurements of along-valley winds and instrumented tethered balloon soundings of wind, humidity and temperature at several locations along the valley floor. Details about the measurements have been given by Horst et al. (1987).

The integrated cross-valley budget terms are calculated as a function of height above the valley floor in the coordinate system shown in Figure 1. The budget calculations assume three things: 1) that the cross-valley temperature variations are unimportant, 2) that the turbulent heat fluxes are significant only at the ground, and 3) that the vertical velocity can be computed from the along-valley wind divergence. The resulting budget can be expressed as

$$\frac{1}{S_2 - S_1}\int_{S_1}^{S_2}\Bigg[\underbrace{\rho C_p \frac{\partial \bar{\theta}}{\partial t}(z)\cdot(y_2 - y_1)}_{a} + \underbrace{\rho C_p\, \bar{U}(z)\bullet\nabla\bar{\theta}(z)\cdot(y_2 - y_1)}_{b} + \underbrace{\rho C_p \int_{y_1}^{y_2}\frac{\partial \overline{w'\theta_s'}}{\partial z}dy}_{c} + \underbrace{\nabla\bullet F}_{d}\Bigg]ds = 0$$

where term a is the local tendency or storage term, term b is the total advective contribution, term c is the surface turbulent heat flux component, and term d is the contribution resulting from the radiative flux divergence. Figure 2 shows the calculated thermal energy budget for one segment of the Brush Creek valley during the 1984 ASCOT field studies. As can be seen in the graph, the sum of the budget terms produces a large residual; this imbalance cannot be explained from analysis of the available data.

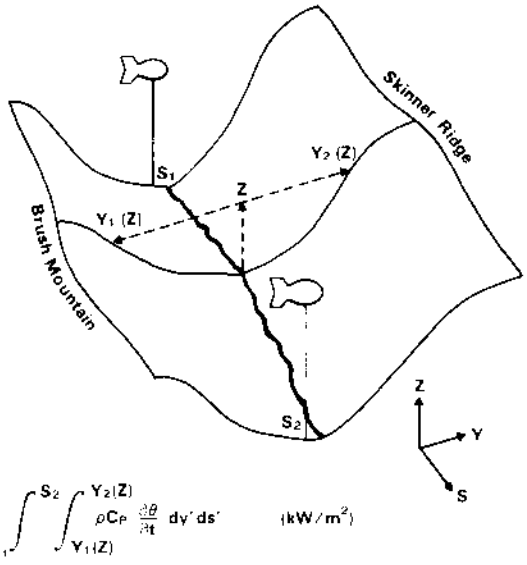

FIGURE 1. Cross-Valley-Integrated Thermal Energy Budget.

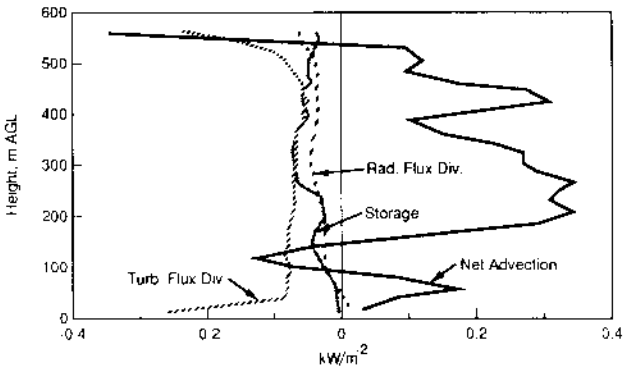

FIGURE 2. Brush Creek Valley Thermal Energy Budget, 01-06 MST September 26, 1984.

Model Simulation

The simulation was produced using the non-hydrostatic mesoscale model described by Bader et al. (1987) in the following configuration. The domain was 36 km long, 4.3 km wide and 4 km deep. An axis of symmetry was imposed at the eastern boundary so that only half of the valley was modeled. This symmetry condition increased the effective domain width to 8.6 km. Grid spacing was 1000 m in the along-valley direction, 100 m in the cross-valley direction and 50 m in the lowest 10 layers in the vertical direction. Above this level, the vertical grid spacing increased logarithmically. The grid spacing above elevated terrain

was reduced slightly according to the coordinate transformation functions used in the model.

The model topography is shown in Figure 3. This idealized model valley is 850 m deep and 6.5 km wide (ridge to ridge) at the mouth. The valley's lower end is U-shaped with the floor width decreasing as a function of distance from the mouth until the sidewalls meet 12 km up-valley. The floor rises with a slope of 0.01 in this lower valley section while the slope increases to 0.02 in the V-shaped upper 6 km. Sidewall slopes are 0.4 below 700 m above the flat plain at the valley mouth and 0.15 between 700 and 850 m elevation above the plain. A flat 850-m-high plateau extends from the ridge crests to the model boundaries.

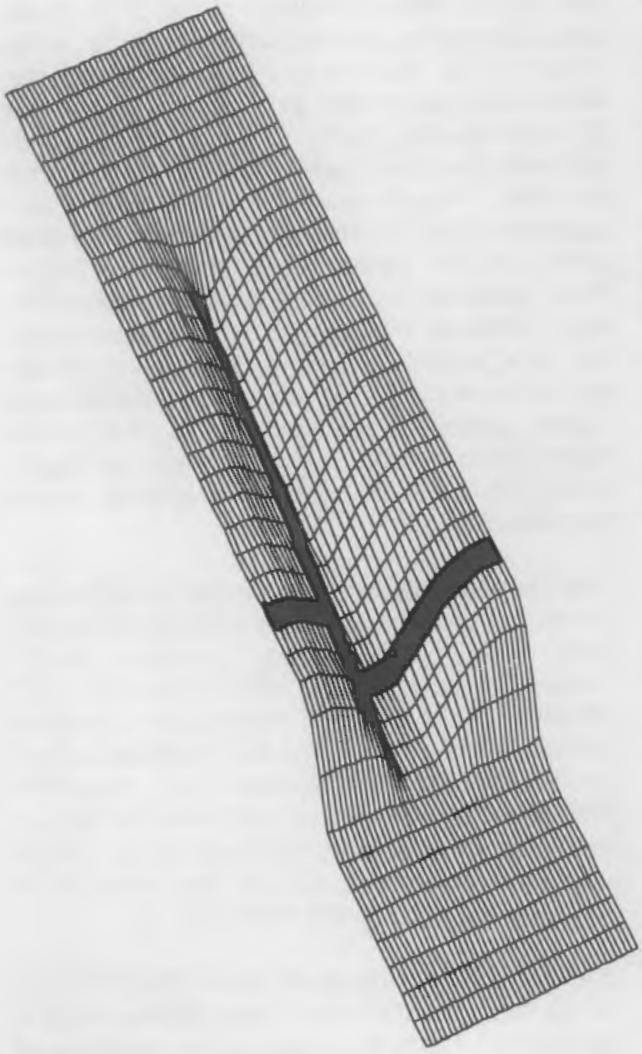

FIGURE 3. Idealized Model Topography.

The simulation started with an isothermal layer in the lowest 1 km topped by a free atmospheric lapse rate of 4 K/km. There was no initial wind. The model was forced by a kinematic heat flux of 0.04 K m/s at the surface (approximately 40 W/m^2) for 2 h. Atmospheric cooling resulting from radiative flux divergence was not simulated, since it is only a minor contribution to the observed cooling.

The model wind and temperature fields were saved on file every 10 min of simulated time. These fields were then interpolated to the budget coordinate system for the shaded section of the valley shown in Figure 3. Cross-valley integrated values of along-valley wind and potential temperature were calculated every 50 m in the vertical. Cross-valley integrated vertical velocities were computed from the integrated along-valley wind divergence in a manner similar to that used in computing the earlier budget. These integrated velocities and temperatures were then averaged over the last 30 min of the simulation to compute the advective contributions to the model budget. The contribution from the surface turbulent heat flux was constant. The local storage term was calculated by differencing the integrated potential temperatures at the beginning and end of the 30-min period.

Results

The thermal energy budget calculated from the model simulation is shown in Figure 4. The modeled and observed budgets both contain a residual after all terms are summed. In the

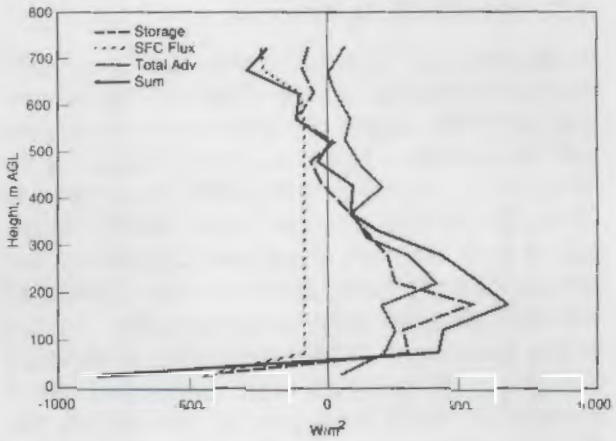

FIGURE 4. Model Budget.

modeled budget, the storage term is large and positive in the lower elevations, whereas the observed budget shows a small net cooling in the same part of the valley. In both cases, the advective contributions tend to be large and positive, except for one small region in the observed budget. Since the model is not prone to measurement error, only the small errors in interpolation, which are diminished by the integration process, and the fact that both budgets fail to close suggest that some of the assumptions used to calculate the budgets are wrong. Testing the assumption that cross-valley differences in the temperature and velocity fields are insignificant is an obvious place to start. The turbulent heat fluxes may also provide a significant contribution. An additional simulation, which will look at the effect of these assumptions on the calculated budgets, has been completed but not yet analyzed.

References

Bader, D. C., T. B. McKee, and G. J. Tripoli. 1987. "Mesoscale Boundary-Layer Evolution Over Complex Terrain. Part 1: Numerical Simulation of the Diurnal Cycle." *J. Atmos. Sci.* 44:2823-2838.

Horst, T. W., K. J. Allwine, and C. D. Whiteman. 1987. "A Thermal Energy Budget for Nocturnal Drainage Flow in a Simple Valley." In *Preprints, Fourth Conference on Mountain Meteorology,* August 25-27, 1987, Seattle, Washington. American Meteorological Society, Boston, Massachusetts.

Planning for the Oak Ridge Experiment 1990: Climatology and Modeling

J. C. Doran and C. D. Whiteman

In January and February of 1990, DOE's ASCOT program conducted a meteorological field experiment at ORNL as part of a planned emergency response exercise. The focus of the ASCOT activities was to improve forecasting operations at ORNL by gaining a better understanding of the role of local thermally developed circulations that form in the Tennessee Valley and their interaction with synoptic-scale flows above the valley. As part of the planning for this experiment, preliminary climatological analyses were performed and a numerical model was run to investigate the dynamics of the interaction between circulations of different scales. Both aspects of this work are continuing. Initial results are shown below.

Climatology

Initial climatological analyses used wind data from the 30-m level of a meteorological tower at ORNL for 1987 and the corresponding National Weather Service (NWS) upper-air data from Nashville, Tennessee. Analyses were focused on determining whether winds in the valley are thermally driven or are channeled by upper winds and whether stability has an effect on the valley wind directions.

Thermally driven wind systems in valleys reverse direction twice per day, with down-valley winds during nighttime and up-valley winds during daytime. The bi-directionality of valley winds, and the day-night reversal, are diagnostic features of thermal wind systems. Analysis of the ORNL tower data showed a bi-directionality of the winds (Figure 1) but also showed that, during daytime, winds were equally likely to be blowing down-valley (D-V) as up-valley (U-V). During nighttime, winds are somewhat more likely to blow down-valley than up-valley. These characteristics of the ORNL wind system suggest that winds are predominantly channeled into the Tennessee Valley by the larger-scale winds and pressure gradients above the valley, although local thermal forcing plays a significant role, especially at night. A further characteristic of the winds is their very low speed (Figure 2). These low speeds again suggest that the thermal forcing of the winds is weak and can be significantly influenced by synoptic-level winds above the valley.

The analysis above suggested that a relationship be sought between upper-air wind directions and wind directions within the Tennessee Valley. Table 1 illustrates these relationships for 1987, showing joint frequency distributions for wind directions at the tower and at the 850-mb pressure level (~1500 m MSL) above Nashville. Note that Nashville is 209 km west of ORNL and that the joint probability distribution includes two data points per day, corresponding to the release times of the rawinsondes, at 0615 and 1815 EST.

Rawinsonde observations show that 850-mb winds come predominantly from the two western quadrants. There are relatively few instances of easterly winds aloft, especially at upper levels. As

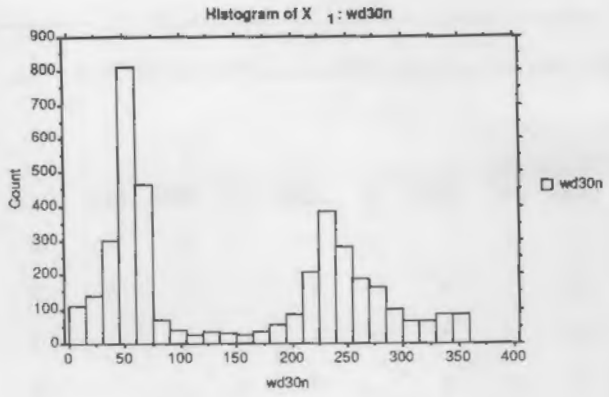

(a)

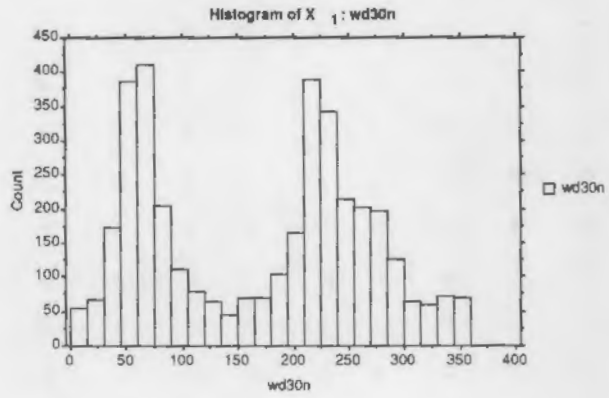

(b)

FIGURE 1. Wind Direction Frequency Distribution for (a) Night and (b) Day, 30-m Level, ORNL Tower, 1987.

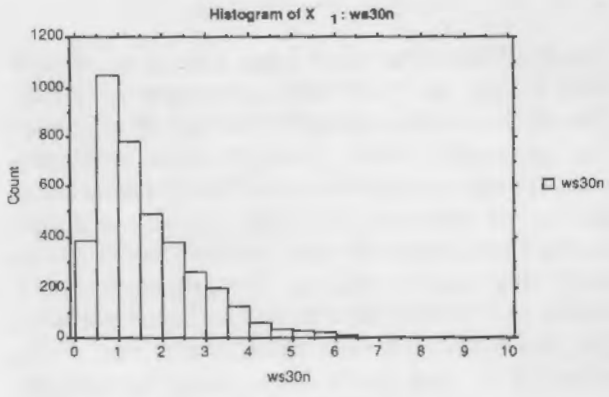

FIGURE 2. Wind Speed Histogram, 30-m Level, ORNL Tower, 1987.

expected, tower winds blow predominantly up or down the valley axis. Using all the rawinsonde data regardless of time of day, we found that winds blow down-valley at ORNL when winds aloft are from the directions N-E-S-SW. When winds aloft are from SW through N, winds within the valley blow up-valley. Thus, when winds aloft shift from SW through WSW the winds in the valley may suddenly reverse direction. This result is similar to wind behavior in the Rhine Valley, as documented by Gross and Wippermann (1987).

Climatological investigations are continuing for the ORNL area, using tower and rawinsonde data from 5 years and focusing on additional topics including stability relationships and day/night differences in valley wind systems and their coupling with winds above the valley. In this work, rawinsonde data will be interpolated from surrounding NWS stations to determine geostrophic wind directions over the valley center.

Dynamic Modeling

Numerical simulations with a mesoscale model (Mahrer and Pielke 1977; Arritt 1985; Doran and Skyllingstad 1989) have been used for a preliminary study of the wind behavior described above. A modeling domain approximately centered on the ORNL area and measuring about 215 km on a side was used for the calculations. A stable temperature profile was assumed to exist over the region, and a geostrophic wind of 10 m/s was specified. The model was run for a period of 2 h of simulated time without any heating or cooling of the surface. The simulations were intended to estimate the effects of terrain channeling of external winds but exclude possible contributions from locally developed thermal circulations.

The geostrophic wind direction was varied between 300° and 350° (roughly NW to N) and the resulting wind patterns were examined. Winds in the ORNL area and the Tennessee Valley north and east of ORNL tended to blow up-valley under these conditions. This behavior is in general agreement with the observations described previously.

TABLE 1. Joint Frequency Distribution–850-mb Wind Direction at Nashville versus the Wind Direction at 30 m on the ORNL Tower, 1987.

Tower Wind Direction	850-mb Wind Direction																	
	N	NNE	NE	ENE	E	ESE	SE	SSE	S	SSW	SW	WSW	W	WNW	NW	NNW	Miss	Total
N	5	2	0	0	0	1	1	0	2	2	1	2	0	2	2	3	0	23
NNE	5	3	1	0	0	0	0	0	0	5	1	5	2	4	1	2	0	29
NE	8	7	9	1	1	3	1	5	7	18	16	11	8	6	14	2	1	118
ENE	5	4	7	2	7	3	6	4	8	8	14	9	4	7	6	4	1	99
E	3	1	2	2	1	2	2	2	8	7	9	9	5	1	6	2	2	64
ESE	1	1	0	0	1	0	1	1	2	0	1	1	0	0	2	3	0	14
SE	0	1	0	0	0	0	0	1	0	0	1	1	1	3	0	0	1	9
SSE	0	0	0	1	0	0	0	0	0	1	1	0	0	1	1	1	0	6
S	1	1	0	0	0	0	0	0	1	2	4	2	2	1	0	0	0	14
SSW	0	1	0	0	0	0	2	0	2	0	12	4	2	2	1	3	0	29
SW	3	1	0	0	0	0	0	0	1	9	8	22	13	12	2	4	1	76
WSW	0	1	0	0	1	0	0	0	2	7	5	16	10	12	8	2	3	67
W	2	1	0	0	0	0	1	3	2	1	5	5	8	8	8	9	0	53
WNW	3	1	0	0	1	0	0	0	0	0	4	4	6	3	11	11	1	45
NW	2	0	0	1	0	0	0	0	0	0	1	1	4	1	3	6	2	21
NNW	6	1	1	1	0	0	0	1	0	2	1	2	1	2	2	7	0	27
Miss	4	3	2	0	0	0	0	1	1	3	5	4	6	2	3	2	0	36
Total	48	29	22	8	12	9	14	18	36	65	89	98	72	67	70	61	12	730

Figure 3 shows an example of the wind field generated for a geostrophic wind from 300°.

Observations also show, however, that downvalley winds are often observed at night even when the winds aloft are from directions covered in these simulations. We believe that at least two additional features will be required in the model if such behavior is to be seen in further simulations. The first is the extension of the modeling domain to include the higher terrain in the northern portion of the Tennessee Valley, and the second is the inclusion of surface cooling. The combination of additional terrain blocking to the northeast and katabatic forcing down the valley may be sufficient to counter the channeling effect simulated up to this time.

The modeled wind fields have also been used to help design the 1990 field experiment at ORNL. The model results indicated a number of regions in the Tennessee Valley in which the near-surface wind speeds and directions may be relatively sensitive to the ambient wind fields above the valley. Surface and upper-air wind measurements will be made at a number of these sites; these measurements will provide data useful for understanding the relationship between synoptic and local winds in the ORNL area and its surroundings and will also serve as a good test of the model's ability to realistically simulate the wind fields in the region. If the model is successful, it may provide a valuable supplement for forecasting that can be applied to problems of emergency preparedness.

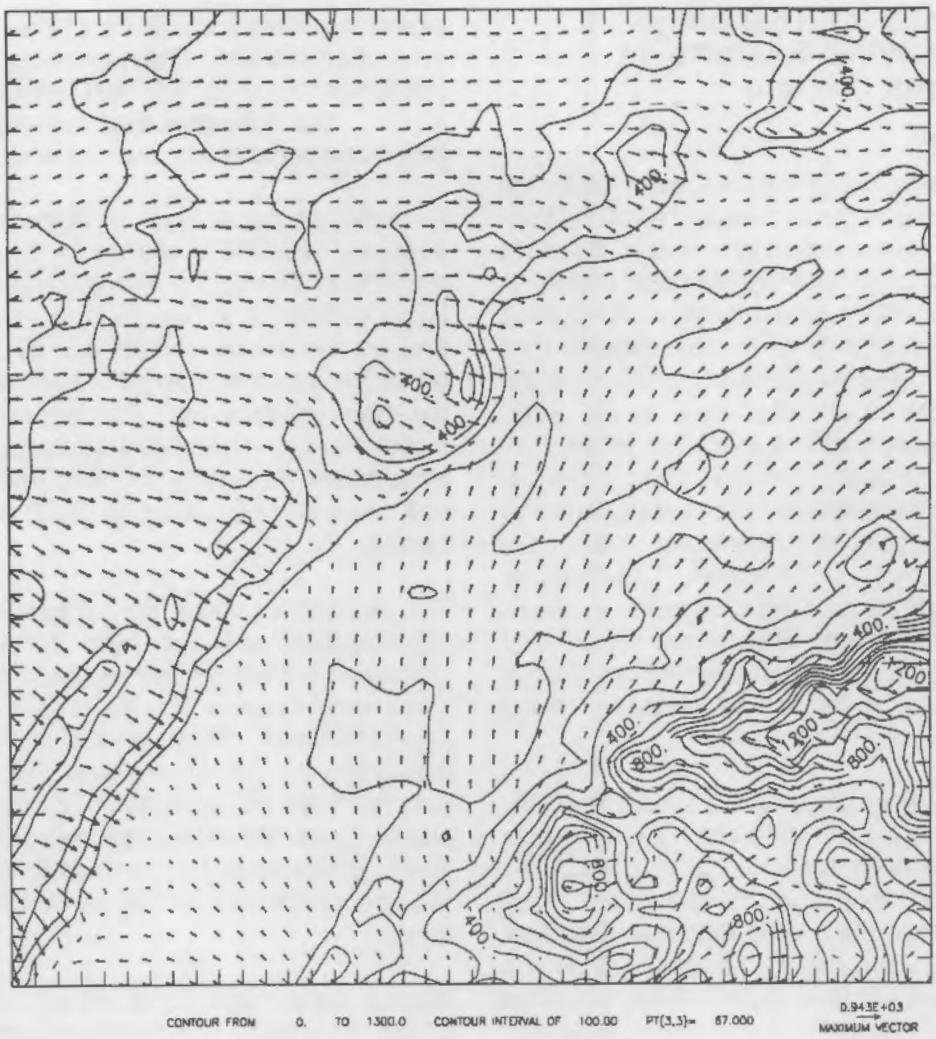

FIGURE 3. Modeled Wind Velocities 10 m Above the Surface for a 10-m/s Geostrophic Wind from 300°. Terrain height contours are in meters.

References

Arritt, R. W. 1985. "Numerical Studies of Thermally and Mechanically Forced Circulations Over Complex Terrain." Ph.D. Dissertation, Colorado State University, Fort Collins, Colorado.

Doran, J. C., and E. D. Skyllingstad. 1989. "Observed and Modeled Terrain-Induced Shear in Tracer Trajectories." In *Preprints, Sixth Joint Conference on Applications of Air Pollution Meteorology*, January 30-February 3, 1989, Anaheim, California. American Meteorological Society, Boston, Massachusetts.

Gross, G., and F. Wippermann. 1987. "Channeling and Countercurrent in the Upper Rhine Valley: Numerical Simulations." *J. Climate Appl. Meteor.* 26:1293-1304.

Mahrer, Y., and R. A. Pielke. 1977. "A Numerical Study of the Air Flow Over Irregular Terrain." *Contrib. Atmos. Phys.* 50:98-113.

Observations of Thermally Developed Wind Systems in Mountainous Terrain

C. D. Whiteman

In August 1988, a workshop was convened by the American Meteorological Society (AMS) in Park City, Utah, to review recent progress in the study of atmospheric processes over complex terrain. A volume in the AMS's Meteorological Monograph series, *Current Directions in Atmospheric Processes Over Complex Terrain*, summarizes the material presented and discussed at the workshop. The monograph is expected to be published in the late spring of 1990. The chapters of the volume were written by the researchers who were invited to speak at the workshop. A summary of the chapter by C. D. Whiteman, "Observations of Thermally Developed Wind Systems in Mountainous Terrain," follows. This chapter summarized recent research being conducted in DOE's ASCOT program, as well as related research being conducted in Europe and Japan.

Slope and valley wind systems are local thermally driven circulations that form frequently in complex terrain areas. Recent research has focused on the temperature structure along the slope and valley axes that leads to these wind systems. Two new tools being used in these analyses include the topographic amplification factor, which quantifies the role of the topography in producing bulk temperature gradients along a valley's axis, and atmospheric heat budgets, which identify key physical processes leading to changes in temperature structure. Both tools are in an early stage of development, are being applied primarily to steady-state nighttime periods, and are leading to new concepts and understanding.

Recent climatological evidence in Austria's Inn Valley and in several Colorado valleys supports the concept that valley winds are driven by horizontal pressure gradients that are built up hydrostatically by the changing temperature structure along a valley's length. Topographic amplification factors appear to be useful in assessing the strength of valley wind systems. Several components of valley atmospheric heat budgets have proven difficult to measure, and large imbalances are being experienced. Several recent experiments, in a range of climatological regimes, suggest that measured nighttime surface sensible heat fluxes are too small to result in balances. This may be caused by measurement errors or by nonrepresentative measurements. The advective and radiative flux divergence components are also uncertain.

A simple conceptual model of diurnal wind and temperature structure evolution in deep valleys is presented. During the morning transition period, upslope flows form over heated valley sidewalls and compensatory subsidence over the valley center produces warming that eventually reverses the down-valley winds. The key role of vertical motions in transferring energy through the valley atmosphere during the morning transition period has been demonstrated by field and modeling studies.

The evening transition period has received little observational attention, and the key physical processes are not yet well known. Investigation of slope wind systems has focused mostly on the nighttime flows. Flows on the sides of isolated mountains are reasonably well understood when external flows are weak, but slope flows on valley sidewalls are complicated by the continued evolution of temperature structure within the valley and the strong influence of the overlying along-valley flows.

Recent experiments have shown that thermally driven flows within the topography may be influenced in subtle ways by the overlying circulations. This influence is nearly always present to some extent but has not yet been systematically investigated. Recent research on strong winds that issue from a valley's exit at night and on tributary flows is briefly summarized, and some comments are made on Maloja winds and anti-wind systems. The chapter ends with a summary of topics needing further research.

Reference

Whiteman, C. D. 1990. "Observations of Thermally Developed Wind Systems in Mountainous Terrain." Chapter 2 in *Current Directions in Atmospheric Processes Over Complex Terrain* (W. Blumen, ed.), *Meteorological Monographs* 45:5-42, American Meteorological Society, Boston, Massachusetts.

Atmospheric Mass and Heat Budgets for a Canyonland Basin

C. D. Whiteman, J. M. Hubbe, and J. C. Doran

In recent years, the first attempts have been made to evaluate individual components of atmospheric mass and heat budgets in valleys and basins to investigate the thermal forcing and sources of air that support the local circulations. Such experiments have now been conducted for Colorado's Brush Creek valley (Whiteman and Barr 1986; Vergeiner et al. 1987; Horst et al. 1989), Austria's Inn Valley (Freytag 1985, 1987), Switzerland's Dischma Valley (Hennemuth 1985), Japan's Aizu Basin (Kondo et al. 1989), and Japan's Akaigawa Basin (Maki et al. 1986). These investigations, by and large, have been exploratory experiments in which individual budget terms were evaluated using small data sets. Since many of the terms could not be properly evaluated with available data, key terms were calculated as residuals in the budgets. Significant heat budget imbalances are a feature of the experiments in which the terms were independently evaluated, and recent lidar and tethersonde observations in valleys have revealed difficulties with the evaluation of along-valley and vertical advection terms. As part of DOE's 1988 ASCOT field program, we conducted a special experiment in Colorado's Sinbad Basin to investigate further the effects of topography on atmospheric heat budgets. Preliminary results from this experiment were presented at the International Conference on Mountain Meteorology and ALPEX (Whiteman et al. 1989) and are summarized below.

The atmospheric heat budget equation for a volume v can be written as follows:

$$\underbrace{\int \rho c_p \frac{\partial \bar{\theta}}{\partial t}\, dv}_{a} = \underbrace{-\int \rho c_p \nabla \cdot \left(\bar{V}\,\bar{\theta}\right) dv}_{b}$$

$$\underbrace{-\int \rho c_p \nabla \cdot \left(\overline{V'\theta'}\right) dv}_{c} \qquad (1)$$

$$\underbrace{-\int (\theta / T) \nabla \cdot \mathbf{R}\, dv}_{d} \quad [W]$$

This equation specifies that the rate of change of heat storage in an atmospheric volume (term a) depends on the convergence of potential temperature flux by the mean wind (term b), convergence of turbulent sensible heat flux (term c), and convergence of radiative flux (term d) in the atmospheric volume. In practice, Equation (1) is generally normalized by dividing each of the terms by the drainage area of the basin so that different valleys can be compared, and the resulting quantities are in the familiar units of W/m^2.

The experiments attempted to evaluate the individual terms of this equation and the basin atmospheric mass budget equation, using assumptions that could be made in the special topography and climatic regime of the Sinbad Basin (Figure 1). The Sinbad Basin is a 7- by 15-km, oval-shaped, arid basin drained by a single narrow valley, the Salt Wash. Since the basin is arid, condensation and evaporation of water within the basin atmosphere were ignored in Equation (1). Frequent soundings

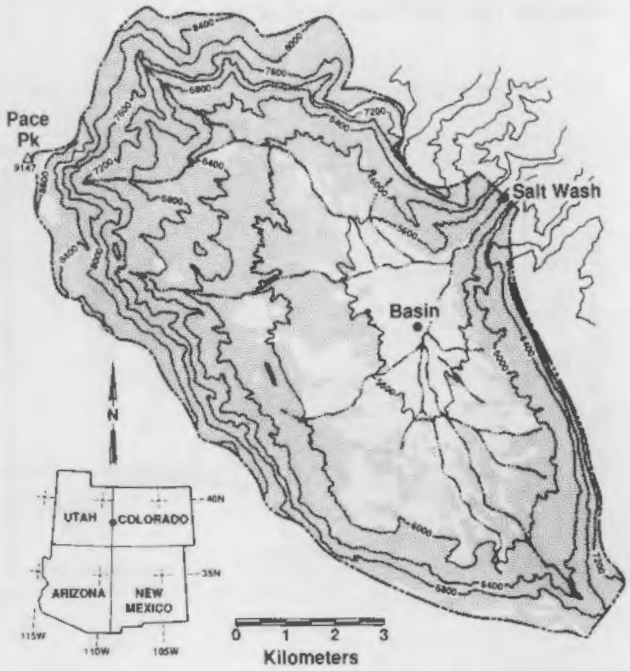

FIGURE 1. Topographic Map of the Sinbad Basin, Colorado, Experimental Area. The contour interval is 400 feet (122 m). The two observation sites are indicated with heavy dots. The stippling indicates the areas of the basin covered with forest or shrub vegetation.

of wind and temperature were made using tethered balloon data collection systems at the two basin sites during the evening and nighttime period of July 15-16, 1988. Supporting surface energy budget component measurements were made at the basin sites.

During nighttime, the mass outflow through the basin's narrow drainage canyon was at the rate of 1 to 2 kilotons/s, producing a compensatory mean subsidence of 0.02 m/s at the top of the basin and a net advective warming of the basin atmosphere at the average rate of 25 W/m^2 (Figure 2). Evaluation of the nocturnal atmospheric heat budget showed that the basin atmosphere lost heat at an average rate of 45 W/m^2, radiative losses were 20 W/m^2, and sensible heat flux from the atmosphere towards the ground, calculated as a residual, was 50 W/m^2. A discrepancy occurred between this calculated sensible heat flux and sensible heat flux estimated from surface energy budget measurements on the basin floor (Figure 3). There, nighttime radiative losses (62 W/m^2) were nearly balanced by an upward flux of heat from the ground (69 W/m^2) so that the sum of latent and sensible heat flux was quite small.

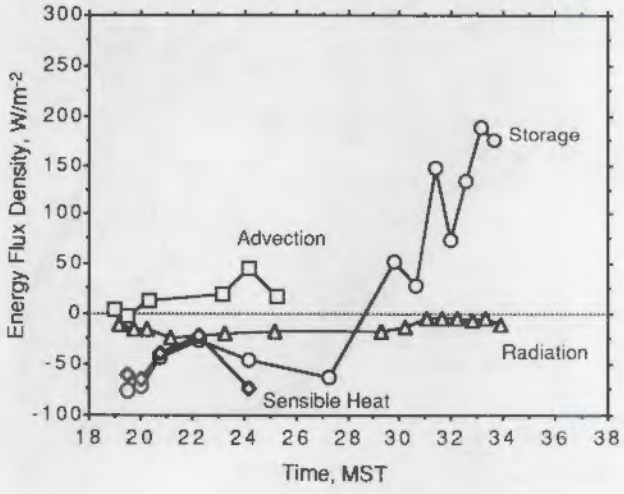

FIGURE 2. Components of the Sinbad Basin Atmospheric Heat Budget, July 15-16, 1988. All energy balance terms are normalized (i.e., divided) by the drainage area of the basin at its top (2214 m MSL). Shown are the rate of change of heat storage (term a in Equation 1), advection, i.e., mean potential temperature flux divergence (term b), turbulent sensible heat flux divergence (term c), and radiative flux divergence (term d).

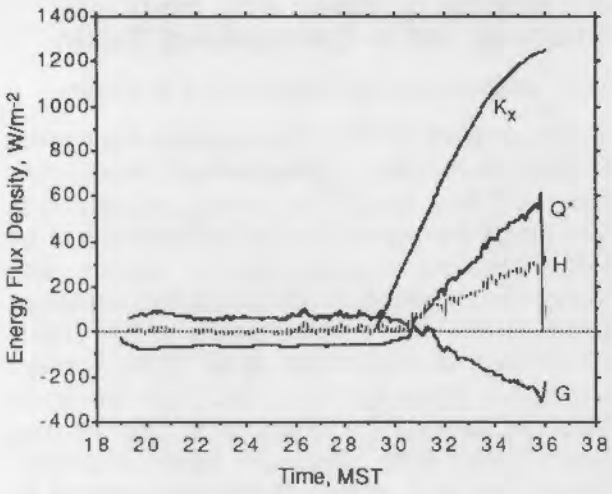

FIGURE 3. Components of the Surface Energy Balance at the Sinbad Basin Site, July 15-16, 1988. K_x is extraterrestrial solar radiation, Q* is net radiation, H is sensible heat flux, and G is ground heat flux.

During daytime, surface energy budget components (Figure 3) were larger than the nighttime values, with magnitudes increasing abruptly about 1 h after astronomical sunrise. Much of the net radiative gain went into sensible heat flux initially, but both the ground and the atmosphere received large amounts of energy during daytime. By noon, the basin atmosphere was receiving energy at the rate of nearly 300 W/m^2 and heat flow into the ground was at the rate of 250 W/m^2.

Four explanations seem possible for resolving the discrepancy between nighttime sensible heat flux as measured at the basin floor site and basin-wide sensible heat flux as calculated as a residual in the atmospheric heat budget equation: 1) measurement errors, 2) inappropriate assumptions in the atmospheric heat budget, 3) the "oasis effect," and 4) nonrepresentativeness of the basin floor energy budget measurements. Similar discrepancies have been previously reported in other more topographically complicated valleys and basins. Since the question of the thermal forcing of local wind systems in valleys and basins is of general interest relating to air pollution and environmental issues, we are focusing further effort on evaluating the atmospheric heat budget approach using Sinbad and other data sets. Other ASCOT investigators are using dynamic models to investigate assumptions used in the analysis regarding

turbulent sensible heat flux at the basin's top, and we are proposing new field experiments that can help to resolve this question.

References

Freytag, C. 1985. "MERKUR-Results: Aspects of the Temperature Field and the Energy Budget in a Large Alpine Valley During Mountain and Valley Wind." *Contrib. Atmos. Phys.* 58:458-476.

Freytag, C. 1987. "Results from the MERKUR Experiment: Mass Budget and Vertical Motions in a Large Valley During Mountain and Valley Wind." *Meteor. Atmos. Phys.* 37:129-140.

Hennemuth, B. 1985. "Temperature Field and Energy Budget of a Small Alpine Valley." *Contrib. Atmos. Phys.* 58:545-559.

Horst, T. W., K. J. Allwine, and C. D. Whiteman. 1987. "A Thermal Energy Budget for Nocturnal Drainage Flow in a Simple Valley." *Preprints, Fourth Conference on Mountain Meteorology*, August 25-28, 1987, Seattle, Washington. American Meteorological Society, Boston, Massachusetts.

Horst, T. W., D. C. Bader, and C. D. Whiteman. 1989. "Comparison of Observed and Simulated Nocturnal Valley Thermal Energy Budgets." *Extended Abstracts, International Conference on Mountain Meteorology and ALPEX*, June 5-9, Garmisch-Partenkirchen, FRG.

Kondo, J., T. Kuwagata, and S. Haginoya. 1989. "Heat Budget Analysis on Nocturnal Cooling and Daytime Heating in a Basin." *J. Atmos. Sci.* 46:2917-2933.

Maki, M., T. Harimaya, and K. Kikuchi. 1986. "Heat Budget Studies on Nocturnal Cooling in a Basin." *J. Meteor. Soc. Japan* 64:727-740.

Vergeiner, I., E. Dreiseitl, and C. D. Whiteman. 1987. "Dynamics of Katabatic Winds in Colorado's Brush Creek Valley." *J. Atmos. Sci.* 44:148-157.

Whiteman, C. D., and S. Barr. 1986. "Atmospheric Mass Transport by Along-Valley Wind Systems in a Deep Colorado Valley." *J. Climate Appl. Meteor.* 25:1205-1212.

Whiteman, C. D., J. M. Hubbe, J. C. Doran, and T. B. McKee. 1989. "Atmospheric Mass and Heat Budgets in a Closed Canyonland Basin." *Preprints, International Conference on Mountain Meteorology and ALPEX*, June 5-9, Garmisch-Partenkirchen, FRG, pp. 116-117.

Use of a Nonhydrostatic Mesoscale Model to Simulate Drainage Flows in the Presence of Ambient Winds

J. C. Doran

The nonhydrostatic mesoscale model developed by T. Clark of NCAR (Clark 1977; Clark and Farley 1984) has been obtained and adapted for use on the CRAY 2 at the National Magnetic Fusion Energy Computer Center. The model uses the anelastic approximation to filter sound waves and features a two-way interactive grid nesting scheme that allows portions of the modeling domain to be resolved on scales finer than those used for the entire domain.

The model has been applied to the problem of the interaction between nocturnal drainage winds in a mountain valley and ambient winds outside the valley. Previous numerical simulations have usually assumed negligible ambient winds. However, observations have shown that the strength and structure of the drainage flows in a valley are affected by external winds, and the processes responsible for these effects are not well understood.

A series of numerical experiments is currently being carried out to study this problem. The development and structure of drainage winds in the presence of ambient winds of varying speeds and directions are being simulated, and the general features will be compared to observations taken in Brush Creek valley in Colorado (Clements et al. 1989). Figure 1 gives an example of the computed down-valley wind field along a cross-section through the center of the valley after 6 h of cooling and with an ambient wind of 4 m/s blowing up and across the valley at an angle of 60° to the valley axis. Additional calculations of this type will be used to develop a more complete picture of the behavior of drainage flows in mountainous terrain.

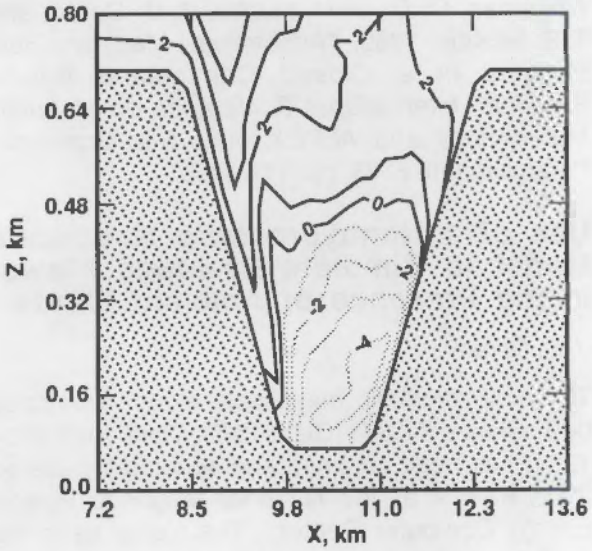

FIGURE 1. Computed Wind Field for Ambient Wind of 4 m/s at an Angle of 60° to the Valley Axis. Solid lines: up-valley winds; dashed lines: down-valley winds. Contours are in units of m/s.

References

Clark, T. L. 1977. "A Small-Scale Dynamic Model Using a Terrain-Following Coordinate Transformation." *J. Comp. Phys.* 24:186-215.

Clark, T. L., and R. D. Farley. 1984. "Severe Downslope Windstorm Calculations in Two and Three Spatial Dimensions Using Anelastic Interactive Grid Nesting: A Possible Mechanism for Gustiness." *J. Atmos. Sci.* 41:329-350.

Clements, W. E., J. A. Archuleta, and D. E. Hoard. 1989. "Mean Structure of the Nocturnal Drainage Flow in a Deep Valley." *J. Appl. Meteor.* 28:457-462.

Large-Scale Atmospheric Transport and Processing of Emissions

LARGE-SCALE ATMOSPHERIC TRANSPORT AND PROCESSING OF EMISSIONS

Research on large-scale atmospheric transport and processing of emissions through storms has continued in the Processing of Emissions by Clouds and Precipitation (PRECP) program and the Multi-State Air Pollution and Power Production Study/Precipitation Chemistry Network (MAP3S/PCN), supported by the Research Aircraft Operations task.

PRECP's purpose has been to examine the source-receptor relationships of regional-scale acid rain impacts through field experiments and modeling activities. Research has addressed the physical and chemical processes within the cloud and precipitation systems; cloud dynamics defining inflow and outflow characteristics, microphysics and in-cloud scavenging properties, aqueous phase chemistry, regional wet deposition patterns, and storm chemistry climatology have received direct attention. Large-scale experiments involving surface-based measurements and aircraft probing frontal and convective storm systems have been a combined effort of Argonne and Brookhaven National Laboratories (ANL and BNL) and PNL and have included other scientists concentrating on other aspects of storm systems. Aircraft and surface data were obtained this year in the Pacific Stratus Investigation, an exercise to determine the levels of chemical emissions from the ocean in the air approaching the west coast of the United States.

Modeling research, which organizes field research results into a descriptive and predictive framework, has emphasized cloud and precipitation chemistry and microphysics. These modeling efforts have also benefitted from strong interfaces with other scientists on related research topics such as photochemistry, synoptic- and regional-scale circulations, and cloud dynamics. This close cooperation is permitting us to integrate a comprehensive modeling description of the combined processes leading to acid deposition. In future PRECP research, model experiments will simulate storm processing of pollutants interactively with analysis of field experiments. The goal of such interaction is to improve understanding and contribute input modules to assessment codes that agencies will ultimately use for policy and regulatory considerations.

The importance of large-scale transport is becoming increasingly evident as PRECP results demonstrate the processing of energy contaminants by clouds, their chemical and photochemical reactions within and beyond their residence in clouds, the production of aerosols by cloud processing, and the interaction between anthropogenic and biogenic atmospheric chemicals. Because of the extent to which energy production and use influence atmospheric chemistry and its role in the global environment, new experiments independent of the concluding National Acid Precipitation Assessment Program research will investigate these processes as well as the redistribution of contaminants on larger scales in the future. Extended models will become increasingly important in numerical experimentation and in hypothesizing focused field experiments to study anticipated behavior. Less frequent but larger-scale confirming field campaigns will be planned in evaluating continental to global-scale distributions and budgets of energy pollutants.

In MAP3S/PCN activities, measurement and analytical capabilities have been advanced to ensure that regional air and surface chemistry distributions and their changes can be characterized sufficiently to anticipate new and growing threats to the environment. Our close association through the MAP3S/PCN network with scientists at universities and other national laboratories and our detailed analysis of precipitation samples from their measurement sites have created a valuable data base serving a host of related investigations on atmospheric chemistry and environmental cycling at their sites and across the network.

Changes in the MAP3S network for the next decade of its operation are being implemented. Recently developed techniques for trace metal evaluations to permit source region signatures for long-range transport to and from the United States are included. We will also examine speciation methods for trace

organometallics such as mercury species, produced in cycling energy-related contaminants between the ocean and atmosphere, as global-scale environmental impacts begin to appear. The need to identify growing levels of energy contaminants in air as well as rain will introduce the investigation of remote detection methods for trace gases and their column-integrated burdens through the troposphere. Similarly, new radiative transfer instrumentation, providing optical depth measurement for aerosol burdens in the troposphere and their size distributions, will be investigated for use at MAP3S stations. As global change issues begin to be addressed, data on radiative transfer through aerosol and cloud layers will be especially important in determining if climate can be altered on a hemispheric and global basis by changes resulting from pollution chemistry.

The studies described in the following articles were supported by:

- **PRECP**
- **MAP3S/PCN**
- **Research Aircraft Operations.**

Large-Scale Atmospheric Transport and Processing of Emissions

Precipitation Chemistry Observations: June 8, 1988, 3CPO Event

M. Terry Dana

Initial precipitation chemistry results from the June 8, 1988, Cloud Chemistry and Cloud Physics Organization (3CPO) event were presented in the 1988 Annual Report (Dana et al. 1989). These included event concentrations (in most cases composites of sequential samples) of sulfate, nitrate, hydrogen (from pH), and ammonium, which are reproduced in Figure 1. Additional examination of these data (plus those for calcium) suggests interesting spatial patterns of precipitation chemistry. The strong acid species (sulfate, nitrate, and hydrogen) show distinctly higher event concentrations in the south-central part of the network, with apparent spatial uniformity within that area. Spatial uniformity is also seen among the north-central sites. Ammonium and calcium, which are expected to have local sources, are more spatially variable, but there is no comparably large difference between the above-noted groups of sites. This suggests that the lower acidity farther north is not particularly due to neutralization by ammonium or soil constituents; equivalently, the acidity to the south is apparently due to higher levels of strong acids.

One can examine the temporal differences, if any, by examination of sequential samples. I have concentrated on two groups of sites that have complete sequential chemistry, shown in Figure 1. Part of the difference in chemistry between the two groups could result from timing of the rainfall or from temporal variations in rainfall rate between the two groups. Figure 2 shows the average end times of the sequential stages. The timing is similar, with the only difference being that the Group 2 sites show a decrease in rate earlier than Group 1 (and thus have one less sequential stage). Also note the near constancy of the rainfall rate (stages are approximately equal volumes, so the slope is inverse rate) except near the end of the event for Group 2.

Figure 3 shows means and plus-and-minus one standard deviations for the two groups. The variance for Stage 3 would be much less if one outlier site (8 mm/h) were removed. The intergroup similarity of the temporal rainfall does not appear to be responsible for chemical differences. As a consequence, comparison of the groups' chemistry is simplified, as one can ignore timing and use stage number.

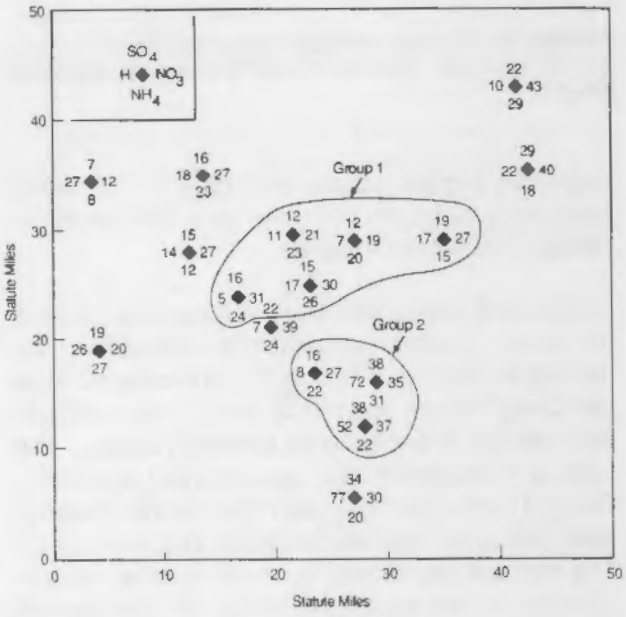

FIGURE 1. Event-Composite Chemistry Data and Groups Selected for Comparison; Concentrations in μm.

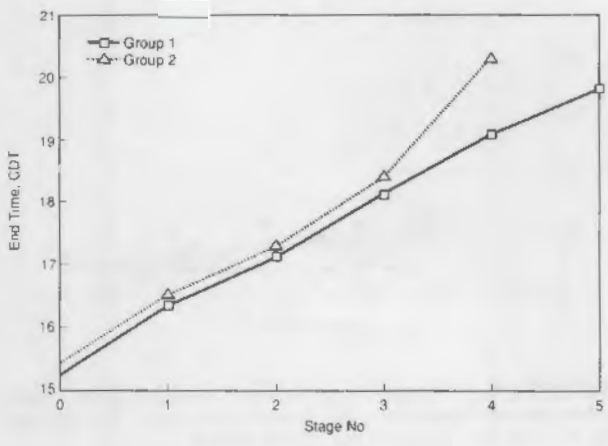

FIGURE 2. Average Sequential Stage End Times.

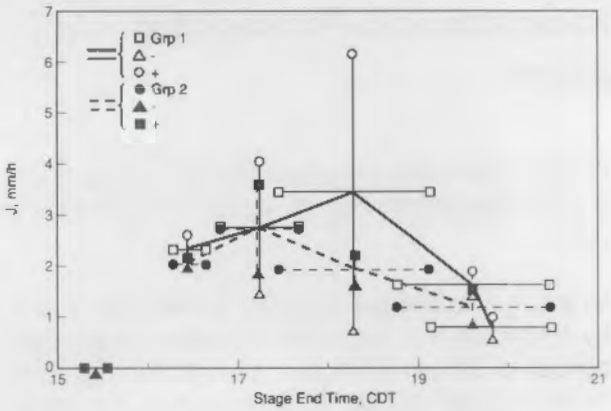

FIGURE 3. Average Stage Rainfall Rates. Bars represent plus-and-minus one standard deviation. Data points on the ordinate represent the start of rainfall.

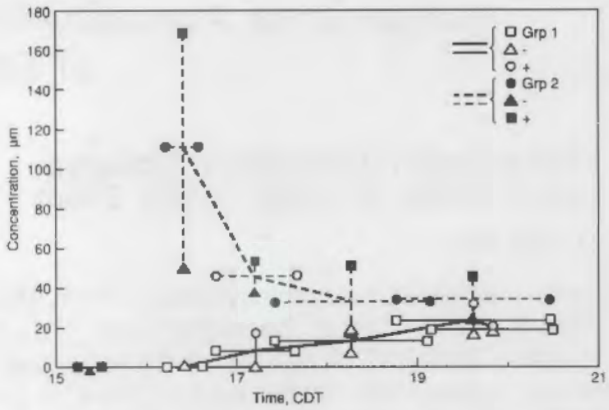

FIGURE 5. Average Stage Hydrogen Concentrations. Bars represent plus-and-minus one standard deviation. Data points on the ordinate represent the start of rainfall.

An overall group comparison (e.g., using "group averages") for chemistry is also only valid if the variance within groups is acceptably small. Figures 4 and 5 show means and plus-and-minus one standard deviations for sulfate and hydrogen concentrations. The intragroup variances are quite small, especially for Group 1. Clearly, the rainfall in Group 2 is more acidic; this is mainly due to increased sulfate and nitrate, especially early in the event.

Figure 6 shows group averages by stage. Sulfate, nitrate, and hydrogen are clearly higher for Group 2, especially in Stage 1. Ammonium and calcium do not vary as much between groups. The

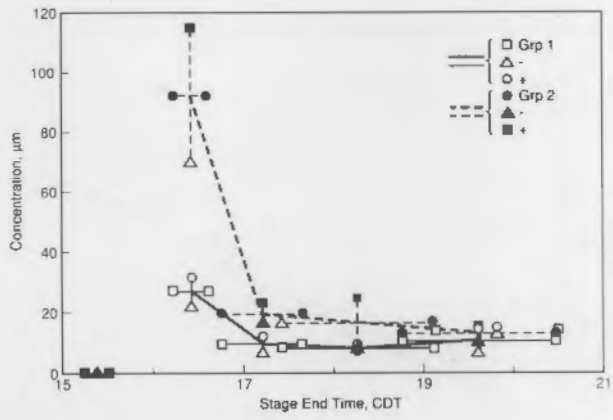

FIGURE 4. Average Stage Sulfate Concentrations. Bars represent plus-and-minus one standard deviation. Data points on the ordinate represent the start of rainfall.

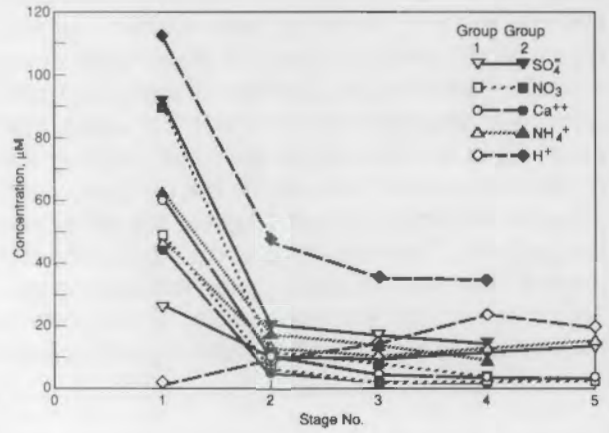

FIGURE 6. Simple Average Concentrations of Sulfate, Nitrate, Hydrogen, Ammonium, and Calcium by Sequential Stage.

expected higher values in Stage 1 for these (especially calcium) correlate with low acidity in Group 1 but not in Group 2.

These data, along with observations made during the event, present two possible explanations for the higher acidity in Group 2: 1) increased local sources of sulfate and nitrate and 2) more efficient precipitation scavenging by convective cells. The surface winds in the area (as observed at a site in Group 1) were northerly, and there were no significant pollutant sources between the two areas. The nearest significant sources were a refinery complex in the southeast corner of the network,

the town of Decatur in the southwest corner of the network, and possibly Champaign-Urbana (east-central). None of these are located in a position to affect Group 2 preferentially. Lightning was observed in the area of Group 2 sites, indicating convective cells in the area that were not seen within Group 1. However, the rainfall rate in Group 2 was not higher as one would expect from an imbedded convective cell or rain band. It is possible that the higher rainfall rate in the central area of a convective cell or cells missed the sampling sites.

Further evaluation of these possibilities (and perhaps introduction of others) may be possible through analysis of the records from the CHILL Doppler and profiler radars. Useful data sets from these and other sources in 3CPO may allow for model simulations that can further explain the spatial chemistry variations.

Reference

Dana, M. Terry, S. D. Tomich, G. W. Dennis, and D. W. Glover. 1989. "Initial Precipitation Chemistry Results from the PRECP-VI June 8 Rain Event." In *Pacific Northwest Laboratory Annual Report for 1988 to the DOE Office of Energy Research, Part 3 Atmospheric Sciences.* PNL-6800 Pt. 3, Pacific Northwest Laboratory, Richland, Washington.

The Concentration and Distribution of Atmospheric Peroxides Over the Pacific Ocean During the Pacific Stratus Investigation (PSI)

R. N. Lee and K. M. Busness

The Pacific Stratus Investigation (PSI), conducted during the late spring of 1989, represented an initial attempt to examine the relationship between natural marine emissions to the atmosphere and cloud albedo and climate. This study took place off the coast of Washington State with atmospheric sampling operations performed using a research vessel (USS McArthur), aircraft (PNL's Gulfstream-1[a] and the University of Washington's Convair C-131),[b] and shore-based measurement systems at Cheeka Peak. The G-1 flew sampling missions in support of this study to complement measurements made by other participating organizations. Organizations contributing to the PSI field program are identified in Table 1.

Aircraft missions, flown along the east-west corridor defining the research vessel track, consisted of soundings from about 100 m up to 5000 m MSL. Sample collection and trace gas measurement were also performed within stratiform clouds. A map of the PSI study area is presented in Figure 1. The map includes aircraft positions corresponding to the profile data reported in this note, their location relative to the McArthur track, and the coastal sampling station. Measurements were restricted to periods of westerly flow in which continental input to the advected air mass was expected to be minimal. In addition to airborne sampling, the ocean surface was characterized by the research vessel, which performed sampling operations up to 300 km off-shore during the 10-day study period. Aircraft missions included fly-bys near the McArthur and Cheeka Peak to compare overlapping measurement systems.

TABLE 1. Organizations Participating in PSI.

National Oceanic and Atmospheric Administration (NOAA) Pacific Marine Environment Laboratory
University of Washington
Pacific Northwest Laboratory
Naval Post Graduate School
Monterey Bay Aquatic Research Institute
National Aeronautics and Space Administration (NASA) Ames Research Laboratory
University of Arizona
Georgia Institute of Technology
Institute of Atmospheric Physics
Institute of Applied Geophysics

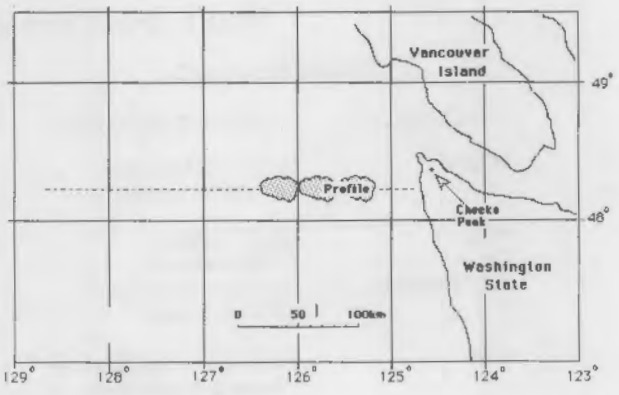

FIGURE 1. PSI Study Area.

(a) Built by Grumman Corporation, Bethpage, New York.
(b) Built by General Dynamics Corporation, Convair Division, San Diego, California.

This note describes initial results from PNL's PSI sampling program. Data acquired during airborne sampling operations represent a unique data set; they provide rare information on concentration profiles of peroxide and other trace gas constituents over the open ocean. The sampling and measurement tasks performed using the G-1 are summarized in Table 2.

While atmospheric peroxide measurements have been made in regions characterized as pristine, most studies have focused on areas impacted by anthropogenic emissions. In this regard, data describing atmospheric profiles are essentially limited to the eastern United States with measurements made by NCAR during the fall of 1984 representing the single most extensive data base. That work, reported by Heikes et al. (1987), included ozone, sulfur dioxide, and peroxide measurements from 500 to about 3000 m MSL. General concentration features observed during that series include the following:

- The vertical concentration structure for H_2O_2 was generally more complex than that of its precursors.
- No correlation was apparent in peroxide and ozone profiles.
- Anticorrelation was observed between SO_2 and peroxide concentrations.
- Peroxide levels were lowest in the mixed layer, increased to a maximum at elevations between 1500 and 2500 m MSL, and decreased, or held nearly constant, up to 3500 m.

In the presence of clouds

- Ambient peroxide concentrations decreased with the magnitude of the decrease related to SO_2 levels.
- Peroxide concentrations frequently displayed a maximum in the region just above cloud tops.

These observations have been generally supported by more recent measurement programs based in the eastern United States, including those conducted by PNL (e.g., 3CPO in the summer of 1988 and the Frontal Boundary Study in the fall of 1989). In contrast to airborne measurements made by PNL during these programs, the PSI series provided an opportunity to examine the distribution of peroxide and other trace gases in a pristine environment.

In addition to trace gas measurement, cloud water chemistry was examined by the collection of bulk samples using a modified impaction collector (Hubert cloud water collector) and a University of Washington-designed Counterflow Virtual Impactor (CVI). The CVI permitted capture of the residual aerosol from evaporated cloud droplets following selective separation from ambient aerosol. Bulk samples were analyzed by ion chromatography (IC) and inductively coupled plasma spectrometry (ICP) for major ionic components. The CVI samples were also analyzed by IC and ICP.

Mercury was collected using a sampling train consisting of a scrubber column, containing gold-coated sand, and a bubbler to collect elemental

TABLE 2. Airborne Measurement and Sampling Systems on the G-1 Aircraft.

In-Flight Measurements		In-Flight Sample Collection	
Parameter	Measurement System	Sample	Sampling Device/ Parameter Measured
NO_2/NO	Luminox LMA-3 with converter system	Cloud water	Hubert cloud water collector/ Cl,NO_3,SO_4=,Na,K
SO_2	TECO Model 43		
O_3	TECO Model 49	Cloud aerosol	Univ. of Wash. CVI, Hi-volume sampler/ Cl,NO_3,SO_4=,Na,K
Total Peroxide	Fluorescence analyzer (NCAR design)		
CCN	TSI Aiken Nucleus Counter (used in conjunction with the CVI)	Elemental Hg and methyl Hg	Adsorption tube and scrubber

and methyl mercury, respectively. Features of this sampling system and subsequent analytical procedures have been described (Bloom and Fitzgerald 1988). In general, trace gas species measured during the PSI flights frequently challenged the detection limits of onboard instrumentation. However, peroxide levels were generally well above the 0.1 ppbv detection limits.

General Flight Plan

Peroxide Profiles

Atmospheric soundings were conducted during each sampling mission. In general these consisted of a slow ascent or descent at approximately 160 m/min interrupted briefly at 600-m intervals to perform instrument zero or calibration checks. Most profiles were conducted in clear air. However, in the presence of extensive cloud coverage, profile measurements included a segment of in-cloud sampling.

Sampling at a Constant Elevation

All instrumentation was up and operating within 30 min of takeoff from the base of operations at Everett, Washington. During transit to the McArthur, sampling was conducted at a single elevation, generally at about 2450 m, well above the top of the marine boundary layer. Data acquired during this period provided information on concentration variability. Once on station, profiles were flown in an area isolated from the C-131 aircraft and the McArthur plume.

Total Peroxide Versus H_2O_2 Concentrations

On most flights, peroxide was measured as total peroxide. However, on the June 8 mission (PSI-6) both channels of the analyzer were operational so as to provide concentration data on H_2O_2 and organic peroxide. Sampling operations conducted during this flight included two soundings as well as in-cloud sampling at approximately 600 m. Concentration profiles for H_2O_2 and organic peroxide are shown in Figure 2 for the period from 2100 to 2115 GMT. During this sounding, both species displayed distinct concentration profiles. As observed throughout the flight, H_2O_2 concentrations were nearly always higher, averaging 75 to 80% of the atmospheric burden. Both H_2O_2 and organic

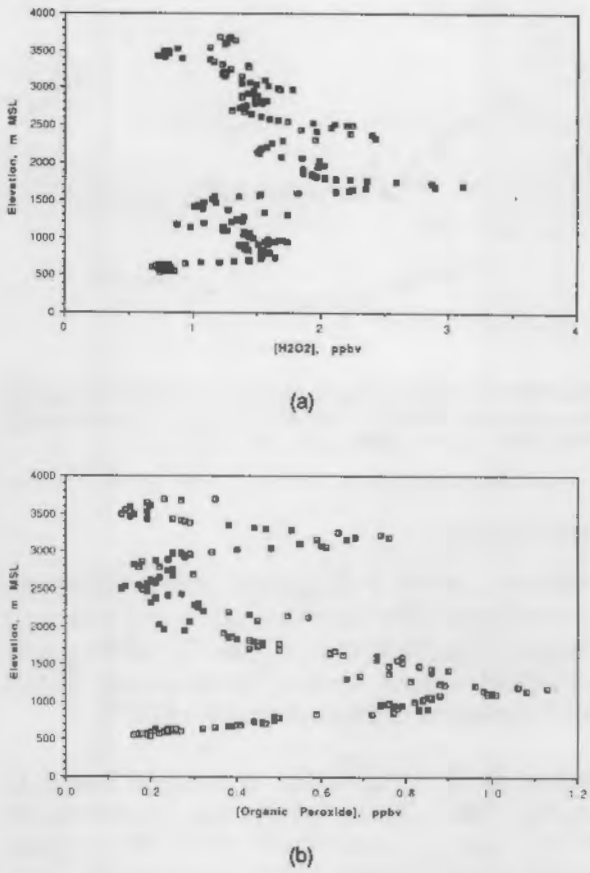

FIGURE 2. 5-Second Average H_2O_2 and Organic Peroxide Concentrations During Sounding from Approximately 550 to 3700 m MSL. June 8, 1989, 2100-2115 GMT. (a) H_2O_2 concentration versus elevation, (b) organic peroxide concentration versus elevation.

peroxide levels rose sharply above cloud tops (~600 m). The organic peroxide concentration peaked at about 1000 m and displayed a secondary maximum at 3100 m. Somewhat less pronounced H_2O_2 peaks were observed at the same elevations while distinct maxima were observed in thin layers centered at about 1600 and 2400 m.

Before the 1400-1415 sounding, sampling was conducted in-cloud at elevations between 500 and 600 m MSL. Five-second average peroxide concentrations are plotted in Figure 3. Also included in this figure are clear air data at cloud height (before 2042 GMT) and an abrupt increase in peroxide levels as the aircraft ascended through the top of the cloud layer at the start of the second profile.

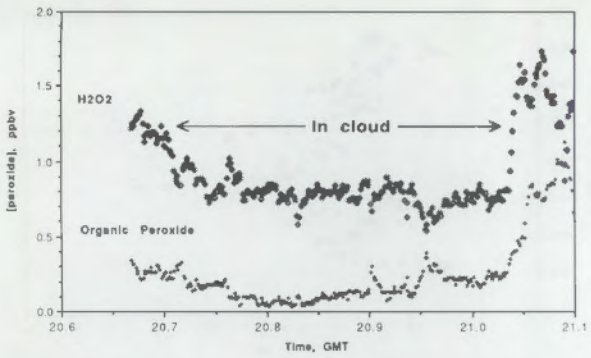

FIGURE 3. 5-Second Average H_2O_2 and Organic Peroxide Concentrations During In-Cloud Sampling at Approximately 550 m MSL. June 8, 1989, 2039-2106 GMT.

References

Bloom, N., and W. F. Fitzgerald. 1988. "Determination of Volatile Mercury Species at the Picogram Level by Low-Temperature Gas Chromatography with Cold-Vapour Atomic Fluorescence Detection." *Analytica Chimica Acta* 208:151-161.

Heikes, B. G., G. L. Kok, J. G. Walega, and A. L. Lazrus. 1987. "H_2O_2, O_3 and SO_2 Measurements in the Lower Troposphere Over the Eastern United States During Fall." *J. Geophys. Res.* 92:915-931.

Overview of the Frontal Boundary Study

K. M. Busness, M. Terry Dana, W. E. Davis, D. W. Glover, R. V. Hannigan, R. N. Lee, D. J. Luecken, J. M. Thorp, and S. D. Tomich

The Frontal Boundary Study (FBS) was conducted in the Columbus, Ohio, area October 5 through November 8, 1989. Participants included PNL, BNL, and ANL. The overall goal was to study transport and precipitation scavenging of atmospheric pollutants near the frontal boundaries of extratropical cyclones. In view of aircraft safety and traffic considerations associated with cold fronts and air mass convective systems, we planned to emphasize the study of warm fronts; however, operational plans for all types of stormy and fair weather were in place. Among the specific objectives of the study were:

- to characterize the pollutant concentrations in air, cloud water, and precipitation in the different air masses associated with a frontal storm, and to compare these to concentrations in surface precipitation
- to determine the nature of the vertical distribution of pollutants in the vicinity of extratropical cyclones with emphasis on the redistribution of pollutants from the boundary layer to the upper troposphere
- to determine the spatial and temporal wet deposition patterns during frontal passage, thereby providing data bases for model evaluation and development.

Measurement systems employed in the study included one aircraft with associated air and water chemistry, meteorological support, and a network of sequential precipitation collectors. Table 1 lists the major instruments and facilities used during FBS. A more detailed description of the G-1 capabilities is given by Busness (1989). Flight plans designed to fulfill the study's objectives were specifically designed with a limited area of operation, namely over the ground network (see below); this allowed for efficient use of aircraft time and effective coordination with Federal Aviation Administration flight control. The basic plan was to make vertical profile measurements at several times during the passage of a front, first to characterize the scavenged air mass, then to evaluate cross-frontal pollutant transport and modification of the profile by frontal dynamics and aqueous-phase chemistry.

TABLE 1. FBS Measurement Capabilities.

Aircraft (PNL Gulfstream-1)	
	Meteorological: temperature, dew point, pressure, wind speed and direction
	Chemical: O_3, NO/NO_x, NO_2/NO, HNO_3, NH_3, PAN, H_2O_2, SO_4, SO_2, CO, Aerosols (major ions)
	Physical: Liquid water content, cloud water collection, cloud droplet aerosols, aerosols (light scattering), UV radiation
Meteorological	
	Standard weather products, AFOS [Columbus National Weather Service (NWS)], Satellite cloud imagery, weather radar (dial-up and Columbus NWS), surface observations, rawinsondes (NWS and PNL system onsite), cloud photography
Network	
	CCARS sequential collectors (major ion chemistry, and selected S-IV and H_2O_2)

The precipitation chemistry network consisted of 40 computer controlled automated rain samplers (CCARS) (Tomich and Dana 1990), located at 36 sites north and northeast of Columbus, as shown in Figure 1. The network size (80 x 80 km) and site spacing (16 km) were designed to provide spatial patterns of precipitation chemistry within a typical acidic-deposition model grid area. Temporal patterns of rainfall and chemistry were defined by collection of sequential samples of approximately 2.5 mm (0.1 in.) rainfall each. Chemical analyses were conducted for the major ionic species for all samples; selected measurements were also made for sulfur-IV (dissolved SO_2) and hydrogen peroxide.

The field study, which concluded immediately before the time of this writing, successfully sampled four major precipitation events. The following is a summary of the events and the measurements obtained. In addition to those listed, rawinsonde flights (approximately every 3 h during the storm period) were flown, near-complete weather radar recordings were obtained, and frequent radar cloud top observations were made.

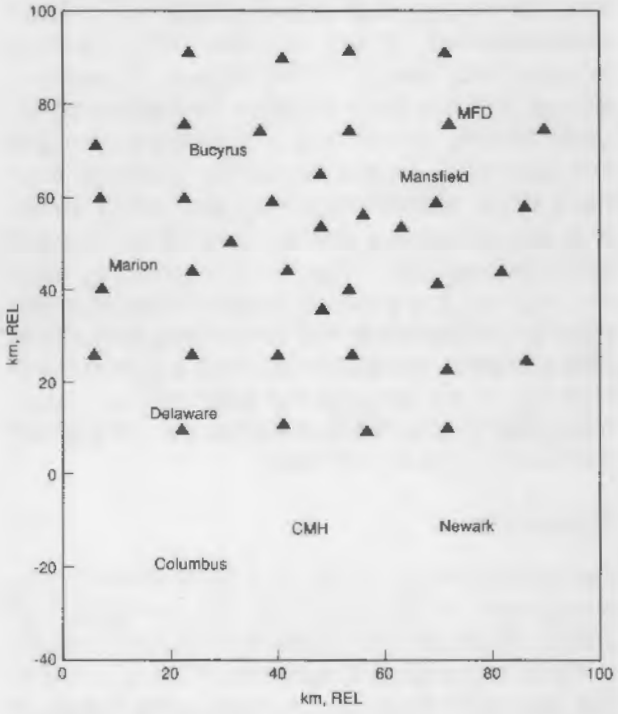

FIGURE 1. The FBS Sequential Sampling Network Area. The Columbus and Mansfield airports are identified by CMH and MFD, respectively.

October 10, 1989

A warm front collapsed before reaching the operational area; sampling was related to warm-sector or pre-cold-front air-mass precipitation. One flight was made over the network 0900 to 1315 GMT: sampling was done at 1000, 1600, and 3300 m (3000, 5000, and 10000 ft) MSL, plus a step-profile from 1000 to 4300 m (3000 to 13000 ft). Sequential samples were collected at 23 sites; precipitation averaged 10 mm from 0800 to 1700 GMT.

October 16-17, 1989

A cold front moving from the north stalled in the center of the network. Prefrontal cells moved along the front, traversing the north half of the network. A separate area of showers covered the south half of the network. Two flights at 1600 to 1904 GMT and 2020 to 2310 GMT on October 16 were made over the network. Both flights included boundary-layer filter measurements, 600 m (2000 ft) increments stair-stepped to 4300 m (13000 ft), and one above-boundary-layer filter. Sequential samples were collected over the entire network; rainfall varied from 0 to 30 mm over the period 0100 to 0500 GMT on October 17.

October 31, 1989

A cold front passed through the network area, but it slowed considerably on approach and became indistinct in the operational area. Two flights, 1250 to 1510 and 1620 to 2010 GMT, were made over the network, but the second was extended west to attempt to penetrate the slowing front. During the first flight, samples were taken at 1000 m (3000 ft) MSL; the vertically integrated filter was used between 1600 and 3300 m (5000 and 10000 ft) MSL. During the second flight, a stepwise profile was obtained between 1000 and 4000 m (3000 and 13000 ft) MSL; the filter was used at 1000 m (3000 ft) MSL; the flight extended to Fort Wayne, Indiana, and the flight returned, sampling at 2000 and 1300 m (6000 and 4000 ft) MSL. Sequential samples were again collected throughout the network; the rainfall was spatially uniform (4 to 6 mm).

November 7, 1989

A warm front aligned east-west across the network slid eastward rather than crossing the network at

sufficient speed to allow more than one flight. Cross-frontal measurements, profiles, and cloud water and filter samples were made during the single flight from 1200 to 1630 GMT. Precipitation was uniform over the network, averaging about 8 mm. The sequential measurements were made at only 12 sites, but some bulk samples were collected at several others, and sulfur-IV and H_2O_2 sequential samples were collected at one site.

Preliminary results indicate that many of the study's objectives were fulfilled: pollutant inflow and detailed spatial and temporal deposition measurements were obtained in all four events, and cross-frontal boundary measurements were made in at least two of the storms. We believe that the FBS measurements will provide unprecedented resources for evaluation of acidic deposition models and will provide valuable information for assessing the effects of frontal storms on the distribution of energy-related air pollutants. Detailed results and analyses will appear in forthcoming reports and open-literature publications.

References

Busness, K. M. 1989. "Development of the G-1 Research Aircraft." In *Pacific Northwest Laboratory Annual Report for 1988 to the Office of Energy Research, Part 3 Atmospheric Sciences.* PNL-6800 Pt. 3, Pacific Northwest Laboratory, Richland, Washington.

Tomich, S. D., and M. Terry Dana. 1990. "Computer Controlled Automated Rain Sampler (CCARS) for Rainfall Measurements and Sequential Sampling." *J. Atmos. Oceanic Technol.* (accepted).

The Effect of Uncertainty in RSM Meteorological Parameters on Predicted Pollutant Wet Deposition

D. J. Luecken and B. C. Scott

Much effort has recently been made to verify that scavenging model predictions are consistent with field measurements. However, predictions of the wet deposition from these models depend heavily on the determination of storm characteristics, i.e., the rainfall rates, the type of rain occurring, and the area over which each type of rain occurs. Model evaluations are difficult if the model does not predict the storm characteristics reasonably well, since pollutant deposition and concentration values depend on the storm characteristics. Unfortunately, meteorological parameters like rainfall rates, type, and areal extent are often expensive and difficult to measure in actual field conditions. Even when the parameters are measured experimentally, a degree of error is associated with each measurement. These errors can be attributed both to the experimental error inherent in the measurement method and to changes in the value over the course of the storm.

This study examines the importance of uncertainties in the meteorological variables used as input to the Regional Acid Deposition Model (RADM) Scavenging Module (RSM). The analysis is accomplished by calculating the cumulative effect that uncertainty occurring simultaneously in five of the most important meteorological input parameters would have on the predicted pollutant rainfall concentration and deposition. The dependence of the magnitude of deposition error on the absolute values and combinations of the meteorological variables is also examined.

This analysis indicates the level of effort needed in future field experiments to measure these parameters and the degree of accuracy important in these measurements. It will also reveal the types of events (and, hence, combinations of variable values) that are more sensitive to meteorological uncertainties. Events with a high rainfall rate and low convective area coverage, for example, may have much different resulting deposition errors than events with low rainfall rate and low convective area coverage. Thus, those events that need the most reliable and concentrated measurement effort will be identified. For scavenging analyses of data already available, we will have a better understanding of the limits of the predicted measurements, for specific types of events, as a function of the meteorological parameters.

Approach

Multiple runs of the RSM, in a stand-alone mode, were used to examine how the deposition of sulfate changed when different combinations of the five meteorological parameters were varied in pre-set increments over a reasonable range of values. The parameters that were varied include:

1. amount of rain from convective activity versus that from stratiform precipitation

2. area of the sky covered by convective rain versus that covered by stratiform
3. total rain rate (which varies with the convective and the stratiform rain rate)
4. height of the tops of convective and the stratiform clouds
5. height of the bases of convective and stratiform clouds.

The chemical input values were held constant for each run so that the deposition differences resulted solely from uncertainties in the meteorological parameters.

The resulting grid of model-predicted depositions was interpolated to a finer-scale grid. The uncertainty range of deposition values was defined by first setting the reasonable uncertainty in each parameter and then identifying the locations of all possible combinations of these uncertainties. For each point in the array, the deposition error was calculated by interrogating all deposition values within this uncertainty range and comparing them with the deposition value (the "exact value") predicted at that point. The largest positive deposition error occurs where the smallest value of deposition within the uncertainty range is found relative to the exact value. Here, the exact value overpredicts the deposition that may actually be occurring considering the uncertainties in the meteorological parameters. Similarly, the highest negative value indicates how much the model may be underpredicting the actual value.

Preliminary Results

The sensitivity studies have been completed for the first four variables, and additional simulations that include uncertainties on the height of the cloud bases are currently being performed. The deposition errors have been analyzed as a function of the fraction of rain from convection, R, and the fractional area covered by convective rain, fc. As expected, the deposition errors increase with the addition of each uncertainty, but the degree to which they increase is highly variable over the array of R and fc values. Some combinations of R and fc, therefore, are highly sensitive to description of cloud-top height, while others are not at all. Uncertainties in R and fc tend to contribute more to the overall error than uncertainties in precipitation rate, J, or cloud top.

Figure 1 shows the largest positive and negative values obtained by simultaneously considering the uncertainties in R, fc, J, and cloud-top height. The deposition uncertainties are given as a percentage of the "exact" value for Case 5, which has an area-averaged rainfall rate of 3.5 mm/h and medium values for cloud-top heights. Overall, including uncertainties in these four variables seems to cause deposition errors averaging ±30%, although there are a few situations where the uncertainties are below ±10% or above ±50%.

The errors tend to be the largest at the edges of the plots, especially where the lowest values of R are involved.

Future Plans

The current analysis will be extended in the near future to cover uncertainties in the cloud base value. The resulting analysis will then be written up and used to help plan future field experiments.

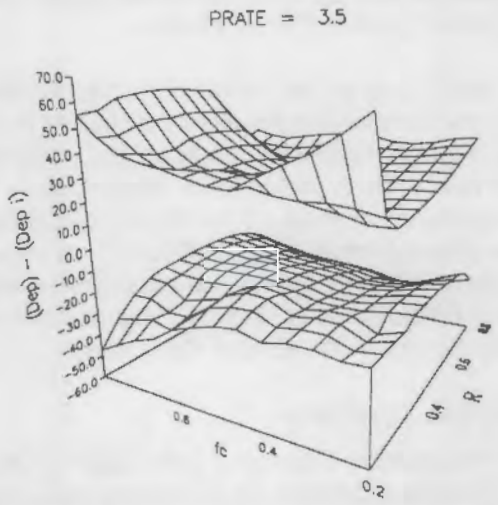

FIGURE 1. Maximum Negative and Positive Differences in Deposition Owing to Meteorological Uncertainties in the Base Case. R is the fraction of rainfall from convection, and fc is the fractional area covered by convection.

The MAP3S Precipitation Chemistry Network in FY 1989

R. N. Lee and W. R. Barchet

The MAP3S Precipitation Chemistry Network completed its thirteenth year of operation (at four of its nine sites) in 1989. This network [see details given by Barchet (1988)] operates in seven states east of the Mississippi River. Network management, site supply, chemical analysis, and data reporting are handled by PNL for the U.S. DOE. Site operation and research are funded separately at each site by the DOE.

Network Operation

Site supply and network management are ongoing operations at PNL. Inventories of site supplies, including sample buckets and bottles, lids, and other field and shipping supplies, are maintained at PNL, and needed supplies are provided to the sites on a regular basis.

Each site collects precipitation samples on a daily (or event) basis. A small portion of the sample is used for field measurement of pH. Another small portion of the sample (20 mL) is treated with tetrachloromercurate to prevent the oxidation of dissolved SO_2. The remaining sample is transferred to plastic bottles for refrigerated storage until the samples are sent to PNL for analysis.

Site audits are a part of network management. Originally, annual site visits were instituted to promote interaction with site operators and ensure the implementation of procedures described in the site operators manual. This objective has been relaxed as a consequence of financial constraints and the operational experience accumulated at the various collection sites. During 1989, an audit was performed at only the Oxford, Ohio, site.

Chemical Analyses

The Precipitation Chemistry Laboratory (PCL) at PNL receives samples on a monthly basis from each site. Chemical analyses and other measurements are made on each sample for pH, conductivity, and ionic concentrations of sulfate, nitrate, chloride, phosphate, ammonium, sodium, calcium, potassium, and magnesium. The methods used for these analyses have been listed in a previous report (Barchet 1988).

Interlaboratory Test-Anions in Wet Deposition

During 1989, the MAP3S PCL was one of nine laboratories participating in the American Society for Testing and Materials (ASTM) D22.06 Round Robin for the Determination of Chloride, Nitrate and Sulfate in Atmospheric Wet Deposition by Chemically Suppressed Ion Chromatography. In accordance with the study protocol, the simulated precipitation samples were analyzed in triplicate with individual samples analyzed on at least two different days. Results of that comparison are reported in Table 1. With the exception of the sample with lowest ion concentrations, representing the lowest ten percentile concentration values of atmospheric precipitation, agreement with reported concentrations is reasonably good. Some outliers are observed at higher concentrations, and there appears to be a slight positive bias associated with nitrate and sulfate measurement.

During 1989, Standard Operating Procedures for equipment preparation and laboratory operations relating to sample handling and analysis procedures have been revised. These procedures are identified in Table 2.

TABLE 1. Results of PCL Analysis of Simulated Precipitation Samples, ASTM D22.06 Round Robin.

Species	Sample	Replicate Analyses, µg/L 1	2	3	Reported Conc., µg/L	Avg. Found/ Reported
Cl^-	1	0.15	0.16	0.19	0.150	1.111
	2	0.26	0.31	0.34	0.300	1.011
	3	0.54	0.58	0.56	0.680	0.824
	4	1.29	1.41	1.32	1.36	0.985
NO_3	1	0.20	0.20	0.20	0.150	1.333
	2	1.13	1.13	1.14	1.08	1.049
	3	2.59	2.60	2.59	2.44	1.063
	4	5.39	5.60	5.41	4.92	1.111
$SO_4^=$	1	0.21	0.20	0.20	0.150	1.356
	2	1.54	1.54	1.52	1.43	1.072
	3	3.55	3.61	3.54	3.23	1.104
	4	7.49	7.60	7.46	6.52	1.153

TABLE 2. Standard Operating Procedures (SOPs) Used by the PCL.

PCL-SOP-1	Sample Receipt and Login
PCL-SOP-2	Field Data Receipt, Filing and Login
PCL-SOP-3	pH and Conductivity
PCL-SOP-4	Anion Analysis
PCL-SOP-5	Automated Wet Chemistry
PCL-SOP-6	Air Filter Treatment/Extraction Procedure
PCL-SOP-7	Cation Analysis
PCL-SOP-8	Alkalinity, Total Acidity, and Gran Titrations
PCL-SOP-9	Analytical Results Login, QC Checks, and Clearance
PCL-SOP-10	Precipitation Chemistry Network (PCN) Data Procedures
PCL-SOP-11	Computer Data Checks
PCL-SOP-12	External QA Clearance, Refiling, and Archival
PCL-SOP-13	Computer Data Reporting
PCL-SOP-14	Equipment Supply for MAP3S/PCN
PCL-SOP-15	Shipping Procedures for MAP3S/PCN
PCL-SOP-16	Preparation of MAP3S/PCN ph Test Samples
PCL-SOP-17	Preparation of MAP3S/PCN Field Blank Samples
PCL-SOP-18	Procedures for Recording Information in the MAP3S/PCN Out Book
PCL-SOP-19	(Reserved)
PCL-SOP-20	(Reserved)
PCL-SOP-21	PreCleaning of Sample Collection and Sample Containers

Data Reporting

Data reporting is an important function of network management. Event data through the end of 1988 reside in the Acid Deposition System data base at PNL and are available for distribution outside of the MAP3S/PNL. Quarterly data reports are regularly distributed to the site operators and principal investigators about 6 months after the end of the quarter. Quarterly data reports through March 1989 have been issued to date. Annual summary reports covering the years through 1987 have been published (e.g., Dana and Barchet 1989). Analytical results are also provided to each site on personal computer disks. These disks are available to others on request.

Summary of Results

Data editing and summarization are carried out at PNL in preparation for calculating annual (as well as seasonal or monthly) precipitation-weighted mean ionic concentrations. Software written to perform these tasks were upgraded during 1989. Data summarization tasks were consequently delayed until 1990.

References

Barchet, W. R. 1988. "The MAP3S Precipitation Chemistry Network in 1987." In *Pacific Northwest Laboratory Annual Report for 1987 to the DOE Office of Energy Research, Part 3, Atmospheric Sciences*, pp. 71-75. PNL-6500 Pt. 3, Pacific Northwest Laboratory, Richland, Washington.

Dana, M. Terry, and W. R. Barchet. 1989. *The MAP3S Precipitation Chemistry Network: Data and Quality Control Summary for 1986 and 1987.* PNL-6885, Pacific Northwest Laboratory, Richland, Washington.

A Test of the RSM Using Data From the Fifth PRECP Field Experiment

W. E. Davis and D. J. Luecken

Only a limited amount of field data has been collected that is useful in testing the wet chemistry portions of scavenging models. In 1987, field measurements were made during the fifth PRECP field study (PRECP-V). The primary purpose of this field study was to study the chemical composition of the air in the vicinity of clouds. However, the field study also produced surface and aircraft measurements during four events that could be used for model testing. In the study reported here, the data sets obtained from four events during PRECP-V were examined to determine if they would be useful for testing the RSM (Berkowitz et al. 1989).

The RSM simulates aerosol and gas scavenging, aqueous-phase oxidation, and wet deposition of sulfur and nitrogen species over an 80 x 80 km grid area. In this study, the area selected for simulation was centered over Columbus, Ohio. Over the grid area, the precipitation is simulated by a mixture of convective and stratiform storms, characterized by the average precipitation, the fractional area of convection, the fraction of rain from convection, and the height of the storm. For a more detailed description of the RSM, see Berkowitz et al. (1989).

Surface Precipitation Data

The surface precipitation data from PRECP-V were available at only five sites shown in Figure 1. The average precipitation over an 80 x 80 km grid cell was difficult to deduce from these limited number of sites. Thus, radar data from Columbus were used to provide the average precipitation for the grid cell and the separation of the precipitation into convective and stratiform components. Radar reflectivity levels are converted to rates of precipitation as shown in Table 1.

Data from four precipitation chemistry sampling sites were available for this study, as shown in Figure 1. In general, the small number of samples available for each simulation (three or four) limits the estimation of the variability of concentrations within the sampling cell to only the range of the observations.

FIGURE 1. Location of PRECP-V Sites.

Aircraft Measurements of Gas and Aerosol Concentrations

The RSM bases its simulation of cloud chemistry and wet deposition on initial concentrations of gases and aerosols at each height in the model domain before cloud formation. The species of aerosol and gases required for input into RSM are listed in Table 2. Three aircraft obtained measurements of gas and aerosol concentrations during PRECP-V; the species measured by each aircraft are also listed in Table 2. The HNO_3 measurements on the DC-3, which measured the boundary-layer air, were found to have high blank concentrations. Since the boundary-layer pollutant

TABLE 2. Chemical Data Input to RSM.

	PRECP-V Measurement Platform		
Species	DC-3 (a)	King Air (b)	Sabreliner (c)
HNO_3(d)	X(e)	X	
NO_3^-(d)	X	X	X
NH_3(a)	X		
H_4^+(d)	X	X	X
SO_2	X	X	X
H_2O_2	X	X	
O_3	X	X	X
$SO_4^=$(d)	X	X	

(a) Operated by PNL.
(b) Operated by NOAA, Boulder, Colorado.
(c) Operated by NCAR.
(d) Filter measurements.
(e) High concentrations on blanks.

TABLE 1. Precipitation Rates for Radar Reflectivity Levels in Stratiform and Convective Storms, Fort Wayne, Indiana.

	Precipitation Rates, mm/h				
	Level 1	Level 2	Level 3	Level 4	Level 5
Stratiform	<2.5	2.5 - 12.7	12.7 - 25.4	(a)	–
Convective	1.27 - 5.1	5.1 - 28.0	28.0 - 56.0	56.0 - 114	114 - 180

(a) No stratiform above Level 3.

concentrations are a vital component for model calculations, these high blanks required the exclusion of HNO_3 and NO_3^- from this study.

Four events were available from PRECP-V for analysis in this study. The dates are shown in Table 3 along with the position of the sampling aircraft relative to the flow of air into the computational cell, i.e., the inflow. On June 12, two of the three aircraft sampled the initial state by measuring the inflow region to the cell. On June 20 and 21, the measurements were less ideal because they were taken downwind from the computational area. However, considerations of other factors make it likely that the measurements taken on these days were representative of the inflow to the cell. On June 25, the DC-3 measurements were to the east of sampling cell and the air flow was from the south. Large point sources of SO_2 and NO_x along the Ohio River may produce strong east-west gradients in pollutant concentrations south of the cell. Therefore, the aircraft measurements on June 25 are potentially unrepresentative of the inflow to the cell.

Results

The RSM was run for the four events, and the modeled results for $SO_4^=$ are shown in Figure 2. For each event, three model runs are made using the minimum, average, and maximum precipitation rates based on the radar echo returns. The average concentrations are plotted for each event along with the range covered by the observed and the modeled concentrations.

For the event of June 12, which had both stratiform and convective components, the modeled concentrations covered a wide range for the three different precipitation rates. The modeled concentrations were higher than the observed concentrations for all three precipitation rates, except in the purely convective component.

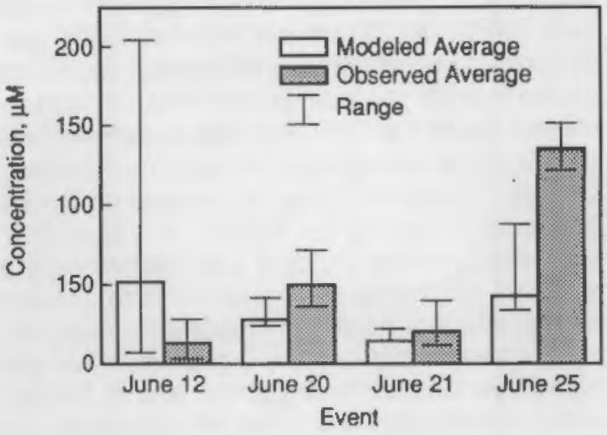

FIGURE 2. Modeled Results for SO_4 Concentrations.

On June 20, only the concentrations predicted using the minimum rainfall rate were within the range of observed concentrations. On June 21, all of the predicted concentrations using the three rainfall rates were within the range of the observed concentrations.

On June 25, the model underestimated the concentrations for all three precipitation rates. The initial gas and aerosol profiles may not be well defined for this case, because of the position of the aircraft during this event.

Conclusions

Three major assumptions are necessary for using the PRECP-V data set to test scavenging models: 1) that the surface precipitation sampling defined the average and range of $SO_4^=$ concentrations over the 80 x 80 km area, 2) that the aircraft sampled the profiles of the aerosols and gases needed as input to the model, and 3) that the precipitation rates calculated from the radar returns represented the average rate of precipitation over the grid cell. By accepting these major

TABLE 3. Aircraft Measurement Positions Relative to Inflow.

Aircraft	June 12	June 20	June 21	June 25
DC-3	inflow	downwind	downwind	out of position
King Air	downwind	downwind	parallel/inflow	
Sabreliner	inflow	downwind	downwind	

assumptions, the model can be run for four events from PRECP-V. Differences between model predictions and observed data will depend somewhat on the validity of these assumptions for the four events. Since the PRECP-V field experiment was not designed specifically for testing scavenging models, it does not have all of the data ideally necessary for testing the models. In this application, we found that the data base did not have a sufficient number of surface samples to account for the natural variability of precipitation rates and $SO_4^=$ concentrations over the grid area. We also found that the positioning of the aircraft for providing initial profiles of pollutant concentrations can cause some degree of uncertainty in the final results. But even with these limitations, the model predictions generally fell within the observed ranges for three of the four events examined.

Scavenging models, such as the RSM, require a large amount of specialized information to rigorously test their predictions against experimental data. The results of this study will be used in the design of future field experiments for collecting the necessary data for testing these models.

Reference

Berkowitz, C. M., R. C. Easter, and B. C. Scott. 1989. "Theory and Results from a Quasi-Steady-State Precipitation-Scavenging Model." *Atmos. Environ.* 23(7):1555-1571.

A Proposed Test of Two Hypotheses Related to Concentration Fluctuations and Residence Times

W.G.N. Slinn

Junge (1974) demonstrated an empirical relationship between concentration fluctuations for trace atmospheric constituents and their atmospheric residence times, T_r. He found that the coefficient of deviation (the standard deviation divided by the mean) was inversely proportional to T_r, with the proportionality constant (0.14 year) the same for all chemicals. Subsequently, a number of authors have searched for a theoretical basis for Junge's relationship (Gibbs and Slinn 1973; Baker et al. 1979; Jaenicke 1982; Hamrud 1983; Slinn 1983; 1988a,b). As stated by Slinn (1988a) [hereinafter Sa]:

> "Hamrud's analysis is particularly illuminating: he emphasizes that Junge's result is more appropriately interpreted, not as a relationship for fluctuations in time at a particular point, but as a measure of the spatial variability of the concentrations. If Hamrud's interpretation is coupled with a part of Jaenicke's concept of finite sampling-time, then the following simple model can be developed."

The resulting simple model has been criticized by Jaenicke (1989), who sees little difference between the model and the one developed by Jaenicke (1982). The response by Slinn (1989) suggests that there are differences and suggests that an experimental test might be able to distinguish between the different hypotheses. The purpose, here, is to describe the proposed test; this brief article has been accepted for publication in *Tellus B*.

Eulerian Versus Lagrangian Times

Figure 1 is used to elucidate measurable differences between the two theories. In Figure 1a, curve 1a(i) shows hypothetical variations of the concentration, C, of some chemical as a function of local (Eulerian) time, t_E. As is well known, there can be many causes of concentration variations; here, to start, assume that the variation is primarily caused by differences in (Lagrangian) travel times between a single source and the detector. Under some conditions (see later), the case of multiple sources can be treated relatively easily, but as mentioned in Sa, there remain a number of restrictions of the theory for the case of a finite area source in a three- (or even two-) dimensional world. Hamrud's numerical calculations give informative examples of these complications and demonstrate that more theoretical studies are needed.

In Figure 1a, curves a(ii), a(iii), etc., plotted only for an Eulerian time interval Δt_E (e.g., the duration of the sampling expedition or sampling campaign), suggest the decomposition of C into contributions from a single source but as a result of these different (Lagrangian) times during which the chemical is assumed to have been in the reservoir. If the detector has a minimum sensitivity or response time, then this decomposition could not proceed

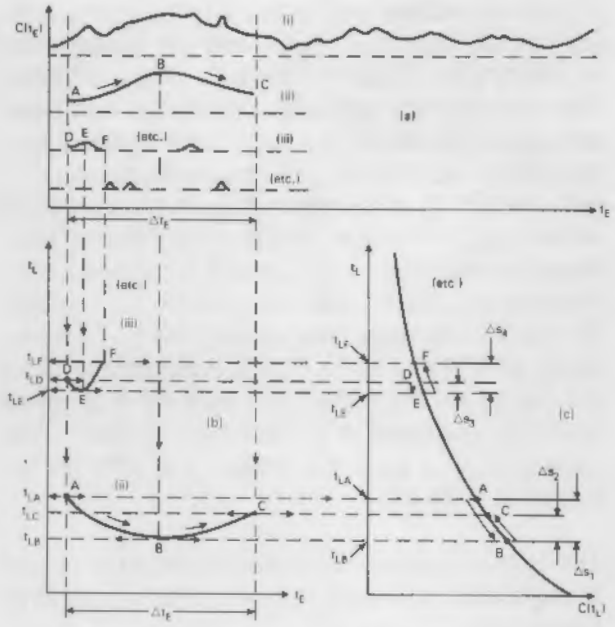

FIGURE 1. Qualitative Sketches of [a] Sampled Concentrations as a Function of (Eulerian) Time, [b] Corresponding Values of Sampled Lagrangian Times, and [c] Corresponding Sampled Concentrations as a Function of Lagrangian Time (with corresponding intervals of Lagrangian time shown at the far right).

indefinitely, but whether or not such limits exist is peripheral to the main point to be demonstrated. Also, no restriction is placed on the duration of the Eulerian sampling interval.

In Figure 1b, curves b(ii) and (iii) suggest distributions in Lagrangian times t_L (during which the chemical resided in the reservoir) for the corresponding curves in Figure 1a. Thus, as illustrations, point A on a(ii) has a corresponding point A on b(ii), point B on a(ii) [with larger concentration than at A] corresponds to point B on b(ii) [larger concentrations corresponding to shorter Lagrangian times], and so on, and similarly for the distributions of Lagrangian times for curve b(iii), etc. By this means, one can hypothetically determine the distribution of Lagrangian times that have been sampled during Δt_E.

The curve in Figure 1c (plotted in a left-handed coordinate system) is the presumed "decay curve" for the concentration as a function of the time during which the chemical has been in the reservoir. The single curve in Figure 1c is for a single source, but the case of multiple sources would seem to proceed similarly. Points A, B, etc. in Figure 1c correspond to those in Figure1b (and Figure 1a), and with them, corresponding Lagrangian time intervals, $t_{LA} - t_{LB} = \Delta s_1$, $t_{LC} - t_{LB} = \Delta s_2$, etc., can be identified. For example, in Figure 1c, A to B corresponds to a time interval when the concentration continued to increase (e.g., because the chemical took a more direct route to the sampler), and then from B to C, continuously longer Lagrangian times are presumed to have been sampled. On the right-most edge of Figure 1c are corresponding ranges of sampled times, Δs_j. In Sa, a "peculiar" coefficient of deviation, F_c (the standard deviation divided by the mean), is calculated by averaging over individual Lagrangian time intervals, Δs_j.

Importantly for what follows, this coefficient of deviation is found in Sa to be independent of the (absolute) Lagrangian time, dependent only on the interval of sampled Lagrangian times, Δs. Specifically, Equation (3b) in Sa, with a typographical error corrected, gives

$$F_c^2 + 1 = \frac{\Delta s}{2T_r} \frac{[1 - \exp\{-2(\Delta s / T_r\}]}{[1 - \exp\{-(\Delta s / T_r\}]^2} \qquad (1)$$

in which T_r is the chemical's residence time. Thus, for example, if a week of Lagrangian times are sampled from B to C in Figure 1c (e.g., at an average "Lagrangian downwind time" of a month), then the calculated F_c would be the same as for a week of Lagrangian times from E to F (e.g., at an average downwind Lagrangian time of a year).

Also important for what follows is that, if the range of sampled times, Δs, is much smaller than the chemical's residence time, then a second-order expansion of Equation (1) for $\Delta s \ll T_r$ gives

$$F_c \rightarrow \frac{1}{\sqrt{12}} \frac{\Delta s}{T_r} \qquad (2)$$

i.e., F_c becomes linearly proportional to $(\Delta s/T_r)$. The result, Equation (2), therefore not only reflects Junge's empirical result, it permits a linear addition of contributions from different sources (superposition), and it suggests that the largest Δs contributes most to F_c. But to suggest that the total F_c can be estimated simply by summing contributions from different records implies that there are no correlations between these records, an assumption that needs investigations, especially for pulsating sinks and sources (e.g., the

biosphere). However, a pulsating source, alone, would make no contribution to this F_c, because when the Lagrangian travel times are identical, the corresponding Δs would be zero (Slinn 1989).

Distributions of Sampled Lagrangian Times

To explain the proposed experimental test of the two theories, it is useful to introduce the concepts shown in Figure 2. To see how Figure 2 might be conceptually constructed, first choose one value for Δt_E (as in Figure 1) and plot a histogram (or probability density function = pdf) describing the distribution of the Δs_j values that were sampled during this one expedition (e.g., a histogram of the Δs_j values shown on the far right-hand side of Figure 1c). Then, what is sketched in Figure 2 (rotated and using a left-handed coordinate system) above the specific Δt_E value is this pdf of sampled Lagrangian times. Note that all of Figure 1 is for one sampling expedition (viz., one Δt_E, say for 10 h) and therefore corresponds to only one pdf on the abscissa of Figure 2 (viz., at Δt_E = 10 h).

It is then assumed that pdfs could be found similarly for all other Δt_E values, and the hypothetical results are sketched in Figure 2. Thus, suppose that a number of sampling expeditions had been conducted (or divide one long data record into a number of subintervals, possibly overlapping), with data record "i" of duration Δt_{Ei} (e.g., a week, a month, etc.). For each, as shown in Figures 1a-c, there is a distribution of sampled Lagrangian time intervals (e.g., from 1 year to 1 year plus a day, from 10 years to 10 years plus a week, etc.). Then the many pdfs sketched in Figure 2 attempt to show the range in Lagrangian intervals Δs that would have been sampled as a function of the duration of each sampling expedition (viz., the pdfs for Δs plotted at each Δt_{Ei}).

The following notes are added to help the reader through other assumed features of this qualitative Figure 2.

- The short-dash line at the top of Figure 2 reflects the suggestion that, for different instruments, there is expected to be a maximum Δs

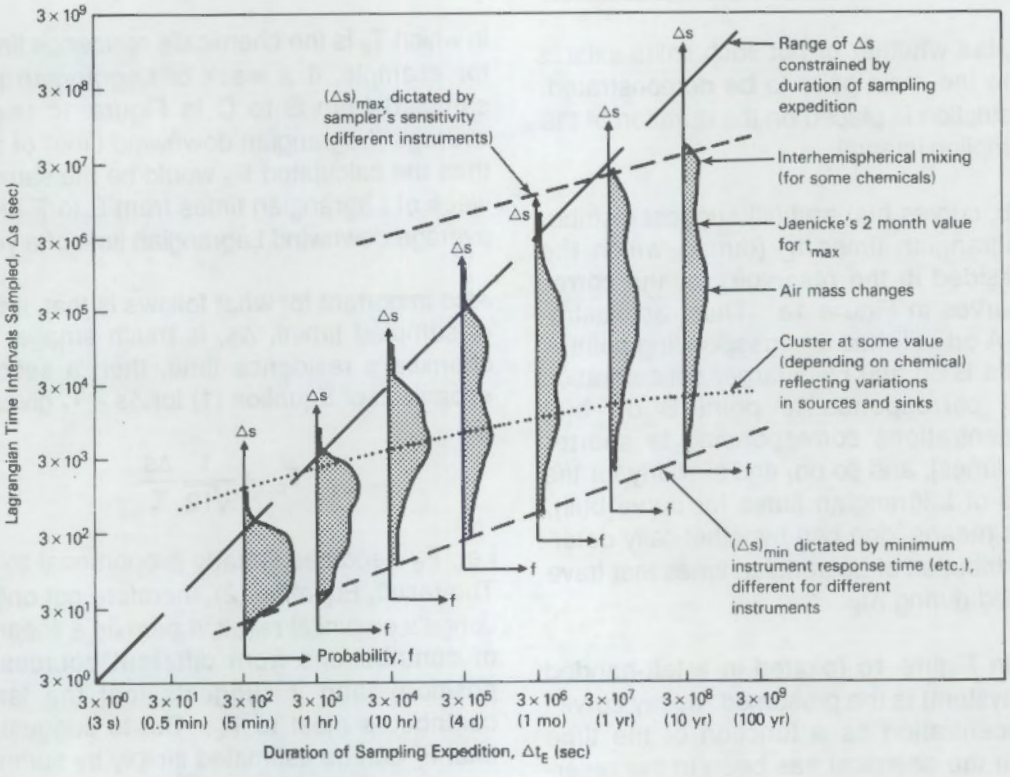

FIGURE 2. Qualitative Sketches of the Distributions of Lagrangian Time Intervals Sampled During Each Measurement Expedition.

that could be sampled because of minimum instrument sensitivity (i.e., for large enough Δs, it is assumed that the signal would be lost in instrument noise).

- The long-dash diagonal line with unit slope, important in what follows, represents an equivalence of the two time intervals, i.e., Lagrangian time intervals equal to the duration of the sampling expedition. It is expected that rarely would one be able to sample *differences* in Lagrangian times larger than the Eulerian time of the expedition (e.g., during a week's expedition, sample differences in Lagrangian times larger than a week, on a single curve of concentration versus Lagrangian time). However, the possibility that $\Delta s > \Delta t_E$ is not inconceivable: transport of the chemical past the sampling station could result in sampling, say during a week, a single "plume" whose differences in Lagrangian times were, say, 2 weeks. But these are expected to be exceptional cases; consequently, the "tails" of the pdfs barely extend past this line defined by $\Delta s = \Delta t_E$.
- The dotted line in Figure 2 schematically suggests that there might be a cluster of sampled Lagrangian times (i.e., a local maximum in each pdf) that reflects some characteristic frequencies for variations in the spatial distributions of either the sources or sinks (or both) for the chemical; this dotted line is curved, since new variations might become apparent as the expedition time increased. Additional clusters in the pdfs are suggested for characteristic times for air mass changes (at times on the order of a week) and for interhemispheric mixing (which might be relevant for some chemicals whose source distributions are not globally uniform).
- Finally, the short-dash line at the bottom of Figure 2 suggests a minimum Δs that could be detected because of limited instrument response time. This line is curved to suggest that different instruments might be used for different Eulerian sampling periods.

Also shown on Figure 2 is the single t_{max} value suggested by Jaenicke and the subject of much of what follows.

Differences in Hypotheses

In contrast to the method in Sa, in which averages were performed over an arbitrary Lagrangian time period, Δs (or, equivalently, over space, as Hamrud perceived), Jaenicke (1982) forms averages of the concentrations from (Eulerian) time zero to a time t_{max}. In his paper he states: "It immediately becomes obvious that a time t_{max} has to be introduced as upper limit of the averaging period." With respect to this t_{max}, Jaenicke (1982) states:

> "We now will try estimating a value of t_{max} for the troposphere. Obviously t_{max} is determined from meteorological parameters and the general mixing of the troposphere and is independent from the individual trace gas species.... The gases with the smallest relative standard deviation... as compared to our model... suggest an apparent t_{max} = 3 month. We tend to assume a t_{max} = 2 month as valid for transport in the troposphere. It remains for future research to [prove] the validity of the above model and the meteorological significance of t_{max} in general and t_{max} = 2 month as a quantity."

In what follows, the goal is to suggest measurements that might be capable of distinguishing between the two models.

Stripped of the theoretical differences between the two models (related to calculations using Lagrangian versus Eulerian times), the practical difference is that Jaenicke has proposed that the constant in Junge's empirical result (0.14 year) has meteorological significance, whereas in Sa, Junge's empirical "constant" is, unfortunately, not a constant, but is found to depend on the Lagrangian times that have been sampled. Thereby, according to Figure 2, it is suggested that Junge's constant depends on a number of variables, including 1) the duration of the sampling expedition, 2) a (complicated) dependence on source and sink distributions, trajectories, etc., and 3) characteristics of the sampling instrument. Of most significance for the present purpose, however, is the suggestion that—especially for short-duration sampling expeditions—the most

important Δs values (at least, those most important for the calculation of F_c, viz., the largest Δs values) will be essentially the (Eulerian) sampling time.

Suggested Test of Hypotheses

Fortunately, some data may already be available that would allow a test of the two hypotheses. To define the suggested test, let δt_E be the time required to obtain a single sample (e.g., 1 s for some instruments, perhaps 1 hr for a filter pack or similar integrator, and possibly longer for other sampling strategies). Choose a number of sampling periods (or "sampling expedition periods" or "averaging periods"), Δt_{Ei} (e.g., a day, week, month, etc.), which can overlap, and calculate the coefficient of deviation F_c for each Δt_{Ei} (i.e., calculate F_c, simply by evaluating the means and standard deviations from each record, for the number of samples $N_i = \Delta t_{Ei}/\delta t_E$). Finally, plot F_c versus Δt_E for the chosen values of the Eulerian averaging periods Δt_{Ei}.

If this were done for gases with fairly long residence times compared to the maximum expedition time Δt_E (e.g., for CH_4, use a maximum Δt_E no longer than a month or so, and for CO_2, no longer than a few months), then it is suggested that the linear result [Equation (2)] would hold, and therefore, it is expected that F_c would increase essentially linearly with Δt_E, especially for small Δt_E. That is, summing over contributions from many Δs_j would primarily give the contribution from the largest Δs, which would be essentially Δt_E, especially for small Δt_E. In contrast, if Jaenicke's model is correct, then it is expected that F_c will be independent of Δt_E.

Although it is readily admitted that the approximations used herein are crude [calculated correctly, the appropriate mean and mean-square values would need to be averaged over the (unknown) distribution of Δs values], it is nevertheless suggested that if experimentalists do find that F_c increases linearly with this $\Delta t_E \approx \Delta s$, especially for small Δt_E, then the initial slope of this line [*lim* $(\Delta t_E \rightarrow 0)$ $\{dF_c/d(\Delta t_E)\}$] should give a better estimate of the residence time than the estimates given by Junge's empirical result or by Jaenicke's model. Specifically, for $\Delta s \ll T_r$, then from Equation (2) the inverse of this slope is predicted to be $\approx\sqrt{12}T_r$.

However, because of the many approximations introduced, not much stock should be put in the constant $\sqrt{12}$. For example, this constant could easily be made a factor of two larger by choosing the representative Δs to be half the value of Δt_E. Also, Hamrud has shown, for example, that variations in the areal distributions of the sources can make large contributions to F_c. Nevertheless, the point emphasized here is that neither Jaenicke's model nor Junge's empirical result predicts any variation of F_c with the duration of the sampling, and if the theory in Sa is valid, it may have value in suggesting how better estimates for T_r can be obtained from F_c measurements by at least eliminating the dependence of F_c on the sampling time. Moreover, it seems that this same technique would apply for chemicals in other reservoirs, e.g., various hydrocarbons in lakes and various carbon compounds in the ocean.

References

Baker, M. B., H. Harrison, J. Vinelli, and K. B. Erickson. 1979. "Simple Stochastic Model for the Sources and Sinks of Two Aerosol Types." *Tellus* 31:39-51.

Gibbs, A. G., and W.G.N. Slinn. 1973. "Fluctuations in Trace Gas Concentrations in the Troposphere." *J. Geophys. Res.* 78:574-576.

Hamrud, M. 1983. "Residence Time and Spatial Variability for Gases in the Atmosphere." *Tellus* 35B:295-303.

Jaenicke, R. 1982. "Physical Aspects of the Atmospheric Aerosol." In *Chemistry of the Unpolluted and Polluted Troposphere*, H. W. Georgii and W. Jaeschke, eds., pp. 341-373. D. Reidel Publishing Co., Boston, Massachusetts.

Jaenicke, R. 1989. Comments on "A Simple Model for Junge's Relationship Between Concentration Fluctuations and Residence Times for Tropospheric Trace Gases." *Tellus*, 41B:560-561.

Junge, C. E. 1974. "Residence Time and Variability of Tropospheric Gases." *Tellus* 26:477-487.

Slinn, W.G.N. 1983. "Air-to-Sea Transfer of Particles." In *Air-Sea Exchange of Gases and Particles*, P. S. Liss and W.G.N. Slinn, eds., pp. 299-405. D. Reidel Publishing Co., Boston, Massachusetts.

Slinn, W.G.N. 1988a. "A Simple Model for Junge's Relationship Between Concentration Fluctuations and Residence Times for Tropospheric Trace Gases." *Tellus* 40B:229-232.

Slinn, W.G.N. 1988b. "Concentrations Statistics for Dispersive Media." *Tellus* 40B:214-228.

Slinn, W.G.N. 1989. "Response to R. Jaenicke." *Tellus* 41B:562-563.

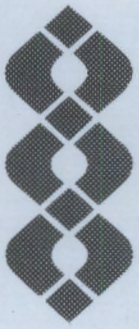

Climate
Change

CLIMATE CHANGE

Climate change research at PNL, like other research efforts aimed at this complex issue, is examining the fundamental controlling processes to reduce serious uncertainties that prevent accurate predictions of climate change and its effects. The program aims to improve data collection and interpretation methods as well as model components and parameterizations so that we may ultimately link observed climate changes to the predictions from the greenhouse hypothesis. Our approach is the development of a scientific information base and tools for analyzing the implications of anthropogenic emissions on the earth's climate. Three areas of research are reported: theoretical examinations, ocean-atmosphere interactions, and source and resource analysis.

Theoretical examinations are seeking explanations for the complicated dependence of climatic data on source and sink distributions and trajectories. The examinations consider not only data, searched for trends that might indicate proof of actual climate change, but also the statistical significance of the data and the validity of the methods used with the data. So far, the theoretical work shows most clearly the complexity of the issues and reveals approaches that must be considered in estimating the extent of climate change.

Ocean research related climate change is examining ocean-atmosphere interaction, ocean circulation and climate modeling, and ocean measurements technology. The program is conducting experimental studies and modeling exchange processes at the air-sea interface for heat, CO_2, and other radiatively active gases. Physical, chemical, and biological processes involved in transfer mechanisms at the sea surface, such as bubble plumes and surface microlayer films, are being studied experimentally. It is recognized that their role in gas transfer must be better understood to reduce uncertainties in predictions of transfer rates. Ocean dynamics that transport and redistribute heat and gases captured at the surface are also not well understood; consequently, parameterizations must be improved to adequately describe the dynamics of the surface mixed layer, transport through the thermocline, and formation of deep water. Improved ocean measurement techniques have been developed, such as a low-cost, ocean profiling system that permits the deployment of arrays of instruments for obtaining seriously needed data, automatically reported through satellites, in planned experiments and for long-term observations in remote areas of the ocean.

The uncertainty regarding sources and emissions of CO_2 and other "greenhouse gases" is under investigation; more complete information on sources and volumes of climate-altering gases is being sought, and development of an advanced global energy emissions model is under way. The goal of the research is to improve the reliability of forecasted emissions of CO_2 and other radiatively active gases. Model development, validation, and uncertainty evaluations depend on improved and expanded data bases, including more definitive information on energy production and consumption practices. The changing technologies and policies of the United States and other countries must be analyzed to anticipate contributions to future emissions of greenhouse gases and their effects on society, particularly on a regional basis.

The regional impacts of CO_2 increases are also being analyzed. Methods are being developed and implemented for analyzing the impacts of climate change and CO_2 increases on natural resources and society at the regional level. Data are being gathered and examined on climatic, environmental, and societal characteristics for a selected region of the United States, and approaches are being developed for predicting the consequences of CO_2/climate change for natural, biological, and human resources.

The progress described in the following articles was supported by the following research tasks:

- **Exploratory Research**
- **Resource Analysis Research.**

Hints of Another Gremlin in the Greenhouse: Anthropogenic Sulfur

W.G.N. Slinn

Changing concentrations of a number of atmospheric chemicals have led to concerns about the possibility of resulting climate changes [e.g., see the reviews by Ramanathan (1988) and by Mitchell (1989)]. Figure 1 illustrates predicted temperature changes if atmospheric CO_2 were increased from 300 to 600 ppm. These predicted changes include 1) stratospheric cooling, 2) tropospheric warming, 3) polar amplification of the tropospheric warming, and 4) approximate north-south symmetry of the temperature changes (with possibly faster response toward new "equilibrium" conditions in the troposphere of the northern hemisphere, because of smaller thermal inertia of land vs. ocean). In this article, these predictions are referred to collectively as the "greenhouse hypothesis."

This article, a summary of a paper accepted for publication in *Atmospheric Environment*, briefly compares the trends of these predictions with data. Emphasis is on discrepancies between predictions of the greenhouse hypothesis and observations. The focus of the submitted paper is the possibility that anthropogenic sulfur has contributed to the observed differences in the changes of surface-level air temperatures for the two hemispheres.

Asymmetric Stratospheric Cooling

Predictions from the greenhouse hypothesis of hemispherically symmetric stratospheric cooling can be compared with the recent asymmetric temperature changes in the lower stratosphere shown in Figure 2. The data suggest 1) little change in 100-50 mb temperatures in the north polar and temperate zones, 2) perhaps a cooling trend in the tropics (the oscillations with period of ~2 years in the equatorial zone are correlated with the quasi-biennial oscillation of equatorial stratospheric winds), and 3) apparent cooling in the south polar zone, possibly related to the destruction of ozone by chlorofluorocarbons (CFCs) (e.g., Tung and Yang 1988).

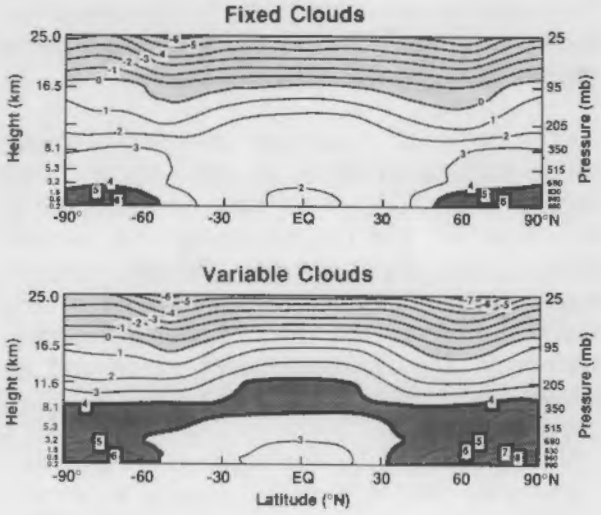

FIGURE 1. Predicted Temperature Changes for Atmospheric CO_2 Doubling from 300 ppm; Figure Sketched from Figure 7 in Wetherald and Manabe (1988).

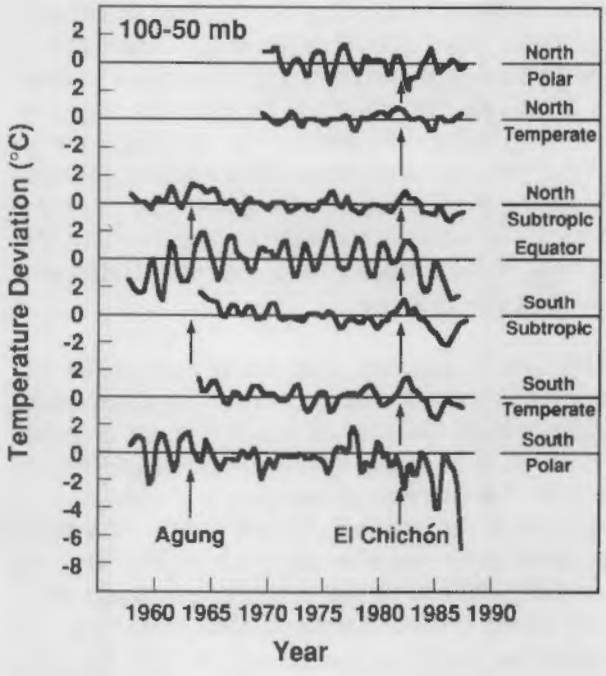

FIGURE 2. Temperature Changes in the Lower Stratosphere As Revealed by Analysis of Radiosonde Data; Sketched from Figure 8 in Angell (1988).

Since the greenhouse gases (CO_2, N_2O, CH_4, CFCs, et al.) have relatively long atmospheric lifetimes, their concentrations should be approximately hemispherically symmetric [or, if anything, the concentrations should be larger in the northern hemisphere (NH), where most of the anthropogenic sources are located]. It therefore would appear difficult to claim support for the greenhouse hypothesis from any of the observed changes in lower stratosphere temperatures; as a minimum, ozone destruction by CFCs has caused difficulties in interpreting these cooling trends in terms of the greenhouse hypothesis. This ozone/CFC complication will be referred herein as the first of several "gremlins in the greenhouse" that appear to frustrate attempts to link observed climate changes to predictions from the greenhouse hypothesis.

Another possible cause of the asymmetric cooling of the lower stratosphere, besides ozone depletion, is asymmetric reduction of heat flux from the troposphere, which in turn could contribute to ozone depletion in the southern hemisphere (SH). It is reasonable that increases in CO_2 and other greenhouse gases could cool the tropical stratosphere (since, by Kirchhoff's law, these gases are both good absorbers and good emitters of longwave radiation and since, in general, the stratosphere is closer to local radiative equilibrium than is the troposphere, with heating via ozone's capture of solar radiation balanced by cooling via greenhouse gases). However, the stratosphere in higher latitudes is not in radiative equilibrium; additional heat is obtained via advection from the tropics and via wave (or eddy or Eliassen-Palm) flux of heat from the troposphere, e.g., associated with extratropical cyclones.

Although it appears that there have been no studies of recent changes in the frequencies of extratropical cyclones in the SH, such changes seem quite possible, given the observed reduction in the number of extratropical cyclones in portions of the NH (e.g., Solow 1989). If a comparable reduction has occurred in the SH, the resulting cooling of the stratosphere could be a root cause of the Antarctic "Ozone Hole;" i.e., the sequence could be 1) decrease in heat flux from the troposphere to the polar stratosphere, 2) increase in polar stratospheric clouds, and 3) decrease in ozone (e.g., Kawahira and Hirooka 1989). Of course, if there has been a decrease in the frequency of high-latitude storms, then there is the question of its cause. One possibility for the NH is a decrease in continental snow cover; another possibility is the observed cooling of the tropical upper troposphere (see the next paragraph). But in turn, causes of changing snow cover or upper tropospheric cooling would require explanations, which at least illustrates the complexity of the climate-change issue.

Tropical Upper Troposphere Cooling

Hints of a second gremlin in the greenhouse can be seen in Figure 3: in contrast with the predictions of warming shown in Figure 1, the data suggest cooling of the tropical upper troposphere. In an attempt to identify the cause of this cooling, consider the heat budget of the tropical upper troposphere: it is dominated by convective heating from the lower troposphere, advection of heat to higher latitudes, and radiative cooling to space. Given the data in Figure 3, suggesting that the lapse rate has increased (thereby suggesting increased convective heating) and that the temperature difference between the upper troposphere of the tropics and the lower troposphere of higher latitudes has decreased (thereby suggesting a decrease in heat flux to higher latitudes), the most likely cause of the observed cooling seems to be increased radiative cooling. In turn, radiative cooling of the upper troposphere appears to be dominated by water vapor (e.g., Stephens and Webster 1981), and it therefore seems reasonable to inquire if there has been a concomitant increase in water vapor in the tropical upper troposphere.

To the author's knowledge, analyses of radiosonde data for changes in water vapor in the tropical upper troposphere have not appeared in the literature, but the possibility that climate models have underestimated changes in upper tropospheric water vapor seems quite large. For example, to obtain the results shown in Figure 1, Wetherald and Manabe (1988) proceeded as follows:

> "At each grid point, cloud is placed in the layer where the relative humidity exceeds a critical value. Otherwise no cloud is forecast. This value for the critical relative humidity (99%) is chosen so that the global integral of total cloud amount is approximately 50%... For the sake of simplicity, it is assumed that all condensed

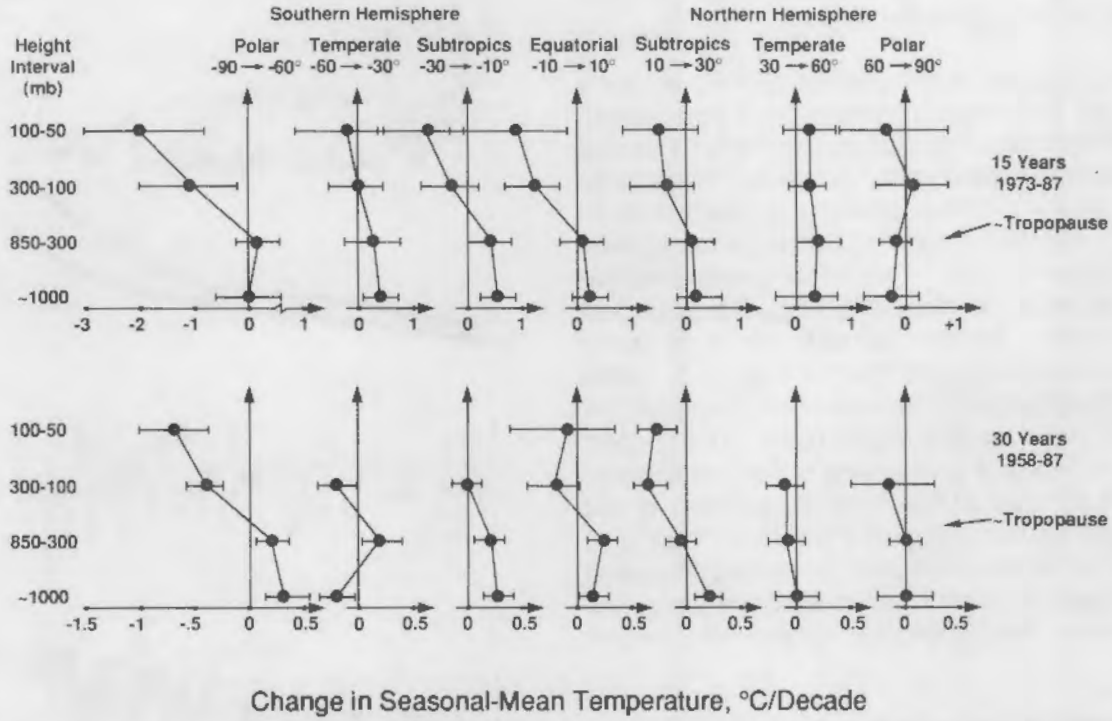

FIGURE 3. In Essence, Changes in Lapse Rates (although notice that the ordinate is for pressure ranges and that the location of the tropopause is only qualitative) As Revealed by Analysis of Radiosonde Data; Drawn by Reading Numbers from Figures 5 and 9 in Angell (1988).

water vapor immediately precipitates out of the model atmosphere despite the fact that cloud cover is placed whenever relative humidity exceeds the critical value."

It is expected that such a scheme would remove far too much water vapor from the model atmosphere.

Polar Amplification and Numerical Errors

Another possible cause of the discrepancy between data and predictions, not only for the case of cooling of the tropical upper troposphere, is numerical errors in climate models: many of the predictions appear to depend on details of the numerical methods. For example, Rind (1988) demonstrates that, when the horizontal resolution of the NASA/Goddard Institute for Space Studies (GISS) model is doubled (from 8° x 10° to 4° x 5° latitude/longitude), the cloud-cover changes in the tropical upper troposphere associated with doubled CO_2 are modified from a 2% *decrease* in cloud cover for the coarser grid to a ~12% *decrease* for the finer grid—and note that neither of these predictions is consistent with the cloud-cover *increase* predicted by Wetherald and Manabe (1988) using the NOAA/Geophysical Fluid Dynamics Laboratory (GFDL) model. As another example, Williamson (1988) demonstrates that when the finite differencing schemes used in the Australian (ANMRC) and European (ECMWF) models are used in the NCAR climate model, the predicted temperatures of the tropical upper troposphere differ by ~10°C when 9 vertical levels are used and by 24°C when 37 levels are used. Williamson writes "It is very disturbing to have the simulation depend so highly on the discrete approximations." As a final example, working with the Canadian Climate Center Model, Boer and Lazare (1988) conclude "The differences in the climates simulated with different model resolutions rival or exceed in magnitude those produced in strong external forcing experiments [e.g., doubling CO_2]." To summarize, it may be that the most troublesome "gremlin in the greenhouse" is the numerics: it is one concern that the physics is inadequately portrayed in the models; it is quite another (and perhaps more serious) concern that

the predictions appear to depend more strongly on the numerics than the physics.

Figure 3 also gives little support for the predictions from the greenhouse hypothesis of polar amplification of lower tropospheric warming. Possible causes of this discrepancy include numerical problems, poorly modeled clouds (e.g., Mitchell et al. 1989), and the unmodeled cooling of the tropical upper troposphere. This cooling would reduce heat advected to the poles (e.g., Nakamur and Oort 1988). Another possible cause of recent surface-level cooling in the Antarctic (e.g., Jones 1988) is subsidence from the cooler stratosphere, and of Arctic cooling, Arctic Haze. The suggestions in Figure 3 of warming of the lower troposphere and lack of hemispheric symmetry of this warming are the emphasis of the submitted paper, but rather than investigate this asymmetry using the relatively short-term radiosonde data, the analysis in the paper uses longer-term surface data.

Changes in Surface-Air Temperature

The top five curves in Figure 4 are used in an attempt to understand the trends of surface-air temperatures for the two hemispheres (the curves at the bottom of Figure 4). The top two (almost coincident) curves in Figure 4, near y = 5, show estimates of the relative influences on direct solar radiation (and, it is assumed, show estimates of proportional reduction in total radiation) from volcanic eruptions in the two hemispheres. Unfortunately, these estimates, based on estimates and radiation data in Lamb (1970) and on more recent data from Mauna Loa and Tucson, Arizona (Sellers and Liu 1988), must be considered as only qualitative.

In Figure 4, the estimate of S emissions (upper curve near y = 4) is from Möller (1984), and the estimate of the influence of greenhouse gases on temperature (lower curve near y = 4) is from Hansen et al. (1988). This greenhouse gas (GHG) curve is not strictly proportional to S emissions for a number of reasons: 1) there have been controls for S emissions but not for GHGs, 2) tropospheric warming is predicted to increase only with the logarithm of the increase in CO_2 concentrations (since the effect of the CO_2 absorption bands is almost saturated), and 3) the recent steep increase in the GHG curve reflects attempts by Hansen et al. to account for recent increases in concentrations of greenhouse gases other than CO_2.

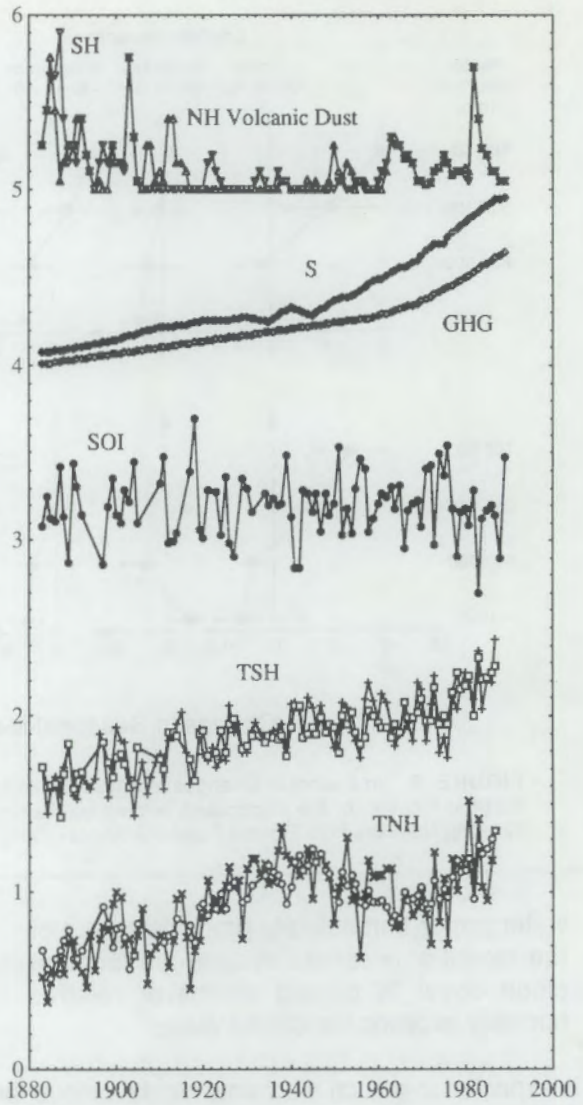

FIGURE 4. Trends in Temperatures of the Southern and Northern Hemispheres and in Other Variables During the Most Recent Century. See text for data sources. Curve identifications: △, NH volcanic dust; ▽, SH volcanic dust; ◆, S; ◇, GHG; ●, SOI; +, TSH; □, regression fit to TSH; x, TNH; ○ regression fit to TNH.

The curve in Figure 4 near y = 3 gives an estimate of the Tahiti-Darwin Southern Oscillation Index (SOI). There are gaps in this record. This SOI curve undoubtedly contains inaccuracies, since it was drawn only from a figure in Ropelewski and Jones (1987). However, these inaccuracies and the inadequacies associated with the choice of an annual SOI (vs. seasonal or summer to spring or summer only) seem to have little influence on the analysis that follows.

The bottom two sets of curves in Figure 4 show the temperature of the southern hemisphere (TSH, near y = 2, symbol +) and northern hemisphere (TNH, near y = 1, symbol x), along with associated stepwise linear regression "fits" to TSH and TNH using as "independent" variables the top curves in Figure 4 (volcanic dust for the respective hemispheres, GHG, S, and SOI). Details of the regression analysis are given in the submitted paper. The temperature data are from Jones et al. (1986a,b) and Jones (1988); the SH data are for land stations only and only in 2.5°- 62.5°S (~27% coverage of the SH); the NH data also include data from weather ships (~58% coverage of the NH).

The TSH seems to be fairly well represented by the regression shown in Figure 4. The *cumulative* percentages of the variance of TSH, "explained" by the indicated functions, and the signs with which they enter the regression equation are: GHG, 55.7%, positive (i.e., heating); SOI, 68.6%, negative (i.e., El Niño heating/La Niña cooling, as expected); SH volcanic dust, 73.0%, negative (i.e., cooling); and a negligible contribution from sulfur. These results are consistent with the expected physics, including the concept that anthropogenic sulfur probably has little influence on the SH.

In contrast with the case for the SH, sulfur does seem to be important for the fit to the NH temperature data. The cumulative contributions to the variances for the terms in the fit to TNH (curve near y = 1 in Figure 4) and the signs with which they enter the regression equation are: GHG, 30.7%, +; sulfur, 51.0%, –; SOI, 54.7%, –; NH volcanic dust, 59%, –. These results, too, are as expected from the physics, but notice that the fit for TNH is not nearly so satisfying (cumulative variance for the four variables = 59.0%) as for TSH (cumulative variances from the same four functions = 73.0%), and it is appropriate to recall the caveat: "correlation does not mean causation!"

Specific problems with the regression fit to TNH seen in Figure 4 include the following: 1) Circa 1940, TNH behaved oppositely from the behavior expected from the SOI (cold period/La Niña in the late 1930s; warm period/El Niño in the early 1940s). 2) The regression is unable to account for the warm period in the early 1960s (possibly then cooled by the eruption of Agung in 1963). 3) Similarly, the regression is unable to account for the warmth of 1981. Unfortunately, these inadequacies in the regression (especially from the behavior near 1940) then propagate within the analysis for the entire period, suggesting both the limitations of the method and the likelihood that important variables/functions are missing, such as a measure of the North Atlantic Oscillation (e.g., see Carleton 1988) and/or the depth of the semi-permanent lows in the NH (e.g., see Niebauer 1988).

Most of the remainder of the submitted paper emphasizes inadequacies and uncertainties associated with these regression fits and explores possible causes (other than S) of the cooling of the NH relative to the SH, but because of space constraints here, these "negatives" will be omitted. Instead, "accentuating the positives," we note the following:

- First, there is the dominant feature that the regression technique uses the variations in volcanic activity and the steady increase of the greenhouse gases to fit the major trend of TSH, and for TNH, the method then adds (or better, subtracts) the sulfur curve to fit the relative cooling trend of the NH since ~1940.

- A second important feature is that the signs with which all terms enter the regression equations are consistent with the expected physics.

- Third, the magnitudes of the terms in the regression equation conform reasonably well to expectations (complete with the expected greater response of the temperature of the NH than the SH, because of greater thermal inertia of the SH). That the magnitudes appear to be reasonable is illustrated in Figure 5, which uses the regression equations to predict TSH and TNH during the next decade for the scenarios listed in the legend.

For these "predictions," the danger of using regression equations outside the ranges of values for the independent variables used in the fits is appreciated, but the forecasts are nevertheless presented, in part to illustrate that the terms conform to the expected physics, and in part to suggest that the appeal of the regression equations will quite likely not evaporate if exposed to only mild criticism. As a final statement supporting the regression equations, it is noted that several

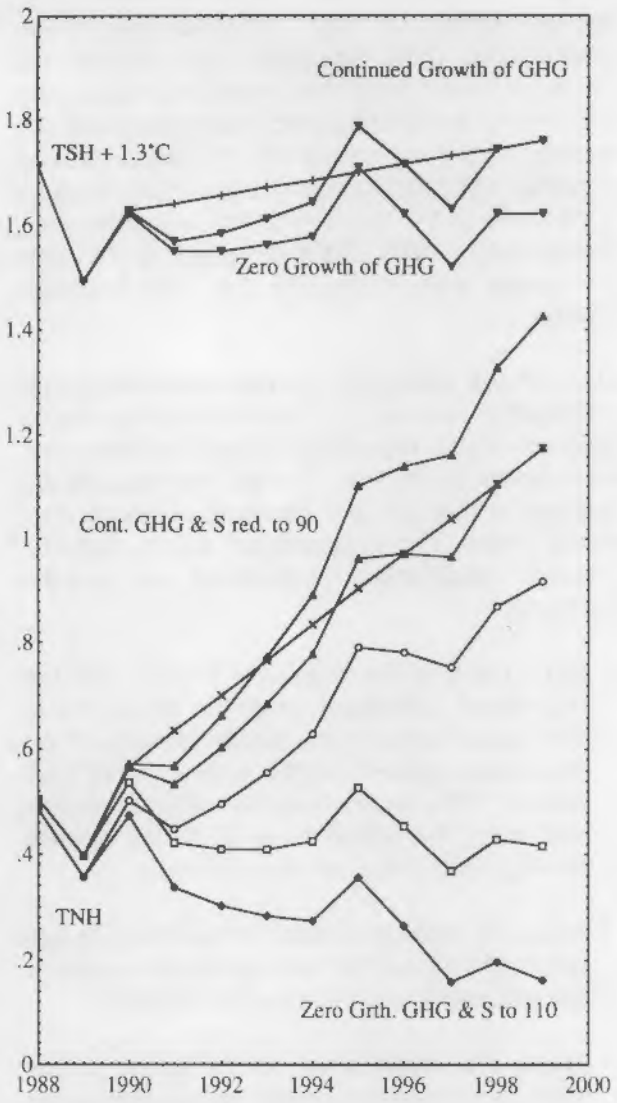

FIGURE 5. Illustrations of the Magnitudes and Signs of the Terms in Equations (1) and (2) for TSH + 1 (three curves at the top) and TNH (curves at bottom) for the Following Cases. Top (TSH + 1): +, (straight line except for the La Niña of 1989) = continued growth of GHG at the rate defined during the 1980s; ▼, continued growth of GHG plus an assumed Agung eruption in 1991, an El Niño in 1995 (SOI = -2) and a La Niña (SOI = +2) in 1997; ▽, same as ▼ except no growth in GHG. Bottom (TNH): x, (straight line except for the La Niña of 1989) = continued 1980s growth of GHG and growth of S emissions to 100 Tg/yr in 2000; ▲, oscillations about x caused by an assumed Agung eruption in 1991, an El Niño in 1995 (SOI = -2), and a La Niña in 1997 (SOI = +2); △, top of the TNH set, same as ▲ but with reduction of S emissions to 90 Tg/yr by 2000; ○, same as ▲ but with S emissions increasing to 110 Tg/yr by 2000 (causing cooling); □, no growth in GHG emissions and S to 100 Tg/yr by 2000; ◇, coolest case, no growth in GHG emissions and emissions of S increased to 110 Tg/yr by 2000.

other ways to develop the equations are outlined in the submitted paper, and all of these [e.g., fitting the temperature difference (TNH-TSH), step-by-step elimination of the variables, fitting longer-term averages of the temperatures, and using a separate data set] generally led to similar results, viz., greater importance of sulfur in the NH than in the SH.

Summary of Tests of Statistical and Physical Significance

For all cases examined, there are concerns about the statistical and physical significance of the results. The second third of the submitted paper addresses some aspects of the statistical significance of the regression equation, and the final third addresses some aspects of their physical significance. In summary, the analyses suggest that the statistics appear to be fairly reliable, but not necessarily the physics. And a pivotal point is that no statistical test appears to be available to test for the significance of missing physics.

To test the statistical significance of the results, an exploration was made of the capability of random sequences and their sums to dislodge the physically significant variables (volcanic dust, S, GHG, SOI) from the regression equations. The results of this exploration gave some confidence in the statistical reliability of the regression equations, since: 1) in no case did a random sequence or its sum "explain" most of the variance, 2) in no case did the introduction of the random or not-so-random sequence (and sums) disrupt the choice of GHG and S for the regression, 3) in no case was there a change in the numerical values for the cumulative contributions to the reduction of variances from S and GHG, and 4) in no case was the sign (with which the variables enter the regression equation) nonphysical. However, changes did occur (for volcanic dust and SOI, for 10- and 30-year averages of the temperatures) when the random sequences were used, suggesting that these terms in the regression (for the long-term average temperatures) are not statistically significant.

With respect to the physical significance of the results, Figure 6 illustrates the concept that, at

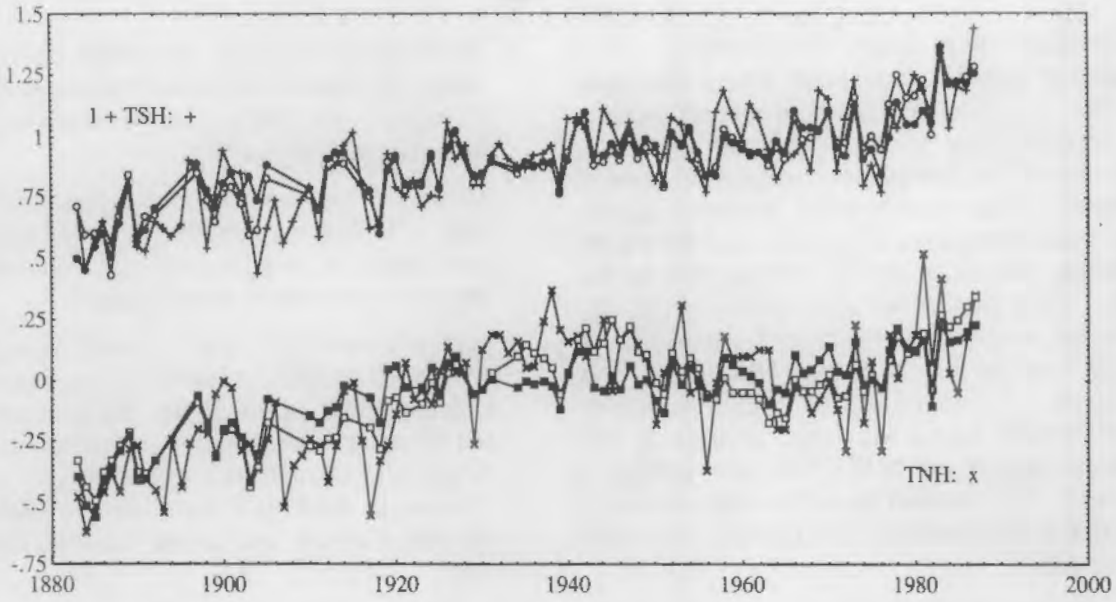

FIGURE 6. Least-Square-Error Regression Fits to Annual Temperatures of the SH (top) and NH (bottom), with x and + Identifying Data, Open Symbols Giving the Regression Using Sulfur and Greenhouse Gases (plus SOI and volcanic dust), and the Solid Symbols Demonstrating a Regression Using Only Natural Variables, i.e., Without Contributions from Sulfur and Greenhouse Gases.

best, statistical fits such as those used herein give only hints of reality. Stated differently, there appears to be no statistical test to evaluate the significance of missing functions/missing physics. Thus, Figure 6 shows the resulting stepwise regression fits to TSH (top curves) and TNH (bottom), both using the four variables as in Figure 4 (volcanic dust, S, GHG, and SOI; open symbols) and (with an almost indistinguishable difference) using only natural variables: volcanic dust, SOI, and running sums (RS) of the dust and SOI; filled symbols. With or without a random sequence and its running sum, the percentage cumulative variances "explained" with these "all natural" regressions are as follows: for the SH, RS SH volcanic dust, 51.7%; SOI, 66.1%; and RS SOI, 68.0%; for the NH, RS NH volcanic dust, 36.4%; NH volcanic dust, 42.1%; and SOI, 48%.

Now, it can easily be argued that this is an artificial exercise: running sums of essentially any variables (be they volcanic dust or random numbers) will provide functions capable of fitting a steady trend in any data. In fact, as shown in the submitted paper, the cumulative variances "explained" using only random variables are quite comparable to those using only natural variables. But on the other hand, it would seem relatively easy to construct arguments, based on physics, to support use of these new variables. For example, the running sum of volcanic dust could reflect the buildup of dust on high-latitude snow and ice (and corresponding reduction in surface albedo). The resulting warming would be consistent with otherwise perplexing data that show a heat pulse in Alaskan permafrost (Lachenbruch and Marshall 1986, Michaels et al. 1988), which appears to have occurred shortly after the eruption of Katmai in Alaska in 1912. Also, this concept of buildup of dust on snow and ice and resulting lowered albedo might explain the dramatic changes in temperature (and dust loadings) at the end of the most recent ice age, approximately 10,000 years ago (Dansgaard et al. 1989). Similarly, the running sum of the SOI could be interpreted as a measure of the net reduction of upwelling of (cold) ocean bottom-water along the east coast of the equatorial Pacific (or equivalently, a net reduction in downwelling of warm water, elsewhere); i.e., part of the observed increase in surface-air temperatures in the SH could be at the expense of minute cooling of the ocean. But it is not the case that these interpretations are being advocated here, only that great caution must be exercised, restraining judgments of the causes of observed climate change.

Consistent with this caution, the wisdom in Fourier's 1827 assessment (as given by

Ramanathan 1988) bears consideration: "The question of global temperatures, one of the most important and most difficult in all natural philosophy, is composed of rather diverse elements, which should be considered under one general viewpoint." Thus, surely great caution is appropriate before advancing explanations of the warming during the most recent century and of the cooling trend in the NH that appeared ~1940, unless the concepts also explain the temperature change that occurred in the NH circa 1815 (cf. Figure 7). And, of course, it is one level of explanation to relate the latter change to the Tambora eruption of 1815 ("the year without a summer"); it is another to explain the warming trend that then seems to have persisted for more than a century.

Conclusions and Recommendations

In this study, three conclusions were reached, and it was found that prejudices could easily influence how two of these conclusions might be stated. The one unequivocal case is the conclusion: *statistics only hint.* Optional ways to state the other two conclusions are given in the following two paragraphs.

One description of the second conclusion is that there are *hints* of "gremlins in the greenhouse." The following is a list of the effects of these gremlins and hints of their identification:

- *Stratospheric cooling*, possibly caused by ozone depletion, but other causes could be changes in dynamics, such as a decrease in heat flux from the troposphere;
- *Cooling of the tropical upper troposphere*, possibly reflecting an increase in water vapor (in turn, poorly modeled in existing climate models because of poorly modeled clouds);
- *Lack of polar amplification of lower tropospheric warming*, possibly caused by cooling of the tropical upper troposphere, subsidence from the Antarctic stratosphere, and pollution in the Arctic, and all quite likely coupled with inadequacies in existing climate models (including numerical errors and poorly modeled clouds); and
- *Lack of approximate hemispheric symmetry in the temperature change of the lower troposphere* (or the warmer SH, rather than the predicted warmer NH), possibly caused by different responses of the two hemispheres to volcanic activity and other meteorological variations, and possibly caused by anthropogenic S emissions.

But from another perspective, this second conclusion could be stated: no data unequivocally support the greenhouse hypothesis.

Similarly, two statements of the third conclusion of this study are readily available. On one hand it can

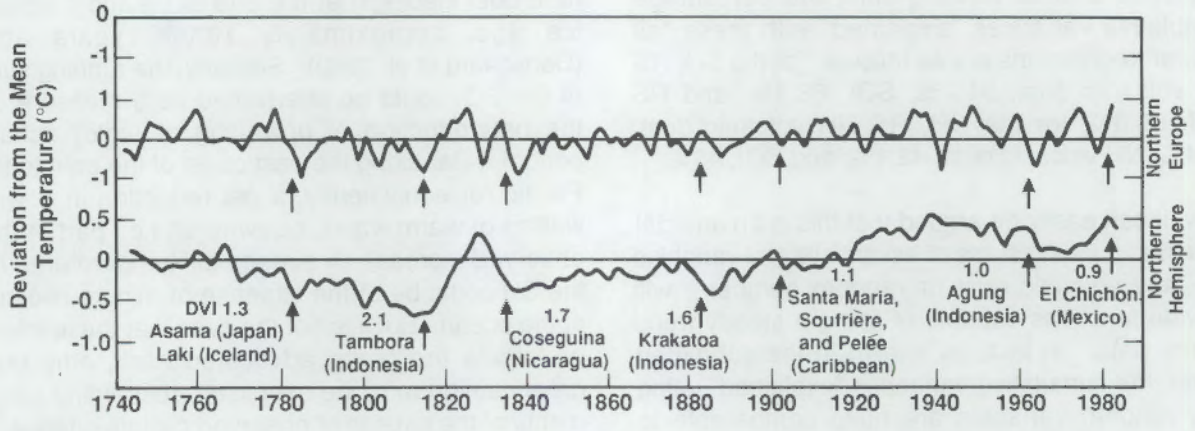

FIGURE 7. Temperatures for Northern Europe and the Northern Hemisphere During the Most Recent ~250 Years; Sketched from a Figure in Angell and Korshover (1985), Where References to the Data Sources Can Be Found.

be said: the concepts that greenhouse gases are warming both hemispheres and that S has retarded this warming in the NH are not inconsistent with the data. On the other hand, the same information (or lack thereof) can be conveyed via: the data are not inconsistent with the concept that all observed changes in the climate are caused entirely by natural processes, such as trends in natural oscillations, volcanic eruptions (and resulting deposition of ash on snow and ice), slight cooling of the ocean, etc. But even though the matter is controversial, the author would seem to be remiss without reporting the *impression* derived from this study that atmospheric chemicals are influencing the climate.

Because of these ambiguities, perhaps the only useful contribution of this study is to provide a vehicle to emphasize the need for additional research. A representative list follows:

- The need for more extensive monitoring and associated data reduction and dissemination is abundantly clear.
- The need for improved climate models is so obvious that it can be summarized by cautioning against placing confidence in any available predictions of climate change.
- From this study, the author is especially sensitive to the need of developing methods for statistical analyses of time series (with more emphasis on signals and less on Gaussian noise).
- Future volcanic eruptions must be defined well (heights of the plumes, ash, sulfur, chlorine contents, etc.), if ever the influence of volcanic eruptions on climate is to become quantitative.
- Radiosonde data should be examined to see if they reveal an increase in water vapor in the tropical upper troposphere.
- There should be continued efforts to try to understand the climatic significance of anthropogenic sulfur (or "Agent X").
- And quite likely of greatest importance is to determine and describe the cause(s) of the climatic changes in the NH that occurred circa 1940 and (if possible) ~1815.

Thus, the only scientifically sound way to define any "anthropogenic signal" in the climate caused by changing atmospheric chemicals (greenhouse gases, sulfur, etc.) seems to be, first, to understand and account for "natural noise." Or, reversing the prejudice in that phrasing: to detect *anthropogenic noise* in the climate, it is advisable first to understand and account for every one of the many significant *natural signals*.

References

Angell, J. K., and J. Korshover. 1985. "Surface Temperature Changes Following the Six Major Volcanic Episodes Between 1780 and 1980." *J. Climate and Appl. Meteor.* 24:937-951.

Angell, J. K. 1988. "Variations and Trends in Tropospheric and Stratospheric Global Temperatures, 1958-87." *J. Climate* 1:1296-1313.

Boer, G. J., and M. Lazare. 1988. "Some Results Concerning the Effect of Horizontal Resolution and Gravity-Wave Drag on Simulated Climate." *J. Climate* 1:789-806.

Carleton, A. M. 1988. "Meridional Transport of Eddy Sensible Heat in Winters Marked By Extremes of the North Atlantic Oscillation, 1948/49-1979/80." *J. Climate* 1:213-223.

Dansgaard, W., J.W.C. White, and J. Johnsen. 1989. "The Abrupt Termination of the Younger Dryas Climate Event." *Nature* 339:532-534.

Hansen, J., I. Fung, A. Lacis, D. Rind, S. Lebedeff, Y. Ruedy, G. Russell, and T. Stone. 1988. "Global Climate Changes as Forecast by Goddard Institute for Space Studies (GISS) 3-Dimensional Model." *J. Geophys. Res.* 93D:9341-9364.

Jones, P. D., S.C.B. Raper, R. S. Bradley, H. F. Diaz, P. M. Kelly, and T.M.L. Wigley. 1986a. "Northern Hemisphere Surface Air Temperature Variations: 1851-1984." *J. Climate and Appl. Meteor.* 25:162-179.

Jones, P. D., S.C.B. Raper, and T.M.L. Wigley. 1986b. "Southern Hemisphere Surface Air Temperature Variations: 1851-1984." *J. Climate and Appl. Meteor.* 25:1213-1230.

Jones, P. D. 1988. "Hemispheric Surface Air Temperature Variations: Recent Trends and an Update to 1987." *J. Climate* 1:654-660.

Kawahira, K., and T. Hirooka. 1989. "Interannual Temperature Changes in the Antarctic Lower Stratosphere -- A Relation to the Ozone Hole." *Geophys. Res. Letters* 16:41-44.

Lachenbruch, A. H., and B. V. Marshall. 1986. Changing Climate: Geothermal Evidence from Permafrost in the Alaskan Arctic." *Science* 234:689-696.

Lamb, H. H. 1970. "Volcanic Dust in the Atmosphere; With a Chronology and Assessment of Its Meteorological Significance." *Phil. Trans. Roy. Soc.*, A. 266:426-533.

Michaels, P. J., D. E. Sappington, and D. E. Stooksbury. 1988. "Anthropogenic Warming in North Alaska?" *J. Climate* 1:942-945.

Mitchell, J.F.B. 1989. "The 'Greenhouse' Effect and Climate Change." *Rev. Geophys.* 27:115-139.

Mitchell, J.F.B., C. A. Senior, and W. J. Ingram. 1989. "CO_2 and Climate: A Missing Feedback?" *Nature* 341:132-134.

Möller, D. 1984. "Estimation of the Global ManMade Sulphur Emission." *Atmospheric Environment* 18:19-27.

Nakamur, N., and A. H. Oort. 1988. "Atmospheric Heat Budgets of the Polar Regions." *J. Geophys. Res.* 93D:9510-9524.

Niebauer, H. J. 1988. "Effects of El Niño-Southern Oscillation and North Pacific Weather Patterns on Interannual Variability in the Subarctic Bering Sea." *J. Geophys. Res.* 93C:5051-5068.

Ramanathan, V. 1988. "The Greenhouse Theory of Climate Change: A Test by an Inadvertent Global Experiment." *Science* 240:293-299.

Rind, D. 1988. "Dependence of Warm and Cold Climate Depiction on Climate Model Resolution." *J. Climate* 1:965-997.

Ropelewski, C. F., and P. D. Jones. 1987. "An Extension of the Tahiti-Darwin Southern Oscillation Index." *Mon. Wea. Rev.* 115:2161-2165.

Sellers, W. D., and W. Liu. 1988. "Temperature Patterns and Trends in the Upper Troposphere and Lower Stratosphere." *J. Climate* 1:573-581.

Solow, A. R. 1989. "Statistical Modeling of Storm Counts." *J. Climate* 2:131-136.

Stephens, G. L., and P. J. Webster. 1981. Clouds and Climate: Sensitivity of Simple Systems." *J. Atmos. Sci.* 38:235-247.

Tung, K. K., and H. Yang. 1988. "Dynamical Component of Seasonal and Year-to-Year Changes in Antarctic and Global Ozone." *J. Geophys. Res.* 93D:12537-12559.

Wetherald, R. T., and S. Manabe. 1988. "Cloud Feedback Processes in a General Circulation Model." *J. Atmos. Sci.* 45:1397-1415.

Williamson, D. L. 1988. "The Effect of Vertical Finite Difference Approximations on Simulations with the NCAR Community Climate Model." *J. Climate* 1:40-58.

A Preliminary Analysis of Deep Convection in an Ocean General Circulation Model

E. D. Skyllingstad

The objective of this research is to assess the negative impact of simple convective overturning algorithms currently used in ocean general circulation models (OGCM). Based on this research, the need for improved parameterizations of deep convection can be determined. The results provide a benchmark for examining new convective algorithms derived from studies of observed and modeled deep convection.

Data Source

Data for this project were obtained from the Community Modeling Effort (CME), which is a part of the World Ocean Circulation Experiment (WOCE). The model data set consists of temperature, salinity, currents, vertical motion, convective activity flag, and tracer age for every 3-day period for 5 years. The model domain covers the North Atlantic from 15°S to 65°N with a grid resolution of 1/3° in latitude and 2/5° in longitude. In the vertical,

the model extends up to 30 levels deep with the grid increment ranging from 35 m at the surface to 250 m below 1000-m depth. In the present work, a subset of the original data is used encompassing the entire Labrador Sea from 50°N to the northern boundary and 37.5°W to the western boundary.

Preliminary Analysis - Flow Structure and Convective Activity

The CME data provide a detailed model simulation of the Labrador Sea region. However, the fine resolution of the data also creates a data accessibility problem. For this reason, preliminary analysis has focused on a limited horizontal section of the model results, with emphasis on variables connected to convective overturning. Of particular interest are the variables referred to as the tracer age and the convective activity flag. The tracer age represents the time since a given parcel of water was in contact with the surface, and the convective activity flag indicates if overturning occurred during the most recent 3-day output period. The tracer age variable is treated as a scalar quantity with both diffusion and convective overturning changing the age value. Both parameters, along with temperature, provide a measure of the convective activity within the model.

It is known from observations that convection in the Labrador Sea extends from about 300 m to 1500 m in depth each winter, depending on atmospheric conditions (Lazier 1980; Gascard and Clarke 1983). By plotting cross sections of the tracer age from the CME data (Figure 1), we can determine a characteristic annual mixed depth for the model. In general, the model mixing is concentrated near the north-central portion of the Labrador Sea. Overall mixing is confined to the topmost 1000 m. With this in mind, we selected a representative level of 577 m for examining the areal extent of modeled Labrador Sea convection.

Model results for this depth are shown in Figures 2 and 3 representing plots of temperature, convective activity, and currents for a given 3-day period during summer, winter, and spring. A number of general characteristics are shown in these figures. First, the flow structure of the Labrador Sea is dominated by a cross current extending from the southern tip of Greenland to the coast of Labrador. Although observations are limited in this region, existing current meter data do not support this important modeled feature

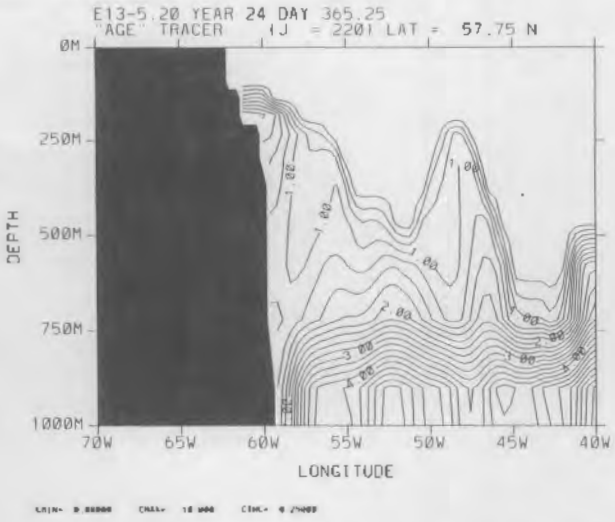

FIGURE 1. Cross-Section of Labrador Sea at 57.75°N Showing the "Age" of a Tracer from the CME Data Set. The age is set to zero at the sea surface.

(Provost and Salmon 1986). The modeled current could be an artifact of the imposed northern boundary conditions at 65°N or a result of the imposed surface fluxes and preferential areas of convection (discussed below).

Mixing at 577 m in the model, as indicated by the convective activity flag, is maximized during the late winter (Figure 3) and covers nearly all of the central region of the Labrador Sea. The mixing occurs late in the season because of the lag between the maximum cooling and the time for convective mixing to reach the reference depth of 577 m. In the summer (Figure 2), mixing has generally ceased; however, the effects of entrained momentum are noticeable with current speeds increased throughout the central gyre. The temperature structure varies with the convective activity, showing a minimum of about 3°C over a large region in winter and over a much smaller area in the fall. Also, a more active Gulf Stream during the summer and fall leads to significant eddy production and westward warm water transport from the eastern boundary.

With active convection, a mixed layer is formed with a temperature structure that tends toward the forced, surface values. Mixing is confined to the center of the Labrador Sea leading to a deep baroclinic zone extending westward along the 59° latitude line, coincident with the Labrador Sea cross current. A lack of mixing in the northern end

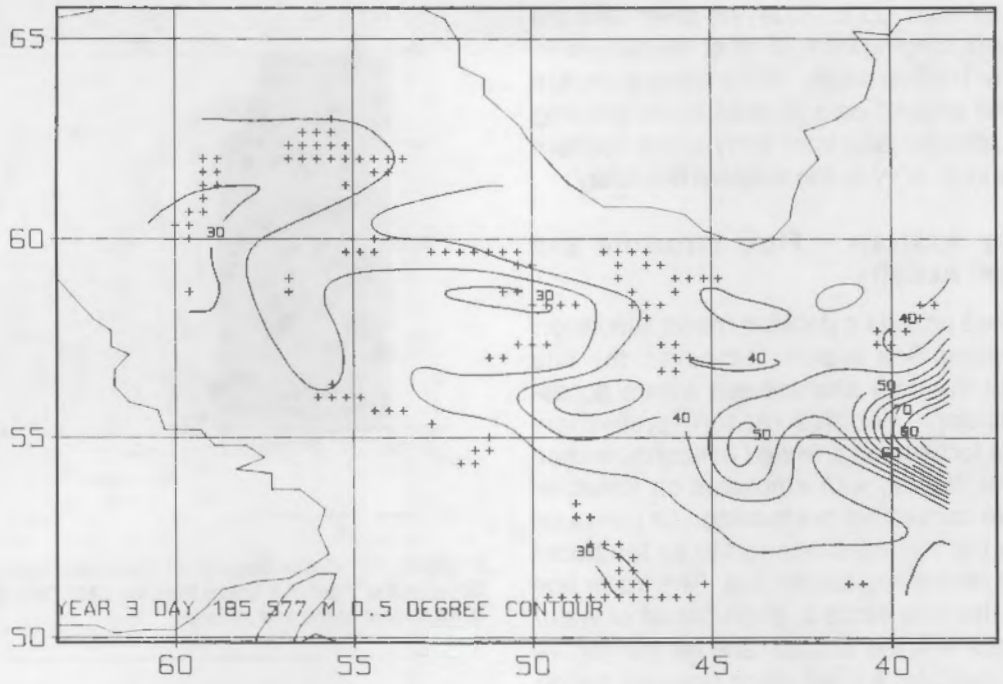

FIGURE 2a. Convective Activity (+) and Temperature from CME Data During Summer.

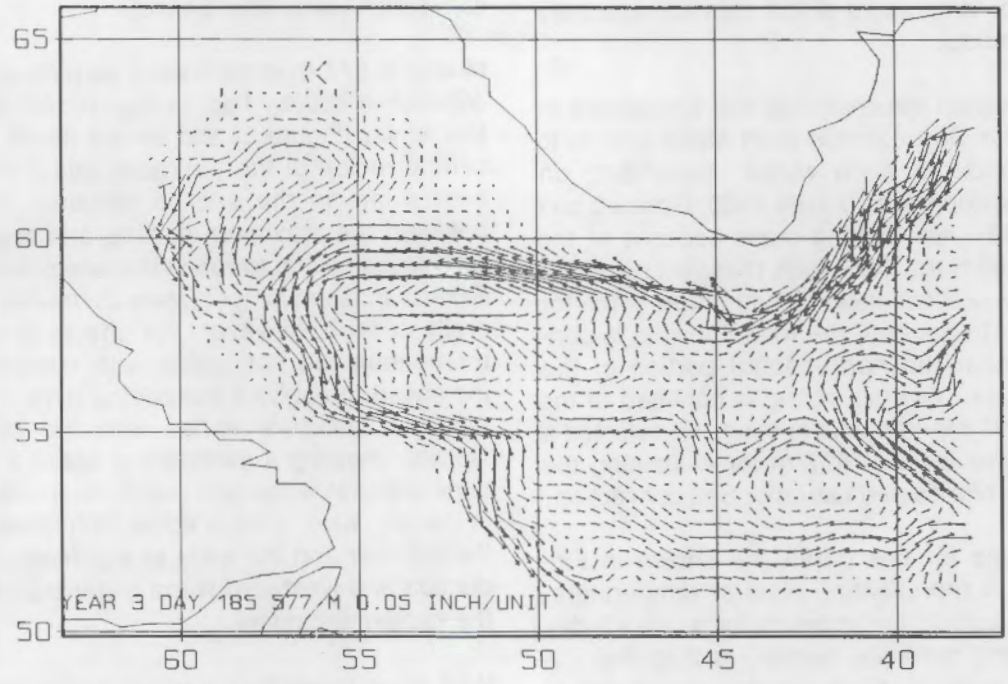

FIGURE 2b. Current Values from CME Results During Summer at 577 m.

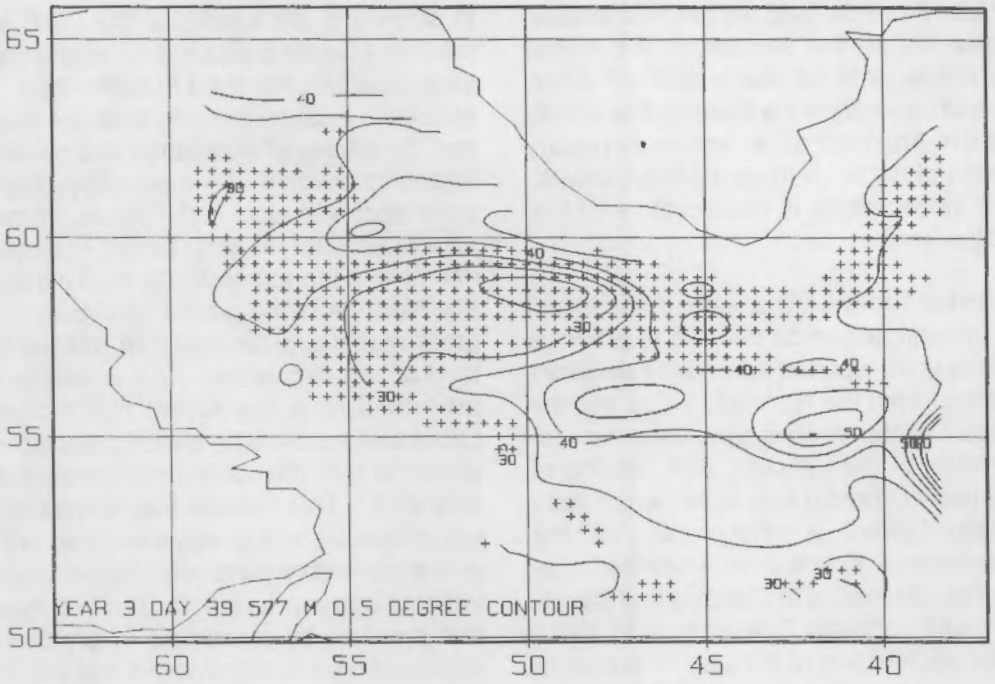

FIGURE 3a. Convective Activity (+) and Temperature from CME Data During Winter.

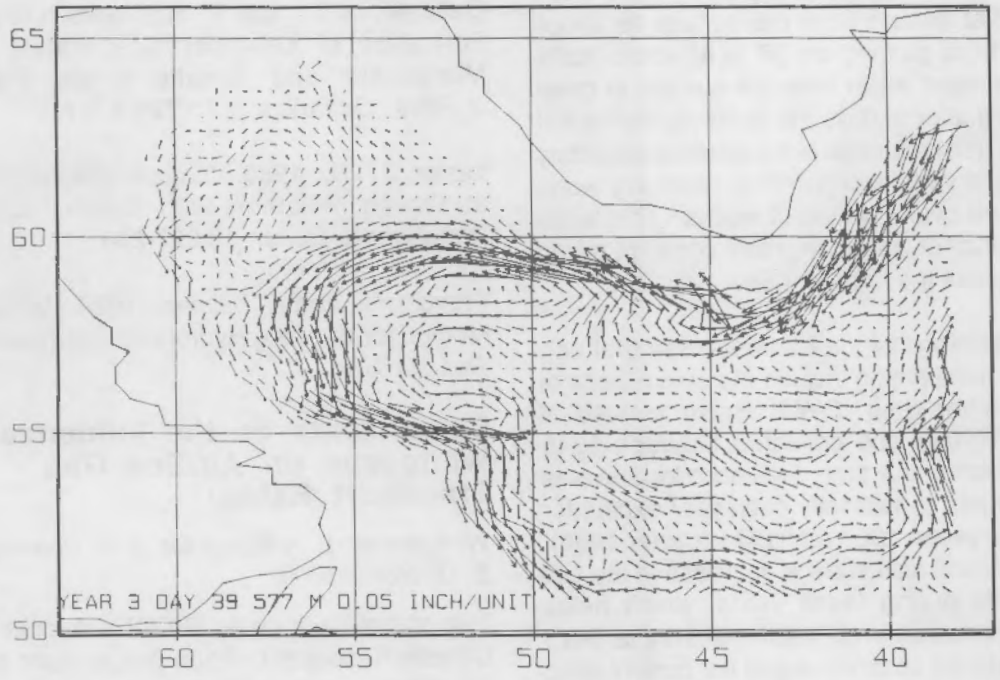

FIGURE 3b. Current Values from CME Results During Winter at 577 m.

of the Labrador Sea may help explain this feature, as convection below the surface in the mixed region does not occur in the stable northern water. The absence of convection is a result of low salinity values that are imposed as a surface boundary condition north of 60°N. A more thorough investigation of the model results is needed to verify this sequence of events.

The production of Labrador Sea water in the model follows the general sequence outlined in previous studies. Water is transported around the southern tip of Greenland from the Norwegian Sea into the Labrador Sea. Winter cooling generates convection in the center of the Labrador Sea, leading to generation of new Labrador Sea water, which exits via the Labrador Current. A major problem with the model is the vertical extent over which the convection is active. According to Gascard and Clarke, convection in the Labrador Sea extends to about 1500 m in the western part of the sea. However, in the model, mixing is limited to about 750 m and is located in the eastern part of the Labrador Sea. This is likely a result of more uniform cooling and the lack of an adequate parameterization of convective elements. Convective plumes have been observed that extend from the surface to about 1500 m. These plumes are 30 to 40 km in scale and can transport water from the surface to great depths in a matter of days. In contrast, the model overturning behaves more like a growing boundary layer, with the vertical penetration gradually working downward over a period of weeks. This leads to the formation of a shallow, more constant mixed layer throughout the Labrador Sea.

Other observations of the Labrador Sea that can be used for comparison include the ship reports of Ocean Weather Ship (OWS) Bravo located at 56°30'N, 51°00'W and collected between 1945 and 1974. During this time, the Labrador Sea was observed to mix consistently each year except for the period between 1967 and 1971 (Lazier 1980). The observations also show a decrease in the sea water salinity during these years, which helps explain the reduction in convective activity at OWS Bravo. Additional observations of the current structure across the mouth of the Labrador Sea are available for performing a budget analysis of sea water entering and exiting the region. The present study will be extended to analyze in greater detail the modeled Labrador Sea in comparison to these observations.

In summary, the results of the CME experiment provide a detailed data set for examining one possible structure for the Labrador Sea. However, questions exist concerning both the flow structure and the effects of no sea ice and grossly parameterized convection. An important problem in large-scale ocean models is the representation of convective activity. In most cases, the ocean is only unstable in the topmost 100 m. This is not true in the North Atlantic where convection occurs to great depth and becomes an integral part of the total ocean circulation. The preliminary analysis presented here has shown that modeling of the Labrador Sea could be affected significantly by the choice of both the cooling and convective parameterization. This implies that modeling the world ocean circulation is in some part tied to the realism of the convective parameterization. Future observational and numerical studies will help alleviate this problem by examining in greater detail the organization and behavior of oceanic convective activity and the net effect of convection on deep water formation.

References

Gascard, J. C., and R. A. Clarke. 1983. "The Formation of Labrador Sea Water. Part II: Mesoscale and Smaller-Scale Processes." *J. Phys. Oceanogr.* 13:1779-1797.

Lazier, J.R.N. 1980. "Oceanographic Conditions at Ocean Weather Ship Bravo, 1964-1974." *Atmosphere-Ocean* 18:227-238.

Provost, C., and R. Salmon. 1986. "A Variational Method for Inverting Hydrographical Data." *J. Mar. Res.* 44:1-34.

Experiments on the Influence of Whitecaps on Air/Sea Gas Transport Rates

W. E. Asher, E. A. Crecelius, J. P. Downing, and E. C. Monahan[a]

Two of the major goals of DOE's Atmosphere and Climate Research Division program are to predict the fraction of CO_2 in the atmosphere resulting from energy use and to determine the possible effects of fossil fuel combustion on the earth's radiation budget and climate. To accomplish these

(a) University of Connecticut, Groton, Connecticut.

goals it is necessary to understand the fate of anthropogenic CO_2 in the global carbon cycle, model interactions among the three main carbon reservoirs (the atmosphere, the ocean, and the terrestrial biosphere), and develop more accurate models of the earth's climatic response to changing levels of radiatively important atmospheric trace gases. Understanding of these systems and their models will be necessary to predict future impacts of continued anthropogenic production of CO_2.

Models of the global ocean carbon cycle that include a parameterization of air/sea exchange processes are currently being developed to calculate the uptake of CO_2 by the ocean. Calculating the global flux of CO_2 into the ocean from the atmosphere requires summation of a series of regional fluxes estimated using maps of global wind fields, air/sea CO_2 concentration gradients, and a wind speed parameterization of the air/sea gas transport rate, k_L. Because the relationship of the gas exchange process with wind speed is poorly known, there may be large errors introduced into the calculation of these regional fluxes through uncertainties in either the relation of k_L with wind speed or the global wind field. Coupled with the oceanic CO_2 concentration measurements to be made in connection with the WOCE and the Global Ocean Flux Study (GOFS), accurate global maps of k_L for CO_2 and other radiatively important trace gases would help reduce the uncertainties in the calculation of their global fluxes into and/or out of the ocean. In addition, global maps of k_L would provide boundary and initial conditions for three-dimensional models of the global carbon cycle. Such maps could be generated from satellite data if k_L could be determined from remotely sensed parameters.

Research is currently in progress, whose main goal is to achieve the capability to predict k_L from the remotely sensed parameter fractional area of whitecap coverage, F_c, at the Pacific Northwest Laboratory's Marine Sciences Laboratory (PNL-MSL). Because it may be possible to determine F_c from satellite measurements of the microwave apparent brightness temperature of the sea surface, correlation of k_L with F_c may allow prediction of k_L with the spatial coverage necessary for accurately calculating global CO_2 fluxes. As an initial step in developing this remote-sensing-based method of determining k_L, we are investigating the conditions under which F_c may be used as a predictor of k_L.

Gas transfer experiments were performed in a 1.3- m x 1.3-m x 2.6-m acrylic tank equipped with a tipping bucket mechanism. The tipping bucket generates bubble plumes by periodically dumping a volume of water into the tank. Computer control of the tipping bucket permits accurate variation of the total volume of water in the bucket and frequency of bucket cycles. This allows control of the intensity and duration of the bubble plumes. In these experiments, O_2 was used as the transporting gas because its concentration in aqueous solution is easily measured using commercially available O_2 electrodes and its transport into water is liquid-phase rate-controlled like CO_2. The tank, tipping bucket mechanism, O_2 electrode, and data acquisition and bucket control computer are shown schematically in Figure 1.

F_c was calibrated in the tank as a function of bucket spill height and spill volume by analysis of video

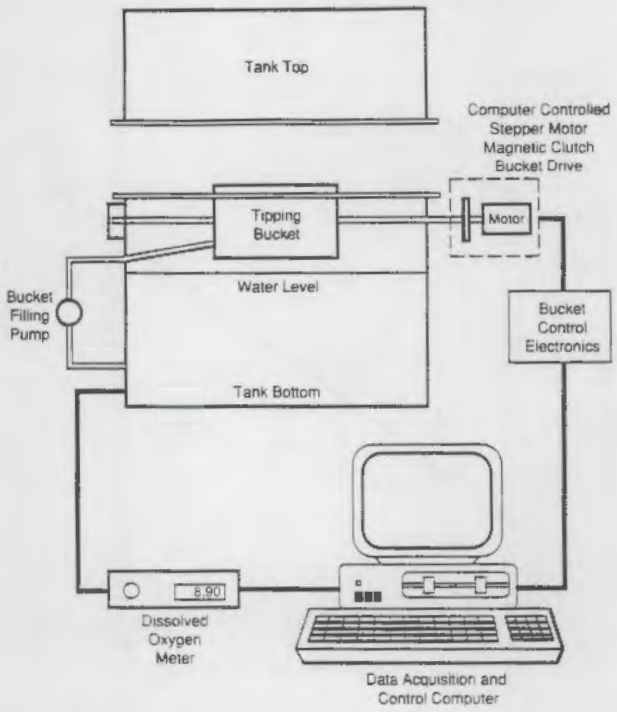

FIGURE 1. Schematic Diagram of the PNL-MSL Whitecap Simulation Tank Showing Computer-Controlled Tipping Bucket Mechanism and Dissolved Oxygen Meter.

records of bubble plume surface area. Calibration of F_c allows generation of a known F_c under a variety of conditions including bucket height above the water surface, tipping volume, and salinity.

Figure 2 is a plot of k_L for O_2 evasion versus F_c for bubble plumes generated by the tipping bucket. The results in Figure 2 clearly show the dependence of k_L on F_c. Because the maximum value of F_c studied here of 0.23 is an order of magnitude below typical oceanic values of F_c observed for wind speeds of approximately 15 m s^{-1}, it is apparent that oceanic whitecaps will have a large effect on air/sea gas exchange rates. Furthermore, these data demonstrate that bubble plumes are very efficient in promoting air/water gas exchange rates. Linear regression of Figure 2 shows that the correlation coefficient of k_L with F_c is 0.94, which suggests that it may be possible to use oceanic whitecap coverages to predict air/sea gas exchange rates.

Further planned work on this project will include laboratory research and two field experiments.

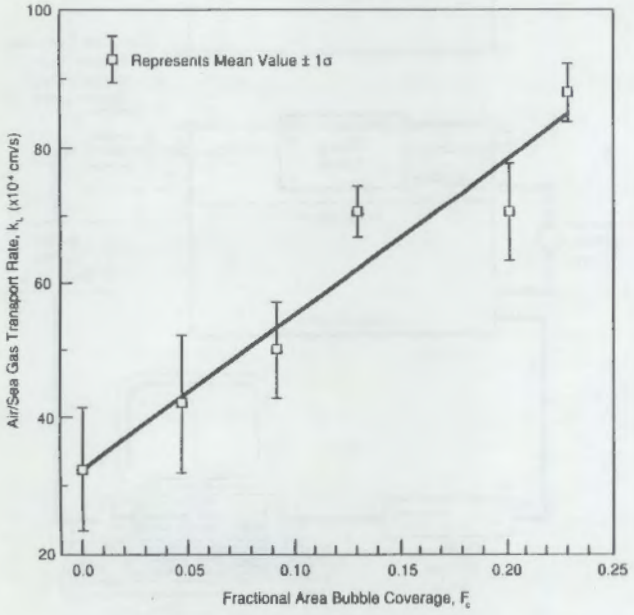

FIGURE 2. Plot of the Air/Sea Gas Transport Rate, k_L, Versus Fractional Area Foam Coverage, F_c, Showing the Enhancement of Air/Water Gas Transport Rates by Bubble Plumes. k_L was determined for oxygen evasion in the MSL tank with bubble plumes generated by a tipping bucket mechanism.

The objective of the future laboraotry experiments will be to determine the relation between k_L and F_c for a variety of gases including CO_2. One field experiment is planned in the Atlantic Ocean with the goal of testing the relationship between k_L and F_c developed in the laboratory studies using oceanic measurements of k_L and F_c. The second of the planned field experiments will be done in a large outdoor wave basin and will determine the relationship between F_c and microwave apparent brightness temperature. The results of this experiment will enable correlation of k_L with the satellite-measurable parameter, passive microwave emissivity of the ocean surface.

A Second-Generation Model of Greenhouse Gas Emissions

J. A. Edmonds, D. W. Barns, W. U. Chandler, and M. J. Scott

The analysis of greenhouse gas emissions has made enormous progress during the course of the past decade. Analysis has progressed from the use of simple time-trend extrapolations to the analysis of emissions of several greenhouse gases with parallel behavioral and optimization models of energy, manufacturing, agriculture, and land-use systems. Our ability to examine potential future scenarios of greenhouse gas emissions, however, is limited by both the lack of good historical data and the modeling tools with which to utilize that data.

The First Generation of Greenhouse Gas Emissions Models

The first generation of models were specialty models that focused on a particular aspect of the emissions problem without regard to how that activity interacted with other human and natural activities. The Edmonds-Reilly model (Edmonds and Reilly 1985), for example, is a global energy model in which the production of commercial biomass has no interaction with the agriculture sector or land use in general. Most forecasts of radiative forcing were made without regard to the interaction of emissions and atmospheric processes. Those that attempt to model this interaction explicitly, for example EPA (1989) and Rotman et al. (1989), produce emission estimates via a set of parallel but unrelated models. This approach has been successful in mapping out a range of uncertainty of future emissions under

business-as-usual circumstances and in providing preliminary analysis of the potential for emissions reduction and associated reductions in atmospheric concentrations of greenhouse gases. But this approach is inadequate to the task of analyzing the link between technical options and the cost of reducing emissions, and is similarly inadequate to understanding how one human or natural system activity interacts with other system activities. The link between technology and emissions has been studied using detailed technology analysis such as that of Goldemberg et al. (1987). While this approach is generally very rich in its technological detail, it is lacking in its description of the relationship between those technologies, and the overall, "macro," scale of human activities (e.g., aggregate energy production and use, or gross national product). There is a clear need for a second-generation model (SGM) capable of linking the so-called "bottom up" approach of researchers like Goldemberg et al. and the so-called "top down" approach of researchers like Edmonds and Reilly.

The Second Generation of Greenhouse Gas Emissions Models

The countries of the world have already embarked on the process of analyzing the cost and effectiveness of emission reduction options as an outgrowth of both domestic initiatives and international activities such as those of the Intergovernmental Panel on Climate Change. Emissions analysis to date has not addressed the issue of cost associated with alternative emissions reduction instruments, which will require a more sophisticated suite of models. The new suite of models must include both a global integrating model and compatible national models. These new models must be capable of analyzing the emissions of all greenhouse gases from all sources, including both those of natural and human origin, and providing an analysis of the interplay between the variety of human and natural activities responsible for greenhouse gas emissions.

Paradigms for SGMs

The development of SGMs will benefit greatly from the application of three simple principles: Problem Orientation, Minimum Modeling, and Parametric Modeling. The overriding design principle is that the model should be *problem oriented.* That is, the design of the model should be derived from an analysis of the underlying problem. In this case the issues to be addressed are

- What are global emissions of greenhouse gases likely to be over the course of the next 5 to 100 years by region and human activity?
- What effect will the exercise of policy instruments to control emission have and what will they cost?
- What effect will new technologies have on emissions?

Minimum modeling means that the model should contain only the information pertinent to answer the research question. If chemical manufacture of chloroflurocarbons (CFCs) is an important activity determining the rate and timing of climate change, it should be included. If it is not, it should be aggregated into a larger, general category of activity.

Finally, the model should be *parametric.* That is, the model should utilize a data base in which all parameters are open to examination and change by the user. The parametric model relies on data drawn from eclectic sources. Econometric, process model output and engineering information *all* are considered in the determination of future parameter values.

In addition, the model should be an *open model.* It is important that model results be reproducible and open to public scrutiny and criticism and that all of the parameters be available for inspection and alteration by model users.

Outline of a Second-Generation Model Design

In light of the above discussion, we have designed and are beginning to program an SGM with the characteristics shown in Table 1. Some of the key features are as follows:

Global Coverage

While the exact number of countries and regions that will be covered by the SGM has not been determined, a global energy data base (GEDB) has been structured for the major greenhouse gas-emitting countries. Table 2 lists the countries and regions covered. Undoubtedly, the final version of

TABLE 1. Features of PNL's Second-Generation Model of Greenhouse Gas Emissions

Global Coverage
Multiple Greenhouse Gases Including: CO_2, CH_4, CO, N_2O, NO_x, VOCs and CFCs
General Equilibrium Analytical Structure
Disaggregated Human Activities Including: Agriculture, Energy, Transportation, Manufacture, Services
Economic Resources: Land, Labor and Capital
Economic Decision Makers Including: Households, Government, and Producers
Capital Stocks: By Vintage of Installation, and Economic Retirement and Retrofit of Existing Stocks
Interactions Between Managed and Unmanaged Ecosystems
Multiple Regions With Key Countries Disaggregated
International Trade in Goods, Services, and Capital
5-Year Time Steps
2100 Forecast Horizon

TABLE 2. List of Countries and Regions of the GEDB

USA	China, Peoples Rep.
Canada	Japan
Mexico	India
Rest of North America	Australia
	Indonesia
Germany, Federal Rep.	Rest of Asia and Oceania
United Kingdom	
France	
Spain	South Africa
Italy	Rest of Africa
Rest of Western Europe	
	Brazil
USSR (Including Asian Part)	Rest of South America
Germany, Democratic Rep.	
Poland	
Czechoslovakia	
Rumania	
Rest of Eastern Europe	

the SGM will include most of these countries and regions as sources of emissions.

General Equilibrium Framework

The SGM will be more than a set of separate modules run in parallel. Each sector will interact with the others. For example, the demand for energy will be dependent of the demands of the agriculture, transportation, manufacturing, services, household, and government sectors while the demand for freight transport will depend of the level of manufacturing output. This means that the interplay between policies that affect, for example, the energy sector will in turn have some implications for the rest of the economy and those energy-economy interactions will be explicitly represented. In addition, the demands for land, labor, and capital will depend on the demands from all five sectors of the economy: agriculture, energy, transport, manufacturing, and services.

International Trade

The global nature of the greenhouse issue requires that international trade issues be addressed. Nations will trade agricultural goods (grain, livestock, other food and fiber, and forest products), energy (oil, gas, coal, and uranium), manufactured goods, services (including returns on foreign investments), and capital (financial and physical). Governments can control international rates of importation and export.

A Modeling Team Approach

The development of the SGM will take at least 3 to 5 years and require the work of research teams at several levels. The model will be designed and built by a team of three to four researchers, supported by research assistants and programmers. Three issues will dominate the model design and development: Economic, Engineering, and Natural Science. The economic issues arise out of the fundamental nature of the problem. That is, the problem is fundamentally one of understanding the allocation of scarce resources over time to competing ends.

Objectives for FY 1989 included forming the core research team, specifying the model structure, and encoding the SGM model skeleton.

In addition to the core model development team, a broader team of collaborators will be required. A network of research organizations is being built both within the United States and the international research communities. We are working with several of the U.S. national laboratories, including ORNL, BNL, and the Lawrence Berkeley Laboratory, to jointly develop this model. We already have concluded an agreement with the Academy of Sciences of the USSR (AS/USSR) to assist in the development of the information needs for the SGM. We have also concluded an agreement with Japan and are seeking other international collaborations. Finally, close cooperation must be maintained between the SGM teams and physical, chemical and biological research efforts with which it intertaces, especially carbon cycle and

atmospheric chemistry groups, to insure usefulness and compatibility.

Progress During FY 1989

Major progress has been made on two fronts in FY 1989. In the area of emissions, the original Edmonds-Reilly model has been modified to forecast emissions of methane (CH_4), the second most important greenhouse gas after CO_2 and N_2O. Progress has also been made on the specification of the capital stock module.

Methane Emissions

Although much of the atmospheric CH_4 is of natural origin (natural wetlands, etc.), a significant portion is anthropogenic, with probably 20% to 30% of the overall total attributable to the production, distribution, and use of energy. However, unlike CO_2, only a small fraction of CH_4 is generated by combustion processes, and the quantitative relationships are much more ambiguous. The Edmonds-Reilly Long-term Energy-CO_2 Model (Edmonds and Reilly 1985), as the name implies, was originally designed to model the emissions of CO_2 resulting from energy production and usage. In extending the model's capabilities to model similar emissions of CH_4, sources of emissions information had to be identified, emissions coefficients assessed, and the final values of the coefficients chosen for the modeling effort.

Energy-related sources of CH_4 include coal mining, natural gas production and distribution, automotive exhausts, burning of traditional biomass, and landfill decay (Barns and Edmonds 1990). Landfills are included because solid waste is a potential energy source, either by direct combustion or by draining and collecting the resulting gas. Methane emissions from coal mining are essentially a function of coal rank and depth, with a wide range of values. A weighted average of 250 cubic feet per short ton yields a world total of about 25 Tg/year at current production rates. Natural gas is mostly CH_4, and losses can occur at any stage of the extraction, distribution, and utilization processes. Using an assessed value of 2% of total production gives a global contribution of about 25 Tg/year. Venting and flaring are generally accounted for in the aggregate; however, it is obvious that only venting is important as a methane emission source. Totals for venting and flaring are available for most countries, but many are of questionable accuracy. If the fraction vented is assessed at one-fifth, the total methane emission is about 15 Tg/year.

The range of methane emissions from automotive exhausts has been extended by incorporating various pollution control measures in some countries; however, the global total is estimated to be only about 1 or 2 Tg/year. Traditional biomass (fuel wood and bagasse) combustion yields another estimated 10 to 15 Tg/year. Finally, landfill emissions from 30 to 70 Tg/year provide one of the largest sources. The sum of the above sources is centered around 110 Tg/year, which in comparison with other similar studies, is in the low end of the range.

Forecasts of future CH_4 emissions were presented at the 14th Congress of the World Energy Conference in September 1989 in Montreal (Scott et al. 1989) and in March 1990 at the annual meetings of the American Association for the Advancement of Science in New Orleans.

Capital Module

The SGM Capital Module utilizes a vintage description of technologies. This has a number of important implications. First, it means that history matters. When a technology is installed it exists and can be operated until its retirement. New technologies affect productivity at the margin. They can only affect historical decisions if they are so attractive (unattractive) that they force prices down to the point when existing technologies are retired early (experience life extension). Another important implication is that once installed, capital is not malleable. It cannot be shifted around from one sector of the economy to another. In fact, once installed, capital costs no longer matter. Once the technology is installed, the decision to operate or idle a technology depends on the ability of the technology to cover its current operating expenses (in market economies).

A technology is described by an array of parameter sets including:

1. production function parameters
2. emissions coefficients
3. capital investment parameters

4. installation parameters (e.g., date of first availability, date of removal from the list of options, nominal lifetime, length of installation period)

5. capacity

6. vintage.

A technology option can be described by the information contained in parameter sets 1, 2, 3, and 4. Once installed, the operating characteristics of a technology can be described by parameter sets 1, 2, 5, and 6.

This model will utilize a simple production function, the CES function.(a) The CES function will be employed for two reasons: First, the function is well behaved; that is, for a wide range of relevant parameter values it never produces counter-intuitive results such as negative demands from production inputs or negative output values. Second, the relationship between the production function in physical terms and the dual cost function is simple.

For the CES production function the function F takes the form:

$$Q = \alpha_0 \left(\sum_{i=1}^{N} \alpha_i x_i^{\sigma} \right)^{1/\sigma}, \qquad (1)$$

where the x_is are inputs to production, and α_i, i=0,..N and σ are parameters. The CES has a number of useful characteristics. It is homogeneous of degree one. That is, doubled input levels result in doubled levels of output.

For the CES production function given in Equation (1), a "dual" cost function can be estimated and is given by

$$C = Q\, \alpha_o \left(\sum_{i=1}^{N} \beta_i P_i^{\tau} \right)^{1/\tau}, \qquad (2)$$

where

$$\tau = -\sigma/(1 - \sigma),$$

and

$$\beta_i = \alpha_i^{(1-\tau)}, \quad i = 1,..,N.$$

Because the CES function is homogeneous of degree zero, the cost of a single unit of production, C/O, is independent of the level of output Q. We also note that the unit cost function is also homogeneous of degree one. This reflects the fact that doubling all prices doubles costs. A demand function for inputs to production also can be estimated.

Greenhouse gas emissions coefficients will be included with each technology description. Emissions will be assumed to be proportional to either the scale of input utilization or output of the technology. Emissions can be calculated simply as

$$E_g = \sum_{i=1}^{N} e_{gi}\, x_i \qquad (3)$$

where x_i are input demand levels for a technology, e_{gi} is the emission coefficient for gas g from input i, and E_g is the total of all emissions of gas g from the technology.

When emissions are released costlessly into the atmosphere, they have no effect on either the cost of production or the optimum demand for investment goods. Releases need not be costless. Like other inputs and outputs from the technology, emissions may be priced. If the cost of a unit of emission of greenhouse gas g is P_g, the effective price of the input used in the technology, W_i, becomes

$$W_i = P_i + e_{gi}\, P_g. \qquad (4)$$

Capital costs are an important determinant of investment decisions. Capital cost per unit of output for a technology in year t are denoted as K(t) and kept as part of the technology characterization. Costs may vary over the period in which the technology is

---

(a) The CES function stands for Constant Elasticity of Substitution. The elasticity in question is not a standard price elasticity, but rather a measure of the ease of substitution of one factor of production for another, output constant. See for example, Henderson and Quandt (1958) for a discussion.

available for selection. The model allows a technology to be introduced at one unit capital cost and for that cost to decline with either time or cumulative installations to a mature technology cost.

Investment decisions in the SGM are based on the nominal lifetime of the technology. This period may differ from both the maximum potential life of the technology and the actual (observed) life of the technology. In the absence of a major renovation of the technology, the actual life of the technology can be no longer than its maximum potential life, TP. The technology can be retired after service for any period shorter than TP years. Investment decisions are made in the SGM based upon expected profit rates, which in turn depend upon parametric forecasts of the prices of inputs and outputs.

The determination of investment among technologies requires a formal and flexible structure capable of analyzing levels of information detail that can differ between regions of the world and between sectors of the economy in a single region. To facilitate the analysis of the interface between technologies, the economy, energy, and greenhouse gas emissions, the model employs a description of technology based on the principle of hierarchy. Hierarchies are applied to two generic classes of technologies: core technologies and accessory technologies.

Core technologies define the technology. There are four hierarchical levels that can be used to subdefine the core technology. At each level, technologies produce the same service and are aggregated to define the next level of the hierarchy. Each level of the hierarchy can be considered to be a market in which technologies compete against each other for market share.

As an example, the electric utility industry's hierarchy is illustrated in Figure 1. The highest level of the hierarchy is electric power generation. At the second level of the technology hierarchy, electric power can be produced using seven generically different technologies: oil, gas, coal, biomass, nuclear, solar, and hydro. Gas can be used as the feedstock for electric power using either boilers or turbines. Turbine technologies can be further subdivided into conventional heavy duty turbines (CHDT), conventional combined cycle turbines

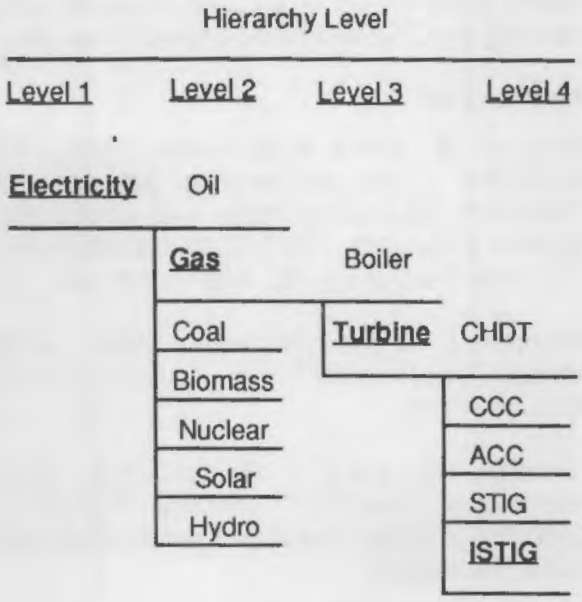

FIGURE 1. The Relationship of ISTIG to the Core Technology Hierarchy of Electric Power Generation.

(CCC), advanced combined cycle turbines (ACC), steam injected gas turbines (STIG), and intercooled steam injected gas turbines (ISTIG).

One of the interesting features of the hierarchical approach is that if information is either not available or not of interest at a given level, the system can be collapsed by providing information at the next level of aggregation only. This provides flexibility in application of the structure among different sectors of an economy and between regions. The most detailed level of the hierarchy is described by a production function of the form given in Equation (1) with an associated dual cost function of the form given in Equation (2).

Summary

It is time to recognize the important interactions that exist among the human activities that generate greenhouse gases and reexamine emissions as a set of interrelated phenomena. The development of a second-generation greenhouse gas emissions model could simplify the analytical framework currently in use, sharpen the focus of the models to greenhouse gas emissions, delete superfluous phenomena, add pertinent detail, and tie the analysis together in a comprehensive interactive analytical framework. The current design effort already has made important strides in this direction.

Work is going forward on greenhouse gases other than CO_2 and CH_4, and model coding has begun.

References

Barns, D. W., and J. A. Edmonds. 1990. *An Evaluation of the Relationship Between the Production and Use of Energy and Atmospheric Methane Emissions.* TR-047, DOE/NBB-0088P, U.S. Department of Energy, Washington, D.C.

Edmonds, J. A., and J. M. Reilly. 1985. *Global Energy: Assessing the Future*. Oxford University Press, New York.

Edmonds, J. A., and D. B. Reister. 1982. *Characteristics of Nested CES Functions*. ORAU/IEA-82-5(M), Oak Ridge Associated Universities, Oak Ridge, Tennessee.

Goldemberg, J., T. B. Johansson, A.K.N. Reddy, and R. H. Williams. 1987. *Energy for a Sustainable World.* Wiley-Easton, New Delhi, India.

Henderson, J. M., and R. E. Ouandt. 1958. *Microeconomic Theory: A Mathematical Approach.* McGraw-Hill Book Company, New York.

Rotman, J., H. de Boois, and J. Swart. 1989. *An Integrated Model for the Assessment of the Greenhouse Effect: The Dutch Approach.* National Institute of Public Health and Environmental Protection, Rijksinstituut voor Volksgezondheid en Milieuhygiaene, Postbus 1, 3720 BA, Bilthoven, The Netherlands.

Samuelson, P. A. 1947. *Foundations of Economic Analysis.* Harvard University Press, Cambridge, Massachusetts.

Scott, M. J., J. A. Edmonds, M. A. Kellogg, and R. W. Schultz. 1989. "Global Energy and the Greenhouse Issue." *World Energy Conference 14th Congress: Energy for Tomorrow.* Paper 2.1.1, Montreal, Quebec, Canada, September 17-22, 1989.

Shepherd, R. W. 1953. *Cost and Production Functions.* Princeton, NJ: Princeton University Press, Princeton, New Jersey.

U.S. Environmental Protection Agency (EPA). 1989. *The Potential Effects of Global Climate Change on the United States*. U.S. Environmental Protection Agency, Washington, D.C.

The Regional Effects of Climate Change and CO_2 Fertilization on the Natural and Human Environment

M. J. Scott, N. J. Rosenberg,[a] and R. M. Cushman[b]

Global circulation models (GCMs) indicate that man-caused increases in greenhouse gases may elevate the average temperature of the earth's atmosphere during the next century to levels not experienced in the last 100,000 years. A question that has received very little systematic attention is this: what are the consequences for human and natural systems?

In the past year, the "greenhouse" issue has moved rapidly from the research domain, where it had existed for years, into the policy domain. Innumerable proposals have been set forth in both the domestic and international policy arena to establish new energy policies to control emissions of CO_2 and other greenhouse gases.[c] These proposals are predicated, of course, on the idea that the consequences for human and natural systems of induced climate change are unacceptable. Given the paucity of information that has been generated in the area of CO_2/climate change effects, however, there is no way either to confirm or reject the conclusion of unacceptable consequences.

(a) Resources for the Future, Washington, D.C.
(b) Environmental Sciences Division, Oak Ridge National Laboratory, Oak Ridge, Tennessee.

(c) The most important of these "radiatively important gases" is CO_2. Other important gases include methane (CH_4), nitrous oxide (N_2O), selected other oxides of nitrogen (NO_x), the cholorofluorocarbon (CFC) family, carbon monoxide (CO), and tropospheric ozone (O_3). The global warming effect of each gas depends on its molecule-by-molecule effectiveness at absorbing infrared radiation and its atmospheric concentration. Analysts usually speak of atmospheric concentration as being radiatively "equivalent to" a certain concentration of CO_2 alone.

The State of the Art

Because GCMs and other climate forecasting tools are not yet sufficiently reliable at a regional level where the effects of climate will be felt, it is clearly too early to "forecast" the effects of climate change. However, it is not too early to begin the process of developing the scientific information base and analytic tools which will be needed to analyze the implications of CO_2/climate change and help formulate responses. If the nation is entertaining the possibility of dramatically altering its energy programs and policies as an outgrowth of concern over induced climate change, then we will need tools to explore the potential consequences, their attendant uncertainties and possible options for adaptation, which can be set against the nearer-term costs and options of alternative energy strategies. Second, a prudent "effects-research" program can help identify the contingent policies and actions that may reduce the costs of adapting to a changed environment. Third, such a program can provide information about which CO_2/climate change variables are important to human and natural systems. This information can be transferred to other domestic and foreign research programs on the carbon cycle, climate, and earth systems. This information can provide useful feedback to these programs and allow them to channel research into the most useful directions.

The current understanding of CO_2/climate change is inadequate to formulate either energy or climate policy, although it does provide a basis to conclude that the potential for adverse consequences from CO_2/climate change exists (Scott et al. 1990; EPA 1989). The current understanding of the environmental, economic, and social effects of CO_2/climate change is based on a fragmented set of studies. With a few exceptions, existing studies have not addressed many of the key problems in predicting the effects of climate, in that for analytical convenience they have focused on *deterministic long-run effects of climate change equivalent to a doubling of atmospheric CO_2 in the steady state, typically for a few resources in isolation.* They have not addressed many of the key issues, which include:

- Time - The climate change will not be felt in today's world, equipped as it is with today's technology, nor will the effects occur for the most part in a world that is steady state. The rate and timing of transient CO_2/climate change may be as important to determining consequences as the characteristics of a theoretical *steady-state* atmospheric concentration of CO_2 and climate. Though unrealistic, theoretical steady states have been used extensively in estimating the effects of climate change.
- Simultaneous Multiple Resource Analysis - Methods must be developed for addressing the interactions of human and natural systems, including methods to analyze simultaneously the interaction of multiple resources within a systems framework, quantify the combined CO_2/climate change interactions, and analyze the effects of technological change and population growth.
- Geographic Disaggregation and Integration - To be meaningful, effects studies must select appropriate geographical entities for analysis--local, regional, global--and because of the interactions between regions, conduct simultaneous multiple region analysis.
- Uncertainty - Studies must develop and apply appropriate uncertainty analysis techniques. In climate effects research and similar natural resource-related social science involving a number of interactions between natural physical processes and economics, computational burden precludes the use of standard Monte Carlo analysis and "what if" sensitivity testing requires such simplifications of the underlying relationships as to be virtually useless. Thus, there is a need to develop more efficient means of generating distributions of potential outcomes from model-based analyses and a need to develop means of assessing the value of external information that permits the sorting among outcomes.

Work began in FY 1989 to develop the scientific information base and the analytical tools necessary to understand the regional consequences of CO_2/climate change, including descriptions of their nature, timing, magnitude and associated uncertainties. Specifically, the research effort has three near-term goals: 1) to develop robust methods and tools of analysis, including systematic analysis of uncertainty using improved computational procedures; 2) to develop the information systems necessary to support CO_2/climate change analysis; and 3) to develop channels of communication

among and between researchers and parties potentially affected by CO_2/climate change (Edmonds et al. 1989). The initial program focuses on a single region of the United States [Missouri, Iowa, Nebraska, and Kansas (MINK)], employs a historical analog climate, and analyzes the interactions of all of the resources resident within that region as they might evolve under current and changing CO_2/climate conditions over the next 50 years. The region was chosen for its relatively simple, natural-resource-based economy, spatially coherent climate, and availability of data on both the region's resources and a potentially meaningful climate analog--the Dust Bowl period of the 1930s. The program is unique in that it addresses all of the research concerns mentioned above, including timing, multiple resources, regional context, and uncertainty.

The program will produce and disseminate information about the effects of CO_2/climate change. This information will be provided in a form usable by DOE in the formulation of national energy policy. This information will also be made available, through reports, forums, and information systems, to the other federal agencies, the states, and to the general public.

During this initial year of the program, analysis has focused on producing an economic and biophysical baseline description of the MINK region and the initial development of models to address the following four major natural resource sectors, the intersectoral biophysical and economic linkages between them, and economic sectors within the MINK region that support them:

- agriculture
- water resources
- forest products
- energy.

Baseline resource information has been collected on the four-state area and in many cases mapped on an ARCINFO geographic information system (GIS) by the ORNL Environmental Sciences Division. Data mapped in this fashion include agricultural production, water use rates from surface and groundwater sources, and species and quality of timber lands. Figure 1, an example of these maps, shows the total water withdrawals for irrigation by county for the MINK region. Many of the results of the regional analysis will be presented in GIS format.

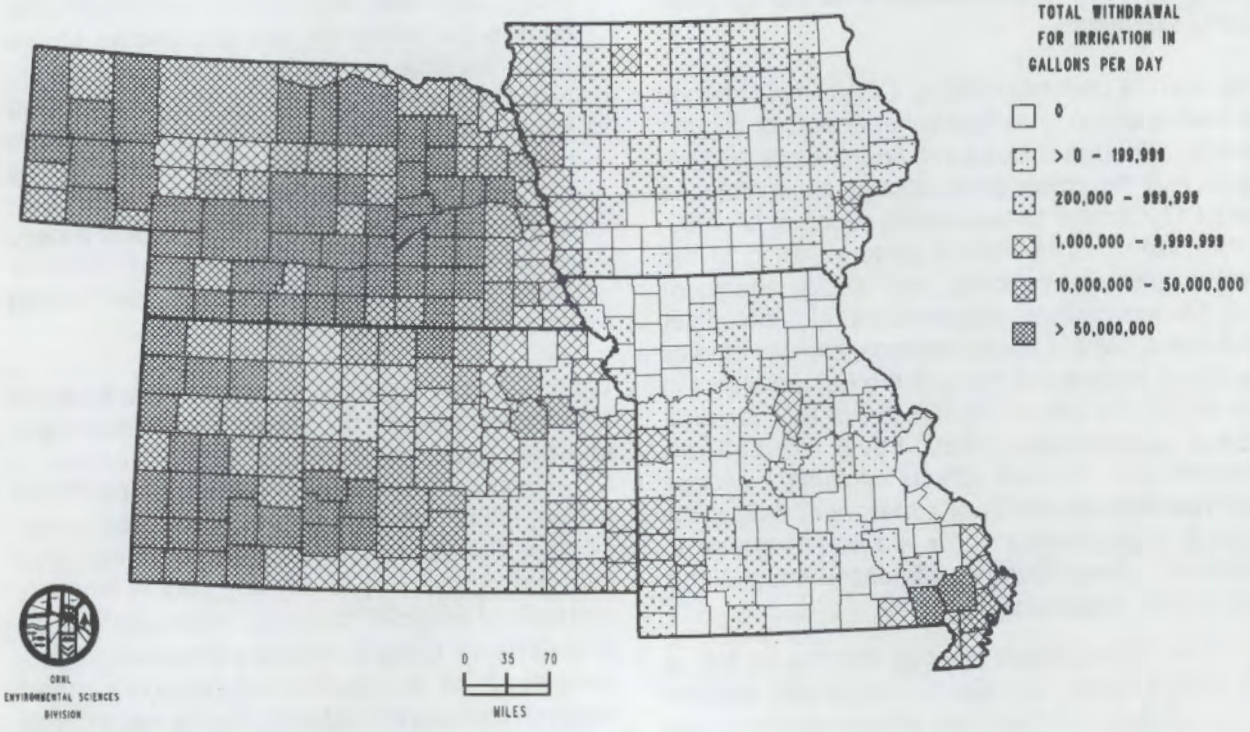

FIGURE 1. Total Withdrawal for Irrigation in Gallons Per Day.

The impacts of climate change on "typical" agricultural cropping systems are being analyzed using a version of the Erosion-Production Impact Calculator (EPIC) computer code originally developed at Texas A&M University (Williams et al. 1984). The EPIC code has been modified in two major ways for this study to incorporate the direct effects of CO_2 on crop growth: 1) An adjustment has been made to the photosynthesis equations in the model based on empirical, species-specific response surfaces for net photosynthesis as a joint function of irradiance and CO_2 concentration, expressed as radiation use efficiency (RUE). RUE is further adjusted for photosynthetic sensitivity to humidity for each species. 2) The Penman-Monteith (P-M) method of calculating evapotranspiration is incorporated in the model (see Martin et al. 1989). P-M expresses evapotranspiration as a function of solar (net) radiation, temperature, humidity, wind speed, and canopy resistance. CO_2 affects canopy resistance by influencing both stomatal resistance (opening and closing of leaf stomates) and leaf area index. Temperature and precipitation data have been collected for some 30 stations of NOAA's Cooperative Climatological Network. Data on solar radiation, atmospheric humidity, and wind have been constructed for these sites from observations at the less numerous First Order Stations throughout the MINK region.

The EPIC model, as modified, has been exercised using baseline (1951-1980) and 1931-1940 "warmer-drier" analog climates under current (mid-1980s) technology. Table 1 shows preliminary results concerning the effects on crop yields of several types of irrigated MINK-region farms. These results assume that farmers do not attempt to minimize the effects of climate change by adjusting farming practices. Adjustments to the impacts of the climate change are to be tested next.

Information has also been developed on a number of "typical" farm operations based on both secondary data from the state departments of agriculture in the MINK region and upon expert opinion from a number of sources in each state. Features that are expected to drive the farm adjustment decisions include the effects of climate itself, expected prices, yields, and costs, specific crop risks, government programs such as price supports, and societal goals as evidenced by state and federal land policies. An example of information provided on these typical farm operations is provided in Table 2 for a corn-soybean operation in northcentral Iowa. Information of the type in Table 2 forms the basis of an expert system that will be used to analyze the response of farm operators to changes in climate (as suggested by Sonka and Lamb 1987). Responses that may prove useful to analyze include changes in land management practices such as no-till agriculture, changes in fertilization practices, changes in crop selection and planting practices (dates, depths, spacing, sequences and patterns), changes in irrigation practices (events, amounts, installation or dismantling), changes in pest management, and changes in harvest practices (timing and drying) (Easterling et al. 1989).

Analysis of water supplies has been concerned primarily with baseline descriptions of groundwater supplies in the region and surface waters originating both inside and outside the region. Effects

TABLE 1. Simulated Changes in Water Use and Crop Yields on Irrigated Farms Under Baseline (1951-80) and Analog (1931-40) Climatic Conditions Using the EPIC Model.

Representative Farms	Change Between the Baseline and Analog Climatic Conditions, %	
	Yields	Water Use
Nebraska: Corn		
A	-8	+19
B	-2	+28
C	-4	+36
D	-6	+25
E	-4	+33
F	-7	+32
Kansas: Corn		
G	-9	+31
H	-5	+15
Crop Rotation I		
Wheat	+13	+18
Corn	-9	0
Sorghum	-15	+23
Crop Rotation J		
Wheat	+3	+17
Corn	-5	+22
Sorghum	-7	+40

TABLE 2. Example Data for Typical Corn-Soybean Farm Operation.

MAJOR SOIL TYPES: Nicollet
Clarion
Webster

ROTATION: Corn - Soybeans (2-year rotation)

			Hectares
Total acres operated:	610		247
Land value per acre:	$1,000		
Acres cropped:	550		223
Cropped acres as share of total:	90%		
Acres rented/leased:	368		149
Cropped acres rented/leased:	67%		
Total value of crop sales:	$85,000	65%	
Total value of livestock sales:	$45,000	35%	
Total value of sales:	$130,000	100%	

CROP 1: CORN

Variety: 110 day (north) Growing degree days: 2450
115-18 day (south)

Acres: 195 Yield: 120 bu/acre
Hectares: 79 Yield: 7.6 mT/hectare

TILLAGE SCHEDULE

Date	Operation	Cost/acre	Cost/hectare	Cost/crop
11/15	Anhydrous App. (40%)	$6.20	$15.31	$1,209
4/1	Anhydrous App. (60%)	$6.20	$15.31	$1,209
4/15	Tandem disc	$3.00	$7.41	$585
4/20	Sprayer (herb.)	$1.90	$4.69	$371
4/22	Field cultivator	$3.60	$8.89	$702
4/25	Planter: row	$5.65	$13.96	$1,102
5/5	Rotary hoe	$1.75	$4.32	$341
6/1	Row crop cultivator	$2.95	$7.29	$575
10/1	Harvest	$23.85	$58.91	$4,651
	Total	$55.10	$136.10	$10,745

INPUTS:

Input	Unit Cost	Amount/acre	Amount/hectare	Cost/acre	Cost/hectare	Cost/crop
Seed	$68.10/bu.	25,000 seeds	61,776 seeds	$19.00	$46.93	$3,705
Lime (pro) (applied once in 6 years)	$25.00/acre			$2.08	$5.15	$406
Nitrogen	$327.27/ton	0.06 T	123 kg	$18.00	$44.46	$3,510
Phosphorous	$353.85/ton	0.03 T	73 kg	$11.50	$28.41	$2,243
Potassium	$275.00/ton	0.04 T	90 kg	$11.00	$27.17	$2,145
Herbicide	$19.00/acre			$19.00	$46.93	$3,705
Land rent	$90.00/acre	130 acres		$90.00	$222.30	$11,700
Hired labor (pro)	$5.25/hour	1247 hours		$33.57	$82.93	$6,547
pro - proportioned across crops			Total	$204.16	$304.27	$33,960
			TOTAL CROP COSTS: CORN	$259.26	$640.36	$44,705
			TOTAL COSTS FOR UNIT OF ESTIMATED PRODUCTION(a)	$1.91/bu	$74.88/mT	

(a) Calculated cost exclude taxes, interest, management overhead, etc.

of climate change on both water supply and demand are being considered, as are effects on both water quality and quantity. Water uses in Missouri and Iowa, the two wetter states, are very different from those in Nebraska and Kansas. For example, in the two wetter states, irrigation accounts for 4% of total offstream water use and 29% of consumptive use. In Kansas and Nebraska, irrigation accounts for 76% of total offstream use and 95% of consumptive use. In some portions of the MINK region, total water use already exceeds mean streamflow, while preliminary analysis shown in Table 3 suggests that 1931-1940 climate conditions may cut streamflows by anywhere from 5% to 70%. Many of the surface waters whose quality supports or partially supports their designated uses may no longer support these uses. Groundwater overdrafts are as high as 50% of consumptive use in some areas within MINK and may increase significantly under analog conditions. Analysis is continuing, particularly of the interaction between irrigation demand by farmers and availability of water supplies.

The forest products resources of the MINK region have been characterized and analysis of the impacts of climate has been begun using the FORET computer code (Solomon et al. 1984; Solomon and West 1987). FORET has been modified for the current project to allow for the possible effects of elevated atmospheric CO_2 concentrations on photosynthesis and water use

TABLE 3. Adjustments in 1985 Mean Assessed Total Streamflows Under the 1931-1940 Climate.

	Millions of Gallons per Day				
	1985 Mean Assessed Total Streamflow with Baseline Climate[a]	Reductions in Streamflows Under the 1931-1940 Climate[b]		Assessed Total Streamflow with the 1931-1940 Climate	1931-1940 Climate Streamflow as a Percent of Baseline Flow
		Reductions in Runoff	Increased Evaporation		
Missouri					
1005	18,204	4,706	1,847	11,651	64
06	20,692	5,822	1,890	12,980	63
07	3,963	20	186	3,757	95
08	9,746	2,926	255	6,565	67
09	34,969	10,940	2,145	21,884	63
10	6,099	2,169	372	3,558	58
11	56,634	17,129	2,990	36,515	64
Arkansas-White-Red					
1101	15,994	1,088	209	14,697	92
03	4,864	371	196	4,297	88
04	28,248	2,019	940	25,289	90
Upper Mississippi					
701	10,506	7,282	52	3,172	30
03	43,972	15,092	451	28,429	65
04	63,926	18,849	510	44,567	70
05	134,677	38,943	3,647	92,087	68
Lower Mississippi					
801	363,321	56,454	4,587	302,280	83

(a) Total assessed streamflow is the flow at the outflow point of the subbasin that would be available if 1) consumption were eliminated, 2) estimated 1985 water transfer and reservoir practices were continued, and 3) groundwater mining were discontinued. This measure takes account of average evaporation under long-term climatic conditions.

(b) These reductions in streamflows are the result of decreased runoff (or increased evaporation) within the hydrologic unit and within all upstream hydrologic units.

efficiency. The FORET model has been used to perform preliminary analysis of forest stand biomass in stocked stands and after clearcutting at points up to 200 years in the future. Figure 2 shows a sample of the results for "typical" stocked stands in Missouri after 200 years of growth. The figure shows biomass response at "current" temperature and precipitation (designated for three locations in Missouri by the asterisks in the figure) and with other, theoretical climates. Taking the location with temperature at 13.5°C and 100 cm precipitation, one might expect total biomass of stocked stands at about 91 tons/hectare after 200 years. With temperatures 3° warmer (16.5°C) and with only 76 cm precipitation, total biomass would be less than 31 tons/hectare. Although not shown here, analysis has also been done of the effects of CO_2 fertilization on individual species.

Regional energy demand and supply issues also are being examined. The baseline description has concentrated on four direct weather-sensitive sources of energy demand (both electric and non-electric irrigation pumping, air conditioning, crop drying, and space heat), which together account for about 30% of all energy used in the region, and two indirect sources of energy demand (fertilizer application and pesticides). Analyses to date show that energy used for irrigation pumping (most of it non-electric) under a 1931-1940 climate might increase by 23% if farmers simply were to try and replace moisture loss without any other adjustments. However, only about 15% of all agricultural energy used in the region is for pumping, meaning that the direct increase in energy would be about 3.5% for the region's farm economy. At the same time, fertilizer applications would likely fall as yields fall, so the net change might be smaller still. The energy/output ratio has fallen sharply in farming in the last decade (by 48%). While this development was no doubt strongly influenced by the rising real price of energy, it does demonstrate the farm sector's capacity to economize on energy without jeopardizing its productivity or ability to expand output. Although water temperatures would be higher and flows less under warmer climate, analysis to date has not identified any major problems with supplies of water for energy within the region, since the major energy use of water (for power plant cooling) mainly represents a diversion

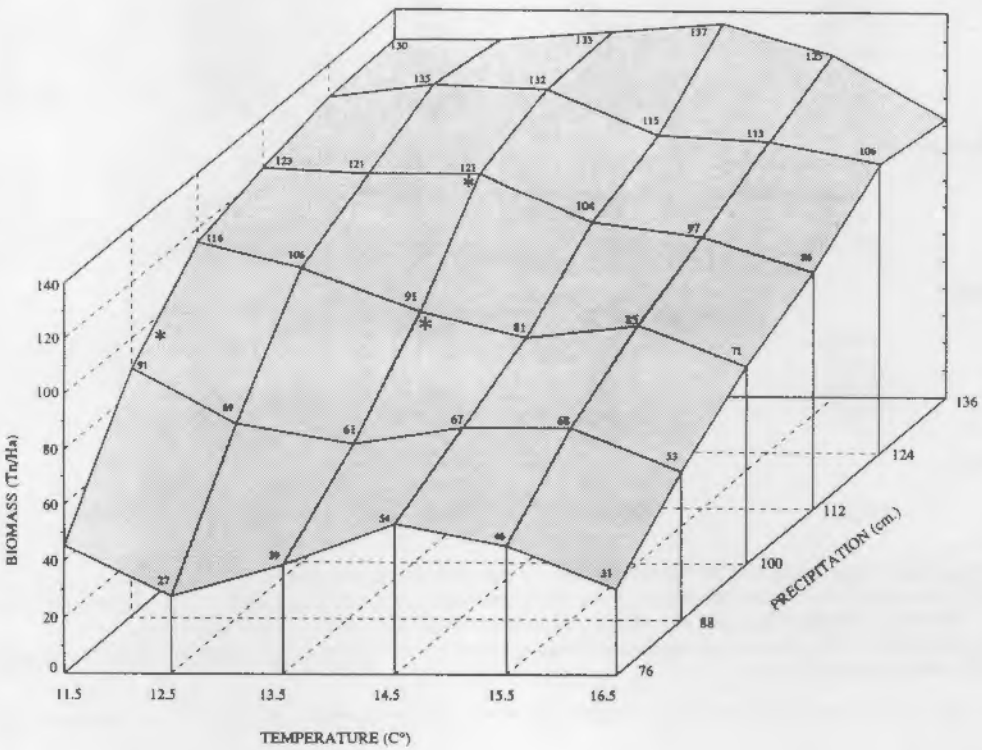

FIGURE 2. Biomass Response to Temperature and Precipitation Stocked Stands After 200 Years--Missouri.

rather than a consumptive use. Flows appear to be adequate for cooling for the region's power plants under reduced flows. Water for hydropower is not an issue in the region, contributing only about 3% to 6% of all electricity generated in the region. However, hydropower may become an issue in regions upstream on the Missouri River system.

Economic integration of the MINK region is being accomplished using the IMPLAN regional input-output model, originally developed for the U.S. Forest Service. During FY 1989, work has focused on collecting economic data and describing the baseline economy so that the IMPLAN modeling system can analyze it. IMPLAN is a flexible modeling system based on a 500-plus sector national input-output table that can be adapted to any state or regional economy in the United States. Although much of the characterization of the MINK economy has been done, appropriate aggregation of the sectors remains to be accomplished, along with identification and measurement of the economic base of the MINK region, appropriate modeling of inputs for the agricultural sector, and exercising the model with climate change.

Studies are continuing at this time. The principal remaining work efforts are development of the expert system for analysis of farmer decisions, technology trends analysis, integration of the regional economy and responses into the IMPLAN system, and analysis of analog climate in the newly developed model system. Completion of this work is scheduled for the end of FY 1990. Concurrent with this effort will be extensive work on uncertainty issues, with some formal analysis being devoted to the problems posed by propagation of uncertainty within and between models. A methodological paper is currently in preparation that addresses strategies for coping with this uncertainty.

Summary

The Resources Analysis Program is involved in analysis of the potential impacts of climate change on natural and human resources at the regional level. The current work represents several advances over previous analyses: 1) the study deals with the region as a whole rather than isolated resources or sectors; 2) CO_2 fertilization and climate change are treated realistically in submodels of plant physiology; 3) technological change and the other effects of time are incorporated in the analysis; 4) regional context is established, with external influences such as world crop prices treated explicitly in expert systems; 5) the analysis also explicitly accounts for uncertainty.

Acknowledgment

The study team also includes Jae Edmonds and Al Liebetrau of PNL, Bill Easterling, Mary McKenney, Pierre Crosson, Michael Bowes, Ken Frederick, Joel Darmstadter, and Roger Sedjo of Resources for the Future (RFF), Carolyn Hunsaker of ORNL, and Gary Yohe and Tom Malone from Sigma Xi.

References

Easterling, W. E., III, M. L. Parry, and P. R. Crosson. 1989. "Adapting Future Agriculture to Changes in Climate." In *Greenhouse Warming: Abatement and Adaptation*, N. J. Rosenberg, W. Easterling III, P. R. Crosson, and J. Darmstadter, eds. Resources for the Future, Washington, D.C..

Edmonds, J. A., R. M. Cushman, W. Easterling, N. J. Rosenberg, T. Malone, G. Yohe, M. J. Scott, and G. M. Stokes. 1989. "Criteria for Selecting a CO_2/Climate Change Region of Study." Paper 89-148.7. Presented at the 82nd Annual Meeting and Exhibition, Air and Waste Management Association, Anaheim, California, June 28, 1989.

Martin, P., N. J. Rosenberg, and M. S. McKenney. 1989. "Sensitivity of Evapotranspiration in a Wheat Field, a Forest and a Grassland to Changes in Climate and Direct Effects of Carbon Dioxide." *Climatic Change* 14:117-151.

Scott, M. J., N. J. Rosenberg, J. A. Edmonds, R. M. Cushman, R. F. Darwin, G. W. Yohe, A. M. Liebetrau, C. T. Hunsaker, D. A. Bruns, D. L. DeAngelis, and J. M. Hales. 1990. "Consequences of Climatic Change for the Human Environment." *Energy and Climate Changes*. Lewis Publishers, Chelsa, Michigan.

Solomon, A. M., M. L. Thorp, D. C. West, G. E. Taylor, J. W. Webb, and J. L. Trimble. 1984. *Response of Unmanaged Forests to CO_2 Induced Climate Change: Available Information, Initial Tests, and Data Requirements.* U.S. DOE TR009, NBB-0053. U.S. Department of Energy, Washington, D.C.

Solomon, A. M., and D. C. West. 1987. "Simulating Forest Ecosystem Responses to Expected Climate Change in Eastern North America: Applications to Decision Making in the Forest Industry." In *The Greenhouse Effect, Climate Change, and U.S. Forests*, W. E. Shands, ed. Conservation Foundation, Washington, D.C.

Sonka, S. T., and P. Lamb. 1987. "On Climate Change and Economic Analysis." *Climatic Change* 11:291-312.

Williams, J. R., C. A. Jones, and P. T. Dyke. 1984. "A Modeling Approach to Determining the Relationship Between Erosion and Soil Productivity." *Transactions of the American Society of Agricultural Engineers* 27:129-144.

U.S. Environmental Protection Agency (EPA). 1989. *The Potential Effects of Global Climate Change on the United States*. Washington, D.C.

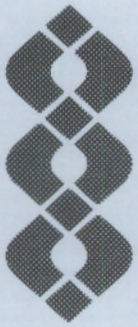

Publications and Presentations

PUBLICATIONS

Allwine, K. J., and C. D. Whiteman. 1988. "Ventilation of Pollutants Trapped in Valleys: A Simple Parameterization for Regional-Scale Disposition Models." *Atmos. Environ.* 22(9):1839-1845.

Bader, D. C., and C. D. Whiteman. 1989. "Numerical Simulation of Cross-Valley Plume Dispersion During the Morning Transition Period." *J. Appl. Meteor.* 28:652-664.

Dana, M. Terry, and W. R. Barchet. 1989. *The MAP3S Precipitation Chemistry Network: Data and Quality Control Summary for 1986 and 1987.* PNL–6885, Pacific Northwest Laboratory, Richland, Washington.

Davis, W. E., A. R. Olsen, and B. T. Didier. 1989. "MLAM Assessment of Radionuclide Air Concentration and Deposition for the Chernobyl Reactor Accident." In *Air Pollution Modeling and its Application.* VII:123-126, Plenum Publishing Corp., New York.

Davis, W. E., A. R. Olsen, B. T. Didier, P. E. Tucker, and D. W. Damschen. 1989. *Surface Footprint from Initial Chernobyl Release as Indicated by the Meso-Alpha MLAM Model.* PNL–7186, Pacific Northwest Laboratory, Richland, Washington.

Doran, J. C., M. L. Wesely, R. T. McMillen, and W. D. Neff. 1989. "Measurements of Turbulent Heat and Momentum Fluxes in a Mountain Valley." *J. Appl. Meteor.* 28:438-444.

Edmonds, J. A., and J. Darmstadter. 1989. "Human Development and CO_2 Emissions: The Current Picture and Long-Term Prospects." In *Greenhouse Warming: Abatement and Adaptation.* N. J. Rosenberg, W. Easterling III, P. R. Crosson, and J. Darmstadter, eds. Resources for the Future, Washington, D.C.

Edmonds, J. A. 1989. "Caveats in Global Energy Modeling--Editorial Response." *Climate Change*, Vol. 13.

Horst, T. W., D. C. Bader, and C. D. Whiteman. 1989. "Comparison of Observed and Simulated Nocturnal Valley Thermal Energy Budgets." *Preprints, International Conference on Mountain Meteorology and ALPEX*, June 5-9, Garmisch-Partenkirchen, FRG, p. 127.

Olsen, A. R., W. E. Davis, B. T. Didier, J. K. Soldat, B. A. Napier, and R. A. Peloquin. 1989. *MLAM Assessment of Air Concentration, Deposition, and Dose for Chernobyl Reactor Accident.* PNL-7197, Pacific Northwest Laboratory, Richland, Washington.

Parkhurst, R. G., and M. Terry Dana. 1989. *Precipitation Chemistry Quarterly Report.* Vol. 21, No. 3, Third Quarter, 1988. Pacific Northwest Laboratory, Richland, Washington.

Pinksterboer, E. F., J. -W. Erisman, H. F. Maas, W.A.H. Asman, A. Waijers-Ypelaan, J. Slanina, and T. W. Horst. 1989. "Spatial Variation in the Ammonia Concentration in a Nature Reserve: Measurements vs. Model Results." *Atmos. Environ.* 23:2259-2265.

Ramsdell, J. V., J. M. Hubbe, G. F. Athey, and W. E. Davis. 1989. *MESORAD Dose Assessment of the Chernobyl Reactor Accident.* PNL–7185, Pacific Northwest Laboratory, Richland, Washington.

Scott, M. J., J. A. Edmonds, A. Liebetrau, and J. M. Hales. 1990. "Consequences of Climatic Change for the Human Environment." *Climate Research*, in press.

Scott, M. J., J. A. Edmonds, M. A. Kellogg, and R. W. Schultz. 1989. "Global Energy and the Greenhouse Issue." In *World Energy Conference 14th Congress: Energy for Tomorrow.* pp. 1-20. Montreal, Quebec, Canada, Sept. 17-22, 1989.

Sisterson, D. L., J. L. Shannon, P. H. Daum, P. J. Kotz, D. J. Luecken, and D. J. Hall. 1989. "The Snowfall Chemistry Collector Intercomparison Test (SCCIT)." *Water, Air, and Soil Pollution* 48:477-488.

Slinn, W.G.N. 1990. "Hints of Another Gremlin in the Greenhouse: Anthropogenic Sulfur." *Atmos. Environ.*, in press.

Slinn, W.G.N. 1990. "Response to R. Jaenicke." *Tellus* 41B:562-563.

Slinn, W.G.N. 1990. "A Proposed Test of Two Hypotheses Related to Concentration Fluctuations and Residence Times." *Tellus* 41B, in press.

Tomich, S. D., and M. Terry Dana. 1989. "Computer Controlled Automated Rain Sampler (CCARS) for Rainfall Measurement and Sequential Sampling." Submitted to *J. of Oceanic and Atmospheric Technology*.

Whiteman, C. D., J. M. Hubbe, J. C. Doran, and T. B. McKee. 1989. "Atmospheric Mass and Heat Budgets in a Closed Canyonland Basin." *Preprints, International Conference on Mountain Meteorology and ALPEX*, June 5-9, Garmisch-Partenkirchen, FRG, pp. 116-117.

Whiteman, C. D. 1990. "Observations of Thermally Developed Wind Systems in Mountainous Terrain." Chapter 2 in *Current Directions in Atmospheric Processes Over Complex Terrain*, W. Blumen, ed., *Meteorological Monographs* 45:5-42, American Meteorological Society, Boston, Massachusetts.

Whiteman, C. D. 1989. "Morning Transition Tracer Experiments in a Deep Narrow Valley." *J. Appl. Meteor.* 28:626-635.

Whiteman, C. D., K. J. Allwine, M. M. Orgill, L. J. Fritschen, and J. R. Simpson. 1989. "Deep Valley Radiation and Surface Energy Budget Microclimates. I. Radiation." *J. Appl. Meteor.* 28:414-426.

Whiteman, C. D., K. J. Allwine, M. M. Orgill, L. J. Fritschen, and J. R. Simpson. 1989. "Deep Valley Radiation and Surface Energy Budget Microclimates. II. Energy Budget." *J. Appl. Meteor.* 28:427-437.

PRESENTATIONS

Dana, M. Terry, and W. R. Barchet. 1989. "Time Trends for Acidic Precipitation Species at MAP3S Network Sites." Abstract submitted for presentation at the Second International Conference on Acid Rain, September 5, Amsterdam, The Netherlands.

Dana, M. Terry, W. E. Davis, J. M. Hales, P. Michael, P. Daum, and L. Kleinman,. 1989. "Pollutant Distributions in Extratropical Cyclones." Abstract submitted for the Fall AGU Meeting, December 1989, San Francisco, California.

Doran, J. C., and E. D. Skyllingstad. 1989. "Observed and Modeled Terrain-Induced Shear in Tracer Trajectories." Presented at the 6th Joint Conference on Applications of Air Pollution, January 29-February 3, Anaheim, California.

Edmonds, J. A. 1989. "Policy Issues Associated with Acid Deposition and Global Climate Change." Presented at IEEE Meeting, February 16, New York.

Edmonds, J. A. 1989. "Forecasting Future Greenhouse Gas Emissions." Presented at Stanford University, February 22, Stanford, California.

Edmonds, J. A. 1989. "Forecasting Future Greenhouse Gas Emissions." Presented at the PNL Global Change Workshop, February 27, Richland, Washington.

Edmonds, J. A. 1989. "Forecasting Future Greenhouse Gas Emissions." Presented to the PNL Technology Planning and Analysis Center, February 28, Richland, Washington.

Gudiksen, P. W., W. E. Clements, R. P. Hosker, Jr., C. D. Whiteman, W. D. Neff, R. L. Coulter, and G. E. Start. 1989. "Field Studies for Determining the Characteristics and Dynamics of Local Circulations." Presented at the Second International Workshop on Real-Time Computing of the Environmental Consequences of an Accidental Release to Atmosphere from a Nuclear Installation, May 15-19, Commission of the European Communities, Luxembourg.

Hales, J. M. 1989. "Model Investigations of Nonlinearities in Wet Removal of Pollutants." Presented at the 198th National Meeting of the American Chemical Society, September 10-15, Miami Beach, Florida.

Hales, J. M., and D. S. Renne. 1989. "Approaches to Determining Source-Receptor Relationships." Presented at the 82nd Annual Meeting of the Air Pollution Control Association, June 26-30, Anaheim, California.

Kerr, R. M., R. Rotunno, W. Wu, and T. W. Horst. 1988. "Length Scales for Rayleigh-Benard Convection." Presented at the American Physical Society Division of Fluid Dynamics Annual Meeting, November 20-22, Buffalo, New York.

Li, S. W., et al. 1989. "Influence of Fog Oil Obscurant Smoke on Soil Microbial Activities." Presented at the American Society of Microbiology Annual Meeting, May 14-18, New Orleans, Louisiana.

Scott, M. J. 1989. "Criteria for Selecting a CO_2/Global Climate Change Region of Study." Presented at the 82nd Annual Meeting and Exposition of the Air and Waste Management Association, June 28, Anaheim, California.

Scott, M. J., 1989. "Global Warming and the Greenhouse Effect: How It Can Change our Lives." Presented at the National Association of Counties 54th Annual Conference, July 15, Cincinnati, Ohio.

Scott, M. J. 1989. "Pacific Northwest Global Climate Effects Case Study: Overview of Resource Implications and Impacts." Presented at Participants Meeting on Pacific Northwest Global Climate Effects Case Study, October 13, Portland, Oregon.

Scott, M. J. 1989. "Global Environmental Change and Socioeconomic Impacts: Estimating Costs to Society." Presented at the Hanford Technical Exchange, October 11, Richland, Washington.

Slinn, W. G. N. 1989. "Constraints from Data on Suggested Influences of Natural and Anthropogenic Sulfur on Climate Change." Presented at the Eighth Annual Meeting of the American Association for Aerosol Research, Symposium on Global Climatic Effects of Aerosols and the Role of Oceanic Emissions on Cloud Properties, October 9-13, 1989, Reno, Nevada.

Author Index

AUTHOR INDEX

Distribution

DISTRIBUTION

No. of Copies

OFFSITE

12 DOE/Office of Scientific and Technical Information

R. E. Alexander
ORPBR, NL
U.S. Nuclear Regulatory Commission
Washington, DC 20545

D. Anderson
ENVIROTEST
1108 N.E. 200th St.
Seattle, WA 98155

J. A. Auxier
IT Corporation
312 Director's Dr.
Knoxville, TN 37701

F. Badgley
13749 41st Street, N.E.
Seattle, WA 98125

R. E. Baker
8904 Roundleaf Way
Gaithersburg, MD 20879-1630

R. W. Barber
EH-131, GTN
U.S. Department of Energy
Washington, DC 20545

A. D. Barker
Battelle Columbus Division
505 King Avenue
Columbus, OH 43201

J. R. Barker
Office of Environmental Audit and Compliance
U.S. Department of Energy
Washington, DC 20545

No. of Copies

H. M. Barnes
ASRL (MD-39)
U.S. Environmental Protection Agency
Research Triangle Park, NC 27711

N. F. Barr
ER-72, GTN
U.S. Department of Energy
Washington, DC 20545

S. Barr
Environmental Studies Group
MS-F665
Los Alamos National Laboratory
P.O. Box 1663
Los Alamos, NM 87544

J. F. Boatman
NOAA/R/E/AR4
325 Broadway
Boulder, CO 80303

L. C. Brazley, Jr.
NE-22, GTN
U.S. Department of Energy
Washington, DC 20545

J. C. Brown
Environmental Studies Group
MS-A114
Los Alamos National Laboratory
P.O. Box 1663
Los Alamos, NM 87545

P. Buhl
FE-232, GTN
U.S. Department of Energy
Washington, DC 20545

No. of Copies

G. Burley
Office of Radiation Programs (ANR-458)
U.S. Environmental Protection Agency
Washington, DC 20460

W. W. Burr
Medical & Health Sciences Division
Oak Ridge Associated Universities
P.O. Box 117
Oak Ridge, TN 37830

L. K. Bustad
College of Veterinary Medicine
Washington State University
Pullman, WA 99164-7010

R. J. Catlin
Robert J. Catlin Corporation
701 Welch Road, Suite 1119
Palo Alto, CA 94304

J. Chang
Atmospheric Sciences Research Center
State University of New York at Albany
100 Fuller Road
Albany, NY 80307

R. J. Charlson
Department of Atmospheric Sciences, AK-40
University of Washington
Seattle, WA 98195

No. of Copies

Council on Environmental Quality
722 Jackson Place, NW
Washington, DC 20503

T. V. Crawford
E. I. duPont de Nemours and Co.
Atomic Energy Division
Savannah River Laboratory
Aiken, SC 29808

J. B. Cunning
NOAA/ERL
325 Broadway
Boulder, CO 80303

P. H. Daum
Brookhaven National Laboratory
Upton, Long Island, NY 11973

K. Demerjian
Atmospheric Sciences Research Center
State University of New York at Albany
100 Fuller Road
Albany, NY 80307

R. L. Dennis
ASRL (MD-80)
U.S. Environmental Protection Agency
Research Triangle Park, NC 27711

G. DePlanque, Director
Environmental Measurements Laboratory
U.S. Department of Energy
375 Hudson Street
New York, NY 10014

No. of Copies

M. H. Dickerson
Lawrence Livermore National Laboratory
L-262
P.O. Box 808
Livermore, CA 94550

R. R. Dickerson
Department of Meteorology
University of Maryland
College Park, MD 20742

H. Drucker
Argonne National Laboratory
9700 South Cass Avenue
Argonne, IL 60439

A. P. Duhamel
ER-74, GTN
Department of Energy
Washington, DC 20545

J. L. Durham
ASRL (MD-59)
U.S. Environmental Protection Agency
Research Triangle Park, NC 27711

C. W. Edington, Director
Board on Radiation Effects Research
National Research Council
2101 Constitution Avenue, NW
Washington, DC 20418

R. J. Engelmann
11701 Karen
Potomac, MD 20854

B. M. Erickson
DOE - Schenectady Naval Reactors Office
P.O. Box 1069
Schenectady, NY 12301

No. of Copies

G. J. Foley
EMSL (MD-75)
U.S. Environmental Protection Agency
Research Triangle Park, NC 27711

T. F. Gesell
Idaho Operations Office
U.S. Department of Energy
785 DOE Place
Idaho Falls, ID 83402-4149

R. D. Gilmore
Environmental Health Sciences, Inc.
Nine Lake Bellevue Building, Suite 104
Bellevue, WA 98005

G. H. Groenewold
Energy and Mineral Research Center
University of North Dakota
Box 8213, University Station
Grand Forks, ND 58202

J. W. Healy
51 Grand Canyon Drive
White Rock, NM 87544

B. Hicks
Atmospheric Turbulence and Diffusion Laboratory
National Oceanic and Atmospheric Administration
P.O. Box 2456
Oak Ridge, TN 37830

R. O. Hunter
ER-1, FORS
U.S. Department of Energy
Washington, DC 20585

No. of Copies

F. Hutchinson
Department of Molecular Biophysics and Biochemistry
Yale University
260 Whitney Ave.
P.O. Box 6666
New Haven, CT 06511

H. Ishikawa
Nuclear Safety Research Association
P.O. Box 1307
Falls Church, VA 22041

A. W. Johnson
Vice President for Academic Affairs
San Diego State University
San Diego, CA 92128

L. J. Johnson
Idaho National Engineering Lab
IRC MS 2203
P.O. Box 1625
Idaho Falls, ID 83415

G. Y. Jordy
ER-30, GTN
U.S. Department of Energy
Washington, DC 20545

F. Koomonoff
ER-12, GTN
U.S. Department of Energy
Washington, DC 20545

R. Kornasiewicz
Mail Stop 1130-55, ONRR
U.S. Nuclear Regulatory Commission
Washington, DC 20555

R. T. Kratzke
NP-40
U.S. Department of Energy
Washington, DC 20585

No. of Copies

D. Lal
Geological Research Division A-020
Scripps Institute of Oceanography
La Jolla, CA 92093

T. V. Larsen
Department of Civil Engineering
University of Washington
Seattle, WA 98195

W. Lauder
Office of Health and Environmental Research
Office of Energy Research
U.S. Department of Energy
Germantown, MD 20545

L. Levin
Electric Power Research Institute
3412 Hillview Ave.
P.O. Box 10412
Palo Alto, CA 94303

Librarian
Brookhaven National Laboratory
Research Library, Reference
Upton, Long Island, NY 11973

Librarian
Colorado State University
Documents Department—The Libraries
Ft. Collins, CO 80521

Librarian
Electric Power Research Institute
3412 Hillview Ave.
P.O. Box 10412
Palo Alto, CA 94303

No. of Copies

Librarian
Atmospheric Sciences Library, AK-50
University of Washington
Seattle, WA 98195

Librarian
Health Sciences Library, SB-55
University of Washington
Seattle, WA 98195

Librarian
Lawrence Livermore National Laboratory
University of California
Technical Information Dept., L-3
P.O. Box 808
Livermore, CA 94550

Librarian
Los Alamos National Laboratory
MS P364
P.O. Box 1663
Los Alamos, NM 87545

Librarian
National Oceanic and Atmospheric Administration
Atmospheric Turbulence and Diffusion Laboratory
P.O. Box 2456
Oak Ridge, TN 37831

Librarian
Washington State University
Pullman, WA 99164-6510

Library
Serials Department (#80-170187)
University of Chicago
1100 East 57th Street
Chicago, IL 60637

No. of Copies

I. R. Linger
ER-63, GTN
U.S. Department of Energy
Washington, DC 20545

D. L. Lundgren
Lovelace - ITRI
P.O. Box 5890
Albuquerque, NM 87185

O. R. Lunt
Laboratory of Nuclear Medicine and Radiation Biology
University of California
900 Veteran Avenue
West Los Angeles, CA 90024

J. N. Maddox
ER-73, GTN
U.S. Department of Energy
Washington, DC 20545

W. J. Madia
Battelle Columbus Division
505 King Avenue
Columbus, OH 43201

J. R. Maher
ER-65, GTN
U.S. Department of Energy
Washington, DC 20545

J. Mahoney
National Acid Precipitation Assessment Program
722 Jackson St.
Washington, DC 20006

B. Manowitz
Energy and Environment Division
Brookhaven National Laboratory
Upton, Long Island, NY 11973

S. Marks
8024 47th Place West
Mukilteo, WA 98275

D. D. Mayhew
ER-63, GTN
U.S. Department of Energy
Washington, DC 20545

H. M. McCammon
ER-75, GTN
U.S. Department of Energy
Washington, DC 20545

C. B. Meinhold
Radiological Sciences Division
Bldg. 703M
Brookhaven National Laboratory
Upton, Long Island, NY 11973

M. L. Mendelsohn
Biomedical and Environmental Research Program
Lawrence Livermore National Laboratory, L-452
University of California
P.O. Box 5507
Livermore, CA 94550

P. Michael
Brookhaven National Laboratory
Upton, NY 11973

C. Miller
P.O. Box 180
Watermill, NY 11976

M. L. Minthorn, Jr.
ER-72, GTN
U.S. Department of Energy
Washington, DC 20545

V. Mohnen
State University of New York at Albany
100 Fuller Road
Albany, NY 80307

B. Morgan
Environmental Division
DOE - Savannah River Operations Office
P.O. Box A
Aiken, SC 29801

H. Moses
ER-74, GTN
U.S. Department of Energy
Washington, DC 20545

P. K. Mueller
Environmental Science Department
Electric Power Research Institute
3412 Hillview Ave.
P.O. Box 10412
Palo Alto, CA 94304

R. Nathan
Battelle Project Management Division
505 King Avenue
Columbus, OH 43201

W. Neff
Wave Propogation Lab, NOAA
325 Broadway
Boulder, CO 80303

N. S. Nelson
U.S. Environmental Protection Agency
Washington, DC 20460

L. Newman
Brookhaven National Laboratory
Upton, Long Island, NY 11973

No. of Copies

W. R. Ney
National Council on Radiation Protection and Measurements
Suite 1016
7910 Woodmont Avenue
Bethesda, MD 20814

Nuclear Regulatory Commission
Advisory Committee on Reactor Safeguards
Washington, DC 20555

M. J. O'Brien
Radiation Safety Office, GS-05
University of Washington
Seattle, WA 98105

A. A. Patrinos
ER-74, GTN
U.S. Department of Energy
Washington, DC 20545

R. Pawr
EMSL (MD-44)
U.S. Environmental Protection Agency
Research Triangle Park, NC 27711

A. A. Pitrolo
Morgantown Energy Research Center
U.S. Department of Energy
P.O. Box 880
Morgantown, WV 26505

D. P. Rall
NIEHS
P.O. Box 12233
Research Triangle Park, NC 27709

No. of Copies

C. R. Richmond
Oak Ridge National Laboratory
4500N, MS-62523
P.O. Box 2008
Oak Ridge, TN 37831-6253

J. S. Robertson
ER-73, GTN
U.S. Department of Energy
Washington, DC 20545

S. L. Rose
ER-73, GTN
U.S. Department of Energy
Washington, DC 20545

R. D. Rosen
Environmental Measurements Laboratory
U.S. Department of Energy
376 Hudson Street
New York, NY 10014

J. M. Rusin
404 W. Halladay
Seattle, WA 98119

L. Sagan
Electric Power Research Institute
3412 Hillview Avenue
P.O. Box 10412
Palo Alto, CA 94304

P. Samson
Atmospheric and Oceanic Sciences
University of Michigan
Ann Arbor, MI 48109

R. A. Scarano
Mill Licensing Section
U.S. Nuclear Regulatory Commission
Washington, DC 20545

No. of Copies

F. A. Schiermeier
Atmospheric Sciences Modeling Division (MD-80)
U.S. Environmental Protection Agency
Research Triangle Park, NC 27711

M. Schulman
ER-70, GTN
U.S. Department of Energy
Washington, DC 20545

R. B. Setlow
Brookhaven National Laboratory
Upton, NY 11973

R. Shikiar
Battelle - Seattle
4000 NE 41st Street
Seattle, WA 98105

P. Silverman
Lawrence Berkeley Laboratory
Bldg. 50A/5104
Berkeley, CA 94720

J. Simmons
Bioeffects Analysis Branch
U.S. Environmental Protection Agency
401 M Street, S.W.
Washington, DC 20460

W. K. Sinclair
National Council on Radiation Protection and Measurements
Suite 1016
7910 Woodmont Avenue
Bethesda, MD 20814

D. H. Slade
ER-74, GTN
U.S. Department of Energy
Washington, DC 20545

No. of Copies

C. Spicer
Battelle Columbus Division
505 King Avenue
Columbus, OH 43201

J. N. Stannard
17441 Plaza Animado #132
San Diego, CA 92128

R. J. Stern
EH-10, FORS
U.S. Department of Energy
Washington, DC 20585

J. F. Stevens
Dayton Area Office
DOE - Albuquerque Operations Office
P.O. Box 66
Miamisburg, OH 45342

E. T. Still
Kerr-McGee Corporation
P.O. Box 25861
Oklahoma City, OK 73125

P. Stone
ER-6, FORS
U.S. Department of Energy
Washington, DC 20585

G. M. Sverdrup
Battelle Columbus Division
505 King Avenue
Columbus, OH 43201

J. Swinebroad
EH-12, GTN
U.S. Department of Energy
Washington, DC 20545

No. of Copies

Technical Information Service
Savannah River Laboratory
Room 773A
E. I. duPont de Nemours & Company
Aiken, SC 29801

R. G. Thomas
ER-72, GTN
U.S. Department of Energy
Washington, DC 20545

U.S. Department of Energy
Environment, Safety and Health Division
P.O. Box 5400
Albuquerque, NM 87115

E. J. Vallario
15228 Red Clover Drive
Rockville, MD 20853

B. Vallet
NORCUS
390 Hanford St.
Richland, WA 99352

C. R. Vest
Battelle, Pacific Northwest Laboratory
Washington Operations
370 L'Enfant Promenade, Suite 900
901 D Street, SW
Washington, DC 20024

G. J. Vodapivc
DOE - Schenectady Naval Reactors Office
P.O. Box 1069
Schenectady, NY 12301

No. of Copies

G. L. Voelz
Los Alamos National Laboratory, MS K404
P.O. Box 1663
Los Alamos, NM 87545

B. W. Wachholz
Radiation Effects Branch
National Cancer Institute
EPN, Room 530
8000 Rockville Pike
Bethesda, MD 20892

M. L. Walker
EH-1, FORS
U.S. Department of Energy
Washington, DC 20585

R. A. Walters
Los Alamos National Laboratory
MS-A114
P.O. Box 1663
Los Alamos, NM 87545

C. G. Welty, Jr.
EH-123, GTN
U.S. Department of Energy
Washington, DC 20545

I. Wender
Department of Chemical Engineering
1249 Benedum Hall
University of Pittsburgh
Pittsburgh, PA 15261

M. L. Wesely
Argonne National Laboratory
Building 203, ER
Argonne, IL 60439

No. of Copies

W. W. Weyzen
Electric Power Research Institute
3412 Hillview Avenue
P.O. Box 10412
Palo Alto, CA 92665

R. W. Wood
ER-74, GTN
U.S. Department of Energy
Washington, DC 20545

Zhu Zhixian
Laboratory for Energy-Related Health Research
University of California
Davis, CA 95616

FOREIGN

E. L. Alpen
University of California Study Center
21 Stratton Ground
London SW1 P2HY
ENGLAND

W. A. Asman
National Environmental Institute
P.O. Box 1
NL-3720 BA Bilthoven
THE NETHERLANDS

D. C. Aumann
Institut für Physikalische Chemie
Der Universität Bonn
Abt. Nuklearchemie
Wegelerstraße 12
5300 Bonn 1
FEDERAL REPUBLIC OF GERMANY

No. of Copies

J. K. Basson
Raad Op Atomic
Atoomkrag Energy Board
Privaatsk X 256
Pretoria 0001
REPUBLIC OF SOUTH AFRICA

A. M. Beau, Librarian
Commissariat à l'Energie Atomique
Département de Protection Sanitaire
BP No. 6
F-92260 Fontenay-aux-Roses
FRANCE

G. Bengtsson
Statens Stralskyddsinstitut
Box 60204
S-104 01 Stockholm
SWEDEN

D. J. Beninson
Gerencia de Protection Radiologica y Seguridad
Comision Nacional de Energia Atomica
Avenida del Libertador 8250
1429 Buenos Aires
ARGENTINA

R. Berkowicz
Air Pollution Laboratory
National Agency for Environmental Protection
Risø National Laboratory
DK-4000 Roskilde
DENMARK

N. Busch
Risø National Laboratory
DK-4000 Roskilde
DENMARK

No. of Copies

Cao Shu-yuan, Deputy Head
Laboratory of Radiation Medicine
North China Institute of Radiation Protection
Tai-yuan, Shan-xi
THE PEOPLE'S REPUBLIC OF CHINA

M. Carpentier
Commission of the E.C.
200 Rue de la Loi
J-70 6/16
B-1049 Brussels
BELGIUM

CEC
DG XII Library
SDM8 R1
200 rue de la Loi
B-1049 Brussels
BELGIUM

Chen Xing-an, M.D.
Laboratory of Industrial Hygiene
Ministry of Public Health
2 Xinkang Street
Deshengmanwai, Beijing
THE PEOPLE'S REPUBLIC OF CHINA

G. H. Clark
Australian Nuclear Science and Technology Organization
Environmental Science Division
Private Mail Bag 1
Menai NSW 2234
AUSTRALIA

No. of Copies

R. Clarke
National Radiological Protection Board
Harwell, Didcot
Oxon OX11 ORQ
ENGLAND

P. Crutzen, Director
Atmospheric Chemistry
Max-Planck-Institut für Chemie
Postfach 3060
D-6500 Mainz
FEDERAL REPUBLIC OF GERMANY

Deng Zhicheng
North China Institute of Radiation Protection
Tai-yuan, Shan-xi
THE PEOPLE'S REPUBLIC OF CHINA

Director
Commissariat à l'Energie Atomique
Centre d'Etudes Nucléaires
Fontenay-aux-Roses (Seine)
FRANCE

Director
Commonwealth Scientific and Industrial Research Organization
Aspendal, Victoria
AUSTRALIA

Director
Laboratorio di Radiobiologia Animale
Centro di Studi Nucleari Della Casaccia
Comitate Nazionale per l'Energia Nucleare
Casella Postale 2400
00100 Roma
ITALY

D. Djuric
Institute of Occupational and Radiological Health
11000 Beograd
Deligradoka 29
YUGOSLAVIA

H. Dovland
Director
Norwegian Institute for Air Research
Elvegaten 52
N-2001 Lillestrom
NORWAY

H. J. Dunster
National Radiological Protection Board
Harwell, Didcot
Oxon OX11 ORQ
ENGLAND

L. Feinendegen, Director
Institut für Medezin
Kernsforschungsanlage Jülich
Postfach 1913
D-5170 Jülich
FEDERAL REPUBLIC OF GERMANY

R. M. Fry
Office of the Supervising Scientist for the Alligator Rivers Region
P.O. Box 387
Bondi Junction NSW 2022
AUSTRALIA

A. Geertsema
SASOL
P.O. Box 95
Sasolburg 9570
REPUBLIC OF SOUTH AFRICA

G. B. Gerber
Radiobiology Department
Commission of European Communities
200 rue de la Loi
B-1049 Brussels
BELGIUM

A. R. Gopal-Ayengar
73-Mysore Colony
Mahul Road, Chembur
Bombay-400 074
INDIA

P. Grennfelt
Swedish Environmental Research Institute
P.O. Box 47086
S-402 58 Göteborg
SWEDEN

S. E. Gryning
Physics and Meteorology
Risø National Laboratory
DK-4000 Roskilde
DENMARK

G. F. Gualdrini
ENEA
3 v. le Ercolani
I-40138 Bologna
ITALY

J. L. Head
Department of Nuclear Science & Technology
Royal Naval College, Greenwich
London SE10 9NN
ENGLAND

O. Hov
Norwegian Institute for Air Research
Elvegaten 52
N-2001 Lillestrom
NORWAY

No. of Copies

P. Hummelshoej
Physics and Meteorology
Risø National Laboratory
DK-4000 Roskilde
DENMARK

K. E. Lennart Johansson
Radiofysiska Inst.
Regionsjukhuset
S-901 82 Umeå
SWEDEN

H. J. Klimisch
BASF Aktiengesellschaft
Abteilung Toxikologie
Z470
D-6700 Ludwigshafen
FEDERAL REPUBLIC
OF GERMANY

L. Kristensen
Physics and Meteorology
Risø National Laboratory
DK-4000 Roskilde
DENMARK

T. Kumatori
National Institute of
Radiological Sciences
9-1, Anagawa 4-chome
Chiba-shi 260
JAPAN

A. Lacser
Israel Institute of
Biological Research
Department of Mathematics
P.O. Box 19
7004 50
Ness-Ziona
ISRAEL

S. E. Larsen
Physics and Meteorology
Risø National Laboratory
DK-4000 Roskilde
DENMARK

No. of Copies

H. P. Leenmouts
National Institute of
Public Health and
Environmental Hygiene
P.O. Box 1
NL-3720 BA, Bilthoven
THE NETHERLANDS

Li De-ping
Professor and Director
of North China Institute
of Radiation Protection,
NMI
Tai-yuan, Shan-xi
THE PEOPLE'S
REPUBLIC OF CHINA

Librarian
Centre d'Etudes
Nucléaires de Saclay
P.O. Box 2, Saclay
Fig-sur-Yvette (S&O)
FRANCE

Librarian
Commonwealth Scientific
and Industrial Research
Organization
314 Albert Street
P.O. Box 89
East Melbourne, Victoria
AUSTRALIA

Librarian
Commonwealth Scientific
and Industrial Research
Organization
Div. of Atmospheric
Research
Station Street
Aspendale, Vic. 3195
AUSTRALIA

Librarian
ECN
3 Westerdiunweg
NL-1755 ZG Petten
THE NETHERLANDS

No. of Copies

Librarian
ENEA (OECD) Health and
Safety Office
38, Blvd. Suchet
Paris
FRANCE

Librarian
Fraunhofer Institute
for Atmospheric
Environmental Research
Kreuzeckbahnstr. 19
D-8100 Garmisch-
Partenkirchen
FEDERAL REPUBLIC
OF GERMANY

Librarian
HCS/EHE
World Health Organization
CH-1211 Geneva 27
SWITZERLAND

Librarian
Kernforschungzentrum
Karlsruhe
Institut für
Strahlenbiologie
D-75 Karlsruhe 1
Postfach 3640
FEDERAL REPUBLIC
OF GERMANY

Librarian
Max-Planck-Institut für
Biophysics
Forstkasstrasse
D-6000 Frankfurt/Main
FEDERAL REPUBLIC
OF GERMANY

Librarian
Ministry of Agriculture,
Fisheries and Food
Fisheries Laboratory
Lowestoft, Suffolk
NR33 OHT
ENGLAND

No. of Copies

Librarian
National Institute of Radiological Sciences
9-1, Anagawa 4-chome
Chiba-shi 260
JAPAN

Library
Risø National Laboratory
DK-4000 Roskilde
DENMARK

Library, Periodicals
Atomic Energy Commission of Canada, Ltd.
Pinawa, Manitoba
ROE 1L0
CANADA

Library
Department of Meteorology
University of Stockholm
Arrhenius Laboratory
S-106 91 Stockholm
SWEDEN

A. M. Marko
Atomic Energy Commission of Canada, Ltd.
Biology and Health Physics Division
Chalk River Nuclear Laboratories
P.O. Box 62
Chalk River, Ontario
KOJ IJO
CANADA

J. C. Nénot
Département de Protection
Centre d' Etudes Nucléaires
BP No. 6
F-92260 Fontenay-aux-Roses
FRANCE

No. of Copies

J. P. Oliver
ENEA (OECD) Health and Safety Office
38, Blvd. Suchet
Paris
FRANCE

N. Parmentier
Département de Protection
Centre d'Etudes Nucléaires
BP No. 6
F-92260 Fontenay-aux-Roses
FRANCE

L. Prahm
Danish Meteorological Institute
Lyngbyvej 100
DK-2100 Copenhagen East
DENMARK

V. Prodi
Department of Physics
University of Bologna
Via Irnerio 46
I-40126 Bologna
ITALY

P. J. A. Rombout
Inhalation of Toxicology Department
National Institute of Public Health and Environmental Hygiene
P.O. Box 1
NL-3720 BA, Bilthoven
THE NETHERLANDS

No. of Copies

M. Roy
Institut de Protection et de Sureté Nucléaire
Department de Protection Sanitaire
Service d'Etudes Apliquées de Protection Sanitaire
BP No. 6
F-92260 Fontenay-aux-Roses
FRANCE

M. Rzekiecki
Commissariat à l'Energie Atomique
Centre d'Etudes Nucléaires de Cadarache
BP No. 13-St. Paul
Les Durance
FRANCE

G. Schnatz
Battelle-Europe eV
Am Römerhof 35
P.O. Box 900160
D-6000 Frankfurt a.M.
FEDERAL REPUBLIC OF GERMANY

R. Skogstrom
Meteorological Institute
University of Stockholm
Arrhenius Laboratory
S-106 91 Stockholm
SWEDEN

J. Slanina
ECN
3 Westerduinweg
NL-1755 ZG Petten
THE NETHERLANDS

H. Smith
Biology Department
National Radiological Protection Board
Chilton, Didcot
Oxon OX11 ORQ
ENGLAND

No. of Copies

J. W. Stather
National Radiological Protection Board
Building 383
Harwell, Didcot
Oxon OX11 ORO
ENGLAND

M. J. Suess
Regional Officer for Environmental Hazards
World Health Organization
8, Scherfigsvej
DK-2100 Copenhagen
DENMARK

Sun Shi-quan, Head
Radiation-Medicine Department
North China Institute of Radiation Protection
Tai-yuan, Shan-xi
THE PEOPLE'S REPUBLIC OF CHINA

J. W. Thiessen
Radiation Effects Research Foundation
5-2 Hijiyama Park
Minami - Ward
Hiroshima 732
JAPAN

M. Thorne
International Commission on Radiological Protection
Clifton Avenue
Sutton, Surrey
ENGLAND

United Nations Scientific Committee on the Effects of Atomic Radiation
Vienna International Center
P.O. Box 500
A-1400 Vienna
AUSTRIA

No. of Copies

R. Van Aalst
Laboratory for Air Research
RIVM
P.O. Box 1
NL-3720 BA Bilthoven
THE NETHERLANDS

D. Van As
Atomic Energy Board
Private Bag X256
Pretoria 0001
REPUBLIC OF SOUTH AFRICA

Vienna International Centre Library
Gifts and Exchange
P.O. Box 100
A-1400 Vienna
AUSTRIA

Wang Renzhi
Institute of Radiation Medicine
11# Tai Ping Road
Beijing
THE PEOPLE'S REPUBLIC OF CHINA

Wang Ruifa
Laboratory of Industrial Hygiene
Ministry of Public Health
2 Xinkang Street
Deshengmanwai, Beijing
THE PEOPLE'S REPUBLIC OF CHINA

Wang Yibing
North China Institute of Radiation Protection
P.O. Box 120
Tai-yuan, Shan-xi
THE PEOPLE'S REPUBLIC OF CHINA

No. of Copies

Wei Luxin
Laboratory of Industrial Hygiene
Ministry of Public Health
2 Xinkang Street
Deshengmanwai, Beijing
THE PEOPLE'S REPUBLIC OF CHINA

B. C. Winkler
Raad Op Atomic
Atoomkrag Energy Board
Privaatsk X256
Pretoria 0001
REPUBLIC OF SOUTH AFRICA

Wu De-Chang
Institute of Radiation Medicine
11# Tai Ping Road
Beijing
THE PEOPLE'S REPUBLIC OF CHINA

Yao Jiaxiang
2 Xinkang Street
Deshengmenwai
Beijing 100011
THE PEOPLE'S REPUBLIC OF CHINA

ONSITE

DOE Richland Operations Office

M. W. Tiernan

Tri-Cities University Center

J. Cooper

Hanford Environmental Health Foundation

M. J. Swint

No. of Copies

2 Westinghouse Hanford Co.

C. J. Perkins
D. E. Simpson

113 Pacific Northwest Laboratory

O. B. Abbey
K. J. Allwine
R. W. Baalman
D. C. Bader
J. F. Bagley
W. J. Bair (15)
M. Y. Ballinger
W. R. Barchet
N. S. Bloom
C. J. Brandt
K. M. Busness
D. B. Cearlock
E. G. Chapman
T. D. Chikalla
E. A. Crecelius
D. S. Daly
M. T. Dana
W. E. Davis
J. C. Doran
R. C. Easter
C. E. Elderkin (5)
J. W. Falco
C. S. Glantz
W. A. Glass
J. A. Glissmeyer
D. W. Glover
R. H. Gray
R. K. Hadlock
J. M. Hales (3)
R. V. Hannigan
P. C. Hays
D. J. Holtink
T. W. Horst
J. M. Hubbe
J. R. Johnson
R. A. Keefe
E. W. Kleckner
N. S. Laulainen
G. L. Laws
R. N. Lee
A.C.D. Leslie
D. J. Luecken
J. A. Malhaffey
M. E. Mericka
J. Mishima
E. L. Owczarski
P. C. Owczarski
J. F. Park
W. T. Pennell
J. V. Ramsdell
D. S. Renne
D. R. Roth
B. C. Scott
D. S. Sharp
R. L. Skaggs
E. D. Skyllingstad
W. G. N. Slinn
J. A. Stottlemyre
J. M. Thorp
B. E. Vaughan
L. L. Wendell (2)
C. D. Whiteman
R. E. Wildung
W. R. Wiley
J. D. Zimbrich
Health Physics Library
Life Sciences Library (2)
Publishing Coordination
Technical Report Files (5)